Comparative study of plasma-treated PCL fibers having different diameters and orientations for enhanced peripheral nerve regeneration

Len Liefooghe

Supervisors: Prof. dr. ir. Nathalie De Geyter, Prof. dr. Rino Morent
Counsellor: Rouba Ghobeira

Master's dissertation submitted in order to obtain the academic degree of
Master of Science in Biomedical Engineering

Department of Applied Physics
Chair: Prof. dr. ir. Christophe Leys
Faculty of Engineering and Architecture
Academic year 2017-2018

GHENT UNIVERSITY

Comparative study of plasma-treated PCL fibers having different diameters and orientations for enhanced peripheral nerve regeneration

Len Liefooghe

Supervisors: Prof. dr. ir. Nathalie De Geyter, Prof. dr. Rino Morent
Counsellor: Rouba Ghobeira

Master's dissertation submitted in order to obtain the academic degree of
Master of Science in Biomedical Engineering

Department of Applied Physics
Chair: Prof. dr. ir. Christophe Leys
Faculty of Engineering and Architecture
Academic year 2017-2018

GHENT UNIVERSITY

Preface

This work was performed at the Department of Applied Physics under the supervision of Rouba Ghobeira, Prof. dr. Rino Morent and Prof. dr. ir. Nathalie De Geyter.

I would like to express my gratitude to some people. In particular my promoters Prof. dr. Rino Morent and Prof. dr. ir. Nathalie De Geyter deserve a word of gratitude for they gave me the possibility to work on this very interesting topic.
I owe Rouba Ghobeira a great deal of respect and gratitude for the help I received with her valuable expertise, support, advise and especially her daily guidance. I hope to make her proud with the dissertation I delivered.
Other people who helped me also deserve a word of gratitude. For starters all the members of the Department of Applied Physics for helping me with fixing numerous day-to-day problems again and again, first and foremost the technician Tim Poelman. I would also like to thank Charlot Philips for her work on the cell tests.
Then, I wish to thank all the people who got this dissertation and read it through. Your comments and critical evaluation have given this dissertation an important added value.
Finally, I would like to thank my family, friends, classmates and roommates for their unconditional support, their much appreciated help and suggestions.

Permission Of Usage

Date:

Signature:

Abstract

Polycaprolactone (PCL) nanofibers are electrospun to create nanofibrous meshes with different fiber diameters (small, intermediate and large) and orientations (random and aligned fibers). The surfaces of these meshes are functionalized by a medium pressure dielectric barrier discharge (DBD) operating in argon. The synergistic effect of different fiber size, orientation and surface chemistry combinations on neuronal cell behavior are compared to choose the optimal fiber conditions capable to enhance peripheral nerve regeneration. Water contact angle (WCA) measurements, X-ray photoelectron spectroscopy (XPS) analysis and scanning electron microscope (SEM) visualizations are performed to examine the effect of the plasma treatment on the fiber surface chemistry and morphology. An increased wettability is seen for all fiber conditions, caused by the incorporation of oxygen-containing functionalities. A treatment time of 15s is chosen since saturation is achieved before fiber damage occurred. An ageing study is implemented to examine the durability of the treated fibers, and shows that the plasma treatment is quite stable since minor decreases in oxygen are observed 7 days post-treatment. Moreover, the ageing behavior is shown to be influenced by the fiber size and orientation. PrestoBlue assay, live/dead staining, SEM measurements and actin cytoskeleton staining are executed to assess the cell metabolic activity, viability, spreading and morphology. Plasma treatment considerably enhances cell spreading, adhesion and proliferation. Furthermore, the fibers with the largest diameter seem to have an adequate porosity that allow the cells to migrate into the bulk of the material. The aligned fibers, additionally, support directional growth of the cells.

Keywords — PCL, electrospinning, plasma activation, fiber morphology, fiber topography, fiber surface chemistry, cell-material interaction.

Comparative study of plasma-treated PCL fibers having different diameters and orientations for an enhanced peripheral nerve regeneration.

Supervisors: Prof. dr. ir. Nathalie De Geyter and Prof. dr. Rino Morent
Counselor: Rouba Ghobeira

Abstract

Polycaprolactone (PCL) nanofibers were electrospun to create nanofibrous meshes with different fiber diameters (small, intermediate and large) and orientations (random and aligned fibers). The surfaces of these meshes were functionalized by a medium pressure dielectric barrier discharge (DBD) operating in argon. The synergistic effect of different fiber size, orientation and surface chemistry combinations on neuronal cell behavior were compared to decide on the optimal fiber conditions capable of enhancing peripheral nerve regeneration. The effect of electrospinning parameters on fiber morphology was studied. Water contact angle (WCA) measurements, X-ray photoelectron spectroscopy (XPS) analysis, scanning electron microscope (SEM) visualizations and an ageing study were performed to examine the effect of the plasma treatment on the fiber surface chemistry and morphology. Live/dead staining, SEM measurements and actin cytoskeleton staining were executed to assess the cell viability, spreading and morphology. Plasma treatment considerably enhanced cell spreading, adhesion and proliferation. Furthermore, the fibers with the largest diameter seemed to have an adequate porosity that allowed the cells to migrate into the bulk of the material. The aligned fibers, additionally, supported directional growth of the cells.

Keywords — PCL, electrospinning, plasma activation, fiber morphology, fiber topography, fiber surface chemistry, cell-material interaction.

1 Introduction

The nerves in the body form the connection between the brain and the organs. Peripheral nerve injuries are quite common and the medical world is actively searching for ways to heal them. Suturing and grafts are possible solutions, but have several drawbacks. The development of tissue engineering however, led to the use of synthetic biodegradable polymers as nerve guidance conduits to lead damaged nerves to the organ that needs innervation such as a muscle. In the design of these conduits, the extracellular matrix (ECM) is the structure which is mimicked. [1] Electrospinning is the method of choice to build a fibrous structure due to the ability to produce thin nanofibers. [2] Polycaprolactone (PCL) is one of these polymers that is extensively studied. The mechanical properties of PCL are surely adequate for the intended use and the ability to electrospin nanofibers makes it a very promising material. [3] Different nerve cells seem to favor different fiber topographies. While some nerve cells perform best on thin fibers, others seem to behave better on thicker fibers. Furthermore the alignment of the fibers also alters the cellular morphology. [4] The electrospinning technique again plays a pivotal role in this, since the scale and orientation features of the electrospun fibers depend on a lot of parameters: solution parameters, process parameters and ambient parameters. [2,5] Different topographies of the nanofibrous mesh will be electrospun and the dependencies of the solution concentration, the collector to tip distance (CTD), the rotational speed and the relative humidity (RH) on the fiber diameter will be investigated with SEM. Unfortunately the surface properties of PCL were not at all desirable. The low surface energy and low wettability were not leading to good cell adhesion, spreading and proliferation. Several approaches to circumvent this inconvenience have been performed such as wet-chemical route, γ- and UV-radiation. The cellular response was better, but these techniques were degrading the nanofibrous mesh. [6] A better technique is the exposure of the PCL nanofibers to nonthermal plasma. This method is solvent-free and modifies the surface adequately without altering the bulk properties. [7] The plasma treatment incorporates functional groups on the surface of the nanofibers, resulting in a more hydrophilic behavior. [3] In this dissertation the PCL nanofibers

will be plasma treated in argon gas using a dielectric barrier discharge (DBD) operating at medium pressure. The effect of the plasma treatment on the polymer surface will be studied by using WCA measurements, XPS and SEM. The main goal of this dissertation however is studying the behavior of olfactory ensheathing cells (OECs) on different nanofibrous meshes. 12 different conditions will be studied (treated vs untreated, small vs intermediate vs large diameter and randomly oriented fibers vs aligned fibers) making use of live/dead staining, actin cytoskeleton staining and SEM visualization.

2 Materials and methods

2.1 Fiber material and fabrication

The fibers were made from PCL pellets with a molecular weight of 80 000 $^{g}/_{mol}$. PCL was dissolved in a mixture of formic acid and acetic acid with a 9:1 ratio to obtain the following concentrations: 20 %, 24 %, 28 % and 32 %. All chemicals were purchased from Sigma-Aldrich in Belgium and used without additional purifications. The fibers were made by electrospinning with the Nanospinner 24 (inovenso, Turkey) and a rotating cylindrical metallic mandrel with a height of 1 cm and a radius of 5 cm. The CTD was adjusted to 20 cm, 17.5 cm, 15 cm and 10 cm. The rotating speed of the collector was 100 rpm for random fibers and 3000 rpm for the aligned fibers. Electrospinning was done at a voltage of 32 kV. The temperature was depending on the weather conditions, but care was taken that electrospinning was only done between temperatures of 20 and 24 °C. The RH was either low (± 20 %) or high (± 50 %). The high RH was possible by using a humidifier inside the process chamber.

2.2 Plasma treatment set-up

The plasma treatment was done by a DBD reactor consisting of a plasma chamber and a power supply. The plasma was generated between 2 circular copper electrodes (diameter = 4 cm). Square (25.0 cm^2) ceramic plates (Al_2O_3) (thickness = 0.7 mm) were used as dielectrics and cover both electrodes. The lower electrode was connected to earth, by either a capacitor (10.4 nF) or a resistor (50 Ω) and the upper electrode was connected to an AC power source (frequency = 50 kHz). The plasma chamber was connected to a pump and filled with argon gas with a controllable flow. The plasma treatment was performed for a variety of treatment times at a stable medium pressure of 5.0 kPa.

2.3 Surface Characterization of the fibers

To visualize the morphology of the PCL fibers a SEM was used (JSM6010PLUS, JEOL, Japan) operating at an accelerating voltage of 7 kV. First, the samples required a golden coating with the sputter coater (JFC1300 autofine coater, JEOL, Japan). Afterwards the average nanofiber diameter was calculated using the ImageJ analysis software (National Institutes of Health, USA). The protocol for cell monolayer on Thermanox was used to fix the cells for adhesion and proliferation.
To evaluate the surface wettability of the PCL nanofibrous meshes, the static WCA was measured with the commercially available Krüss Easy Drop optical system (Krüss Gmbh in Germany). A 2 μl of distilled water was deposited onto the samples and the water contact angle was measured in normal ambient conditions in a laboratory setting.
A PHI 5000 Versaprobe II spectrometer was used to carry out the XPS measurement. A monochromatic Al K_α X-ray source ($h\nu$ = 1486.6 eV), operating at 50 W power (beam size = 200 μm) was focused onto the sample. A pressure of at least 10^{-6} Pa was maintained inside the apparatus. A hemispherical electron analyzer, placed under an angle of 45° with respect to the sample surface normal, was used to detect the photoelectrons.

2.4 UV sterilization

The samples were irradiated for 3 h by a UV lamp of 15 W (Sylvania; 254 nm wavelength). A distance of 45 cm between the lamp and the samples was maintained and the effective UV intensity was 300 $^{\mu W}/_{cm^2}$.

2.5 Cell culture tests

2.5.1 Cell seeding

The olfactory ensheathing cells (OECs) were derived from rat's bulbus olfactorius, cultured in DMEM/F12 (Gibco) with 10 % FCS and 1 % antibiotics and seeded at a density of 10 000 cells per sample.

2.5.2 Live/dead Staining (CaPi) and fluorescence microscopy

Live/dead staining with calcein AM/propidium iodide was carried out to evaluate cell viability of OECs. First of all the PCL fibers were rinsed, then the supernatant was replaced with 1 ml phosphate buffered saline (PBS) supplemented with 2 μl (1 $^{mg}/_{ml}$) prodium iodide (Sigma-Aldrich; P4170) and

2 μl (1 $^{mg}/_{ml}$) calcein AM (ANaspec; 89201). Afterwards the cells were incubated in the dark for a duration of 10 min at room temperature. The samples were washed with PBS and checked under a fluorescence microscope (Olympus IX 81).

2.5.3 Actin Staining

The intermediate actin filaments of the OECs are visualized by first fixing the samples with 4 % paraformalfehyde for a duration of 20 min. The samples were washed 3 times with PBS and permeabilized with 0.5 % Triton X-100 (Sigma-Aldrich; T8787) for 5 min in distilled water. Next the cells were washed again with PBS and subsequently incubated with rhodamine phalloidin (Thermo Fisher Scientific; R415; 1/100). A last PBS wash was carried out and finally the samples were mounted with Vectashield Antifade Mounting Medium with DAPI (Vectorlabs; H-1200).

3 Results and Discussion

3.1 Electrospinning of PCL fibers

To obtain the different fiber conditions, electrospinning parameters were altered. The polymer concentration, CTD, RH and rotational speed were adjusted separately to study their effect on fiber morphology. Increasing the polymer concentration, led to an increase in the fiber diameter. Moreover decreasing the CTD and increasing the RH, resulted in larger fiber diameters. The rotational speed was primarily used to accomplish different alignment: 100 rpm for random fibers and 3000 rpm for aligned fibers. Six different fiber conditions were electrospun, SEM images can be found in figure 1.

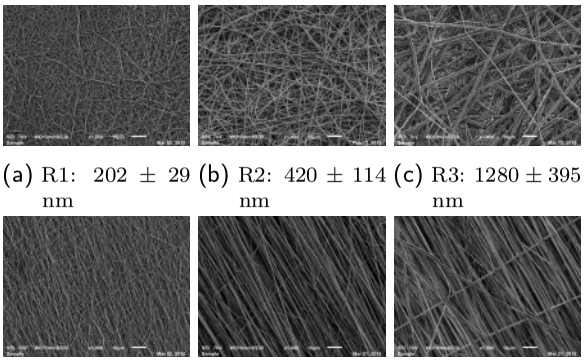

(a) R1: 202 ± 29 nm (b) R2: 420 ± 114 nm (c) R3: 1280 ± 395 nm

(d) A1: 238 ± 81 nm (e) A2: 573 ± 240 nm (f) A3: 1091 ± 463 nm

Fig. 1: SEM images (magnification 1000x) of the different fiber conditions.

3.2 Analysis of the plasma treatment

3.2.1 WCA

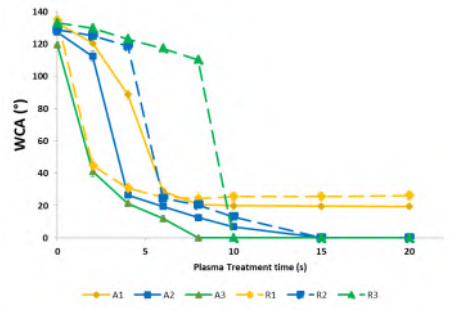

Fig. 2: WCA (°) vs plasma treatment time (s) for all fiber conditions.

Figure 2 shows the evolution of the WCA for argon plasma treatment on all fiber conditions. The untreated samples had a WCA around 130°, thus very hydrophobic. After plasma treatment the WCA started to decrease. All samples became hydrophilic after 10s of treatment. The wettability of the nanofibrous meshes was seen to depend on both the surface topography and the surface energy. Air bubbles get trapped inside the pores and hinders water drops to penetrate into the structure. Thicker fibers are more porous, so more air gets trapped and the WCA increases. But in counterpart thicker fibers also have a higher surface roughness and water penetrates in the surface grooves, so the WCA increases. This competition led to an equilibrium in water spreading. The porosity decreased for aligned fibers, increasing the wettability. The surface energy was studied with XPS analysis and explained the dependency of the plasma treatment on the WCA drop.

3.2.2 XPS

The evolution of the surface oxygen content of the PCL fibers can be found in figure 3. It was clear that the plasma treatment incorporated oxygen functionalities until saturation was reached, around 15s. This explained the drop in WCA after treatment. For all fiber conditions the initial surface oxygen content was around 24.5 % and reached ± 30 %. A closer look at figure 3 showed that, although all fiber conditions showed a negligible difference in oxygen content in the untreated state, the oxygen content developed in a slightly different way during plasma treatment. For the randomly oriented fibers, the saturation was reached earlier. Moreover, in both orientations the bigger diameters had slightly higher surface oxidation compared to the smallest diameters. For the aligned fibers, the macromolecules are

really packed and straight, making plasma incorporation harder. The molecular chains needed thus more treatment time to be broken and functionalized. Furthermore, a bigger diameter was caused by polymer jet experiencing less stretching and thinning, leading to less ordering in the molecular chain arrangement. This implicated that more molecular chains were exposed to plasma resulting in more bonds that were broken, thus more functionalities that could be incorporated into the sample.

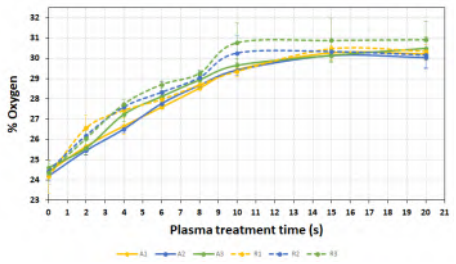

Fig. 3: % Oxygen vs plasma treatment time (s) for the different fiber conditions.

3.2.3 Damage of the plasma treatment

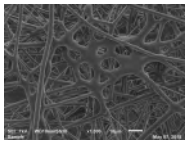

Fig. 4: SEM image (magnification 1000x) of R3 fibers after 1 min of plasma treatment.

SEM images of the nanofibrous meshes were taken after 15s and 1 min of plasma treatment to check if plasma treatment altered the fibrous morphology. Little to no damage was visible on the fibers treated for 15s. But after 1 min the samples, especially the R3 fibers, started to show significant damage (figure 4). Two phenomena took place: some fibers were melting together and some fibers got thinner. The melting was caused by the electrodes that got heated during the treatment because of the high energy supplied by the plasma source. The thinning could be explained by the ion etching effect of the plasma. The differences in severity of the damage can be explained by looking at the mechanical properties of the fibrous meshes. The poor molecular arrangement and crystallinity of the larger fibers increased the degree of freedom for the polymer chains to move. The porous structure seen in randomly oriented fibers can weaken the resilience against deformations as well.

3.2.4 Ageing

An ageing study was performed by analyzing the surface composition of the samples after 1, 3 and 7 days. The results can be found in figure 5. In all the conditions, the surface oxygen content decreased, but not too much. This was due to post-plasma treatment reactions of the surface with atmospheric minorities and due to the reorientation of oxygen containing functionalities towards the bulk of the material. The alignment of molecular chains hindered the incorporated functional groups to move and reorientate, hence the lower hydrophobic recovery on the aligned fibers. The increased degree of freedom in the larger fibers resulted in higher possibility of rotational and translational motion and thus more reorientation of functionalities towards the bulk.

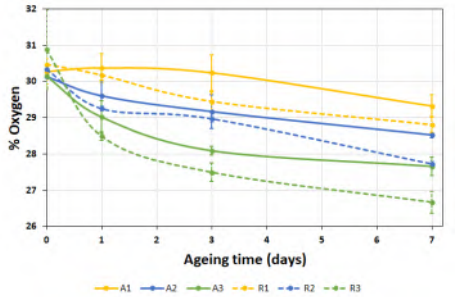

Fig. 5: Evolution of the surface content of oxygen as a function of ageing time (days) for the different fiber conditions.

3.3 Cell Tests

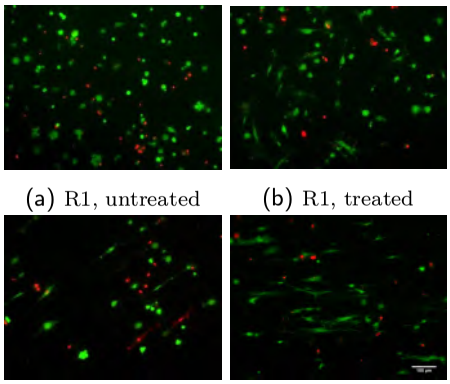

(a) R1, untreated (b) R1, treated

(c) A2, untreated (d) A2, treated

Fig. 6: Fluorescent micrographs after live/dead staining of OECs, cultured for 3 days. (scale bar on (d): 100 μm)

Twelve different conditions were fabricated (untreated vs treated, random vs aligned and small

vs intermediate vs large fiber diameter). OECS were used for the cell tests, they ensheath the non-myelinated neurons of the olfactory system, that is responsible for the sense of smell. [8] The fluorescent microscopic images after live/dead staining of OECs, showed the cells that survived and died, indicated by green and red respectively. In most different conditions more living cells than dead cells were seen. The cells stayed rounded on the untreated samples (figures 6a and 6c) and spread on the treated samples (figure 6b); even along the fiber orientation in case of aligned fibers (figure 6d). The cytoskeleton was visualized with the actin staining, which clearly showed a more spread out morphology of the cells on the treated samples (figures 7b and 7d), while they stayed small and rounded on the untreated samples (figures 7a and 7c).

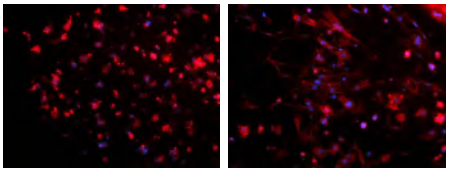

(a) R1, untreated (b) R1, treated

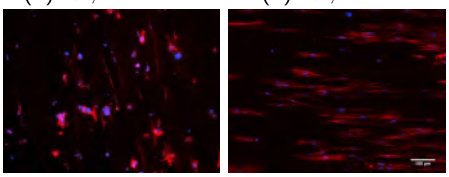

(c) A3, untreated (d) A3, treated

Fig. 7: Actin cytoskeleton staining of OECs, cultured for 3 days. (scale bar on (d): 100 μm)

The cytoskeleton was visualized with the actin staining, which clearly showed a more spread out morphology of the cells on the treated samples (figures 7b and 7d), while they stayed small and rounded on the untreated samples (figures 7a and 7c). The cellular attachment was much better because of the plasma treatment. The aligned fibers showed a highly directional spreading on top of that. Even in the SEM images the difference between treated and untreated was clear. The cells were small and round on the untreated samples (figure 8a), indicating poor cellular attachment. For the plasma treated conditions the cells were elongated and spread out (figure 8d). On the larger fiber diameters, the cells were able to infiltrate the bulk (figure 8h). The pores in the samples with small diameter were too small for the elongated cells to migrate into and the cells formed a covering sheet on top of the mesh (figure 8b). The treated, aligned fibers showed that the cells were following the fiber direction in spreading (figure 8f).

The higher wettability led to better adsorption of proteins, because the oxygen containing functionalities acted as receptor binding sites. The receptors on the cell surface were able to bind to the plasma treated nanofibers.
Important mediators in cell-material interactions were the transmembrane proteins: integrins. At focal adhesion sites, the cell binds to the sample with these integrins.

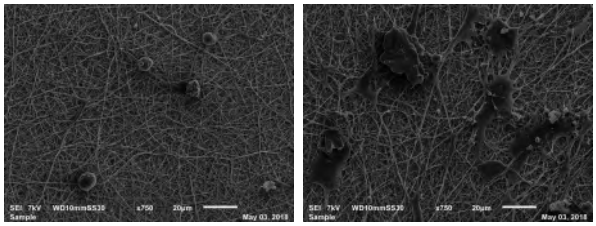

(a) R1, untreated (b) R1, treated

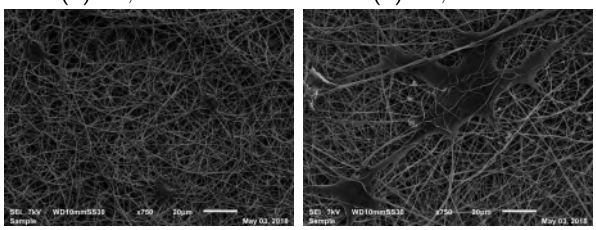

(c) R2, untreated (d) R2, treated

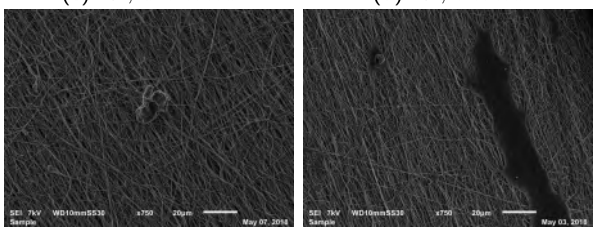

(e) A1, untreated (f) A1, treated

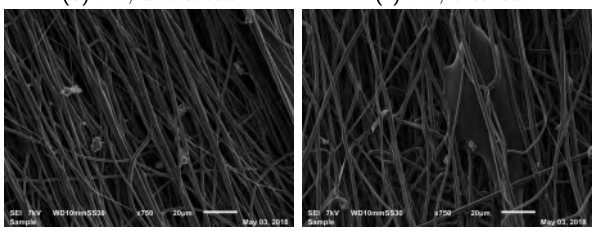

(g) A3, untreated (h) A3, treated

Fig. 8: SEM images (magnification 750x) of of OECs, cultured for 10 days, on different conditions.

They cluster together and evoke signalling pathways, that alters the structure of the filaments of the cytoskeleton among others. The untreated samples did not have a lot of these focal adhesion sites, because they lacked oxygen functionalities. The cells that did attach, showed a three-dimensional rounded morphology. The plasma treated samples were occupied with focal adhesive sites, the cells

showed a two-dimensional spreading and elongation. [9,10]

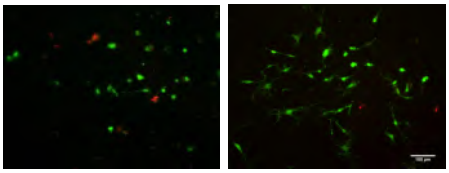

(a) R3, untreated (b) R3, treated

Fig. 9: Fluorescent micrographs after live/dead staining of OECs, cultured for 10 days. (scale bar on (b): 100 μm)

The cells that did attach, showed a three-dimensional rounded morphology. The plasma treated samples were occupied with focal adhesive sites, the cells showed a two-dimensional spreading and elongation. [9, 10]
The live/dead staining at day 10 indicated most cells were still alive. For random fibers, there was a clear difference between the untreated and the argon plasma treated samples. A lot of living cells were present on the treated fibers (figure 9b), much more than on the untreated fibers (figure 9a). Plasma treatment did not only enhance adhesion of the cells, but also their proliferation.

4 Conclusion

This master's dissertation describes a host of advancements concerning the fabrication of nanofibrous meshes suitable for peripheral nerve regeneration purposes, which is a common clinical problem. Six different nanofibrous meshes were electrospun. The effects of a DBD argon plasma treatment on the different fibers conditions, have also been studied extensively. The wettability was higher because the incorporation of oxygen containing functionalities. Surface morphology was also seen to influence wettability. At 15s the fibers were still intact and durable, according to SEM visualization and an ageing study. The main reason for the plasma treatment was the bad biochemical properties of the surface of the fibers. These were altered without changing the bulk of the material.
Twelve different conditions were tested and compared to each other concerning their potential to be utilized as a nanofibrous mesh for polymer conduits used in peripheral nerve regeneration. Cells are sensitive to both their topographical and their biochemical environment. The electrospun nanofibers were responsible for the topographical cues, while the argon plasma treatment was responsible for the biochemical cues. The cellular attachment, morphology and proliferation of OECs were tested on the 12 different conditions. None of the samples showed a high death rate for the cells. The untreated samples showed rounded cells, indicating poor cellular attachment, while the treated samples showed an elongated morphology. The cells showed a directional spreading on the aligned fibers, useful to direct the cells to the right structure to be innervated. The cells were also migrating to the inside of the bulk on the larger fibers, because of the adequately porous structure. The nanofibrous meshes mimic the ECM quite good in these cases. The next step in this research is the fabrication of actual polymeric conduits instead of meshes on coverslips. My suggestion is a bi-layer conduit where the inner lumen is built up out of plasma treated aligned fibers with a mean diameter of around 1200 nm. The outer lumen should consist of randomly oriented fibers, so nutrients can reach the inner volume, but cellular ingrowth deep into the inner volume should be hindered, especially for cells like fibroblasts. These synthesize the ECM, so the available space for the nerve regeneration could be diminished. A little inwards migration could be beneficial, since, during the degradation of the polymer, the ECM should replace the conduit continuously.

Acknowledgements

This master's dissertation was performed at the Department of Applied Physics under the supervision of Rouba Ghobeira, Prof. dr. Rino Morent and Prof. dr. ir. Nathalie De Geyter. I would like to express my gratitude to them for their guidance and support. Furthermore, I would like to thank Charlot Philips for performing the cell tests and the other members of the Department of Applied Physics for their help.

References

[1] G. Lundborg. *Journal of Hand Surgery*, 25(3):391–414, 2000.

[2] R. Ghobeira et al. *European Polymer Journal (submitted)*.

[3] A. Martins et al. *Small*, 5:1195–1206, 2009.

[4] A.T. Nguyen et al. *Journal of Physics: Condensed Matter*, 28, 2016.

[5] N. Bhardwaj et al. *Biotechnology Advances*, 68(3):325–347, 2010.

[6] R. Morent et al. *Plasma Processes and Polymers*, 8(3):171–190, 2011.

[7] T. Desmet et al. *Biomacromolecules*, 10(9):2351–2378, 2009.

[8] S.C. Barnett et al. *Journal of Anatomy*, 204:57–67, 2004.

[9] W. Liu et al. *Colloids and Surfaces B: Biointerfaces*, 113:101–106, 2013.

[10] D. Lepzelter et al. *Langmuir*, 28:5379–5386, 2012.

Contents

List of Figures

List of Tables

List Of Abbreviations

CNS	Central nervous system
PNS	Peripheral nervous system
ECM	Extracellular matrix
PCL	Polycaprolactone
XPS	X-ray photoelectron spectroscopy
rpm	Rotations per minute
DBD	Dielectric barrier discharge
UV	Ultraviolet
WCA	Water contact angle
SEM	Scanning electron microscopy
UHV	Ultra-high vacuum
CTD	Collector-to-tip distance
RH	Relative humidity
R1	Randomly oriented fibers with small diameter
R2	Randomly oriented fibers with intermediate diameter
R3	Randomly oriented fibers with large diameter
A1	Aligned fibers with small diameter
A2	Aligned fibers with intermediate diameter
A3	Aligned fibers with large diameter
OEC	Olfactory ensheathing cell
slm	Standard liters per minute
FCS	Foetal Calf Serum
PBS	Phosphate buffered saline
HMDS	Hexamethyldisilazane

Chapter 1

Neural tissue engineering for enhanced peripheral nerve regeneration - literature review

1.1 Nerves

The nervous system is divided into two parts: the **central nervous system** (CNS) and **the peripheral nervous system** (PNS). The CNS consists of the brain and the spinal cord. Two roots originate from the spinal cord: the ventral root at the side of the belly and the dorsal root, at the side of the back. The ventral and dorsal roots combined form a spinal nerve; the human body normally has 31 pairs of them. The PNS forms the connections between organs and the CNS, via sensory nerves that send information to the brain and motor nerves that send information from the brain to the rest of the body. (figure 1.1)

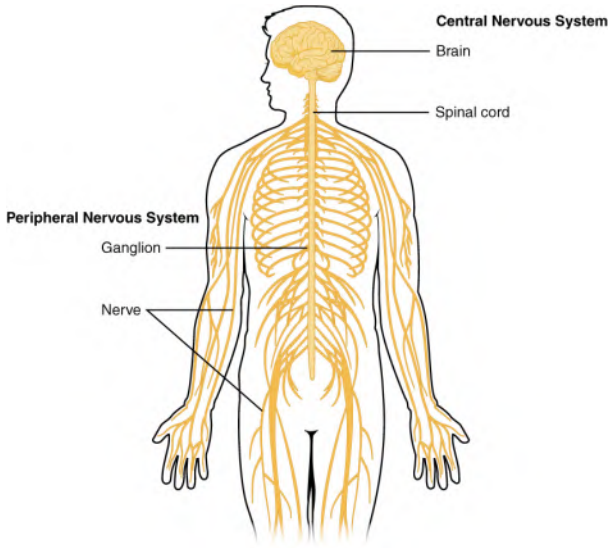

Figure 1.1: Central nervous system (CNS) and peripheral nervous system (PNS). [1]

Each nerve in the PNS is enclosed by a protective layer called **endoneurium**. Myelinated and unmyelinated nerves cluster together forming bundles of neurons called nerve fascicles that in turn are enclosed by the **perineurium**. Veins and arteries are present in between these fascicles to supply the nerves with nutrients and oxygen. The overall structure comprising of nerve fascicles and blood vessels is enclosed by a connective tissue called the **epineurium** (figure 1.2).
Neurons or nerve cells are quite well-known structures, consisting of a **cell body** or **soma**, **dendrites**

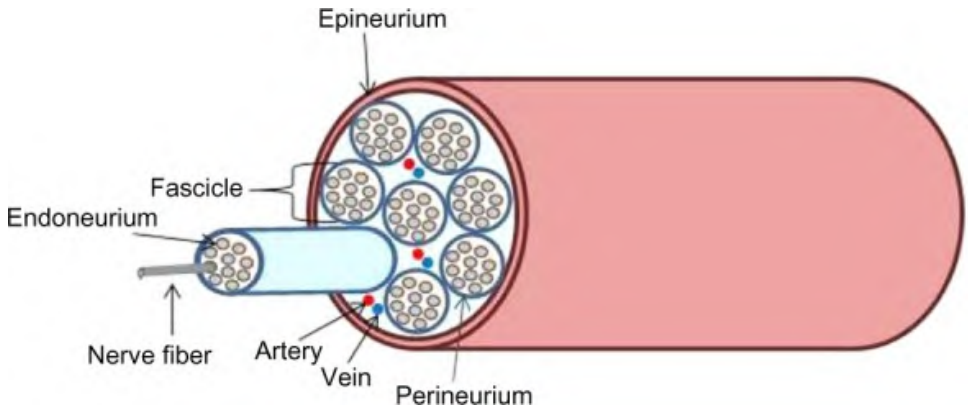

Figure 1.2: Cross-section of peripheral nerve.
[2]

and an **axon**. The dendrites are short structures of the nerve cell receiving information to be processed in the soma. The axon represents a longer structure with a beginning called the axon hillock (responsible for the generation of action potentials). The axon transmits the signal to the axon terminal where neurotransmitters can be released in the synaptic cleft. The neurotransmitters can cause a response in the postsynaptic cell. While dendrites are mostly short, axons can be quite long. The long nerve fiber is enclosed by **myelin sheaths**, produced by oligodendrocytes (in the CNS) or **Schwann cells** (in the PNS). Between successive myelin sheaths there is a small gap called **node of Ranvier** (figure 1.3). Just like in other cells, a cytoskeleton is present inside a neuron. The cytoskeleton is responsible for the shape of the cell and can also conduct transport along the cell. The neuronal cytoskeleton is built out of **microtubules**, **intermediate actin filaments** and **neurofilaments**. The latter consist of specialized protein subunits that are conventionally named neurofilament light (NF-L), neurofilament medium (NF-M) and neurofilament heavy (NF-H). [1–5]

1.2 Peripheral nerve damage and natural regeneration

Following for example a traumatic injury, nerves can be damaged. Whether the nerve is part of the CNS or of the PNS determines the ability of the nerve to regenerate or not. In the CNS, researchers have seen that the environment is not optimal for the healing of damaged nerves. Studies have shown that the myelin in the CNS contains growth-inhibiting proteins and the cleaning up of the damaged parts of the nerves is slower compared to peripheral nerves. [6]
In contrast, the nerves of the PNS do have the ability to spontaneously regenerate. The types of damage can be classified and will heal in a different way. **Seddon's classification** is stated here. First of all, it is important to note that if the soma is damaged, the regeneration will not occur. It only happens when the axon or axon terminal is damaged.

The least severe form of peripheral nerve damage is called **neuropraxia**. The axon, myelin sheath and endoneurium are still intact, but are compressed. In some cases demyelination occurs as well. This leads to blockage of an action potential along the lesion, followed by for example weakening of a muscle. A physician is needed, but surgery is not required for the recovery, that only takes a few days to some weeks. This is frequently observed in athletes.
The second form is called **axonotmesis**. The main difference with neuropraxia is damage to the axon and its myelin sheath, but endoneurium, perineurium and epineurium remain undamaged. In this case the proximal end of the injured axon is able to regenerate. The distal end undergoes a process called Wallerian degeneration (figure 1.4). The axon and its myelin shealth degenerate while macrophages and Schwann cells serve to clear the inside of the endoneurium of the debris left behind. Afterwards, the Schwann cells align and produce growth factors. The tubelike structure is able to guide the injured axon. These tubes are also called Büngner bands. This clearance goes up to the former proximal node of Ranvier from where the axon sprouts again. A **growth cone** is visible at the end of the axon. The

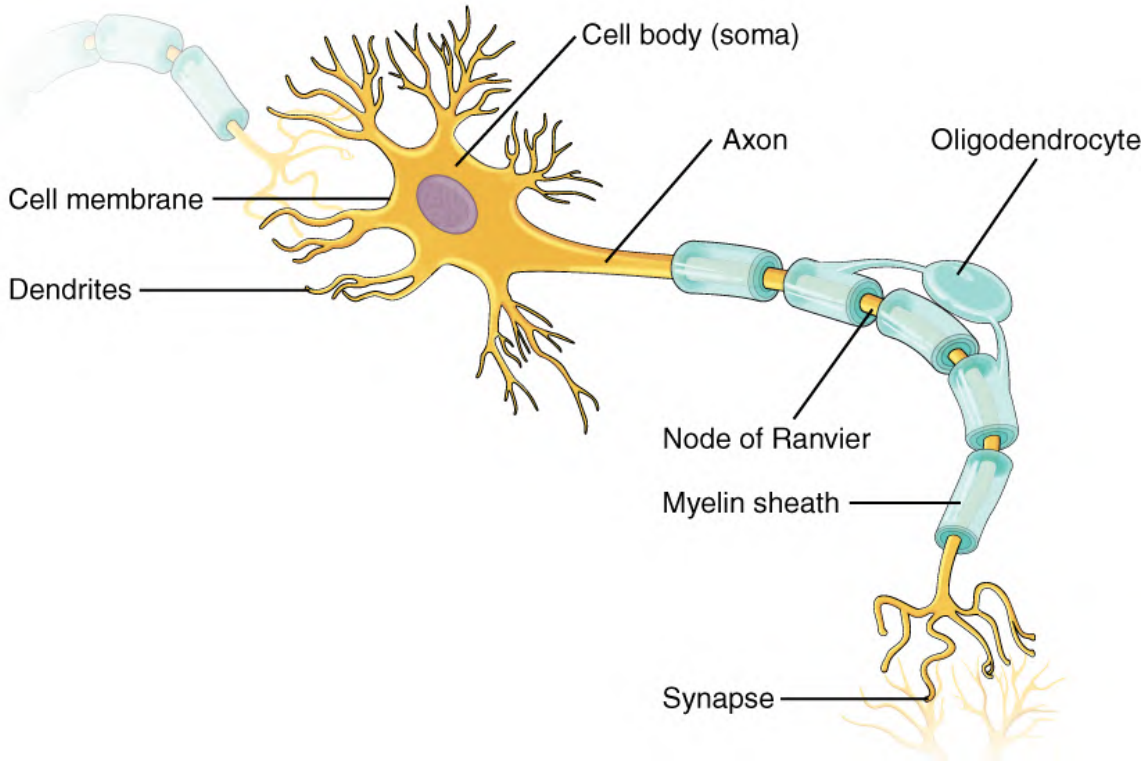

Figure 1.3: Typical appearance of a neuron in the CNS.
[1]

neurons use this subcellular structure to sense and navigate the surroundings. Depending on the type of growth cone, cell and extracellular matrix (ECM), the growth cone can vary largely in area, from 10 μm^2 to 760 μm^2. [7–9] Along the Büngner bands the axon advances, reaching and reinnervating the tissue of interest. The axon grows approximately 1 mm per day. The Wallerian degeneration is however not always as successful, leading to problems such as polyinnervation and misdirection.
The most severe case of nerve damage is called **neurotmesis**. This is characterized by damage to the connective tissues around the neurons. According to whether it is the endoneurium, perineurium or epineurium, that is impaired, the regeneration process will be different. If the endoneurium is damaged, natural regrowth of the nerve is possible similar as in axonotmesis, but mostly not as good. If the perineurium is damaged, regeneration can also take place but will possibly be of poor quality. If the epineurium is involved in the lesion, spontaneous regeneration will not be present. Surgical procedures will be needed to fix this problem. [2, 4, 10–13]

1.3 Medically assisted nerve regeneration

1.3.1 Suturing

A gap somewhere in a peripheral nerve leaves a proximal end and a distal end distinguishable. The two stumps must meet again in order for the proximal stump to regrow along the path of the distal part which is undergoing Wallerian degeneration. The joining of the nerve segments is called coaptation. The spontaneous, natural regeneration of the nerve is however not always a piece of cake. Luckily the medical world is researching how to help the nerve repair as fast and optimal as possible. For this several strategies are applied (figure 1.5).

The most straightforward way is obviously suturing both ends together. The epineurium of both sides is brought together and the alignment is based on the vascular structure of the outside of the epineurium (figure 1.6). An important factor is the suturing material. Fibrin glue seems to be an adequate candidate

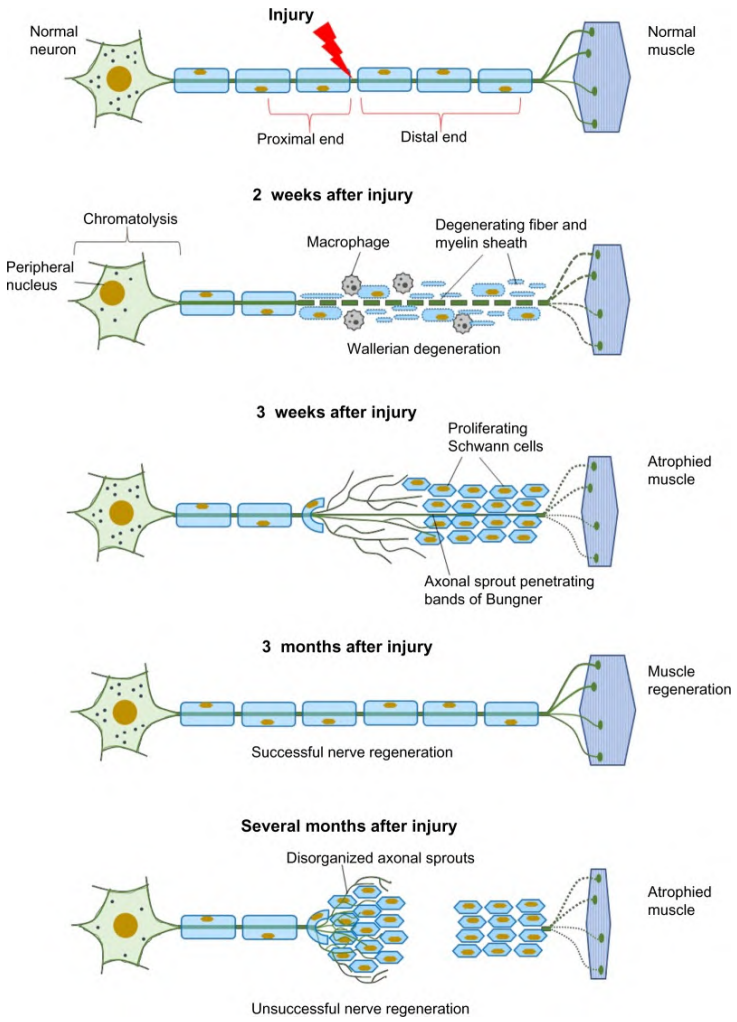

Figure 1.4: Wallerian degradation and nerve regeneration mechanism.
[2]

to avoid irritation.
The inside of the nerve is however not necessarily aligned and this seems to be important as well to attain optimal repair. Another way is to remove a part of the epineurium in both ends and suture the perineurium of the distinct fascicles together (figure 1.7). A critical comparison concluded that both epineurial and perineurial fascicular nerve repairs are equally successful.
Although suturing is the preferential procedure to overcome gaps in the nerve, a problem arises when the gap becomes relatively big as a tension is exerted on both sides of the gap. This could lead to ripping at another site in the nerve. A logical solution for this is bridging the gap. [14]

1.3.2 Grafts

The ECM holds cells together and provides a medium for cells to interact and migrate. This is obviously the gold standard for nerves to regenerate. If we want to create an ideal environment for nerve regeneration, an **autologous graft** would be perfect. This already contains Schwann cells from the host, which play a very important role in the peripheral nerve regeneration. Currently autografts are used for gaps up till 5 cm. [2]
However some problems seem to arise. First of all, the size of the nerve at the donor site needs to be compatible with the size at the recipient site. This already limits the useful nerves. Next to that, the donor nerve is harvested from elsewhere in the body of the patient, thus requiring a second surgical procedure and rendering the donor site vulnerable to loss of sensation and scarring. Furthermore there

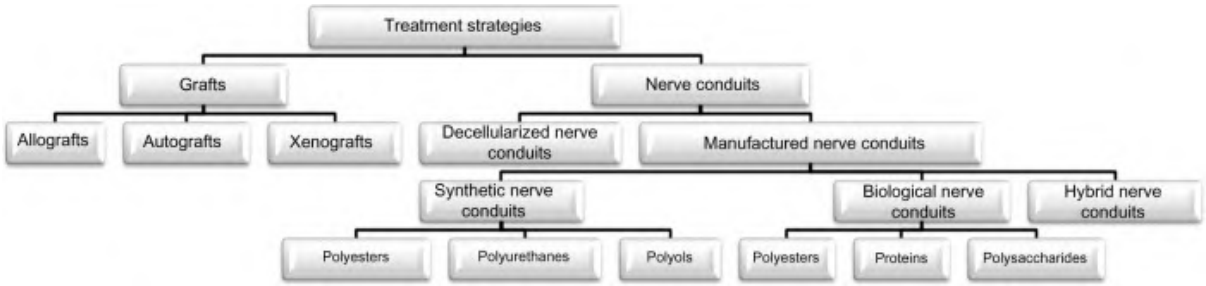

Figure 1.5: Different strategies for medically-assisted nerve regeneration.
[2]

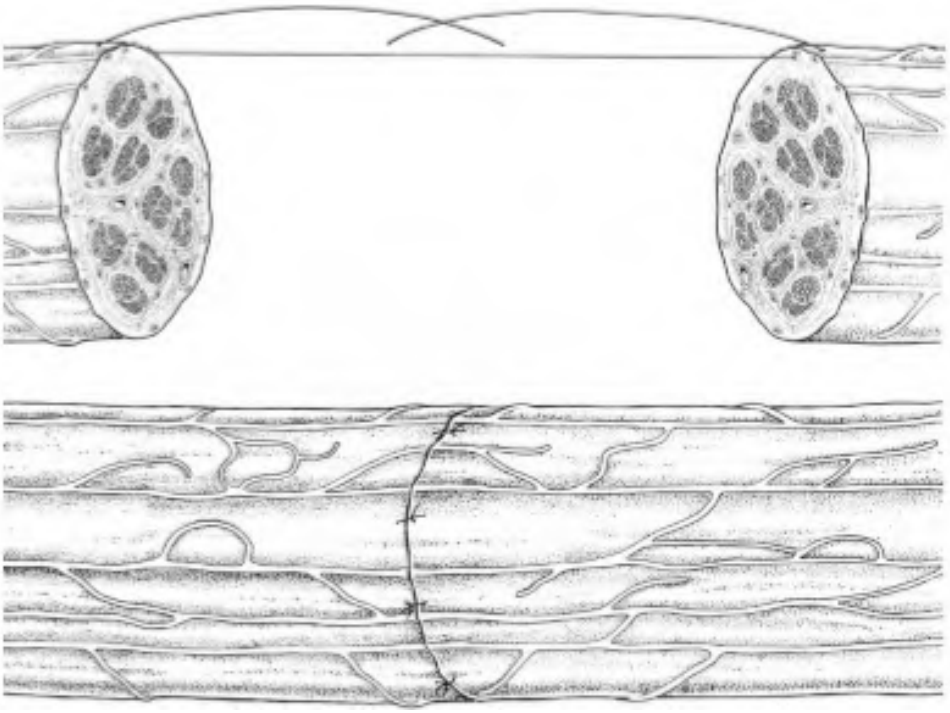

Figure 1.6: Epineural suture.
[14]

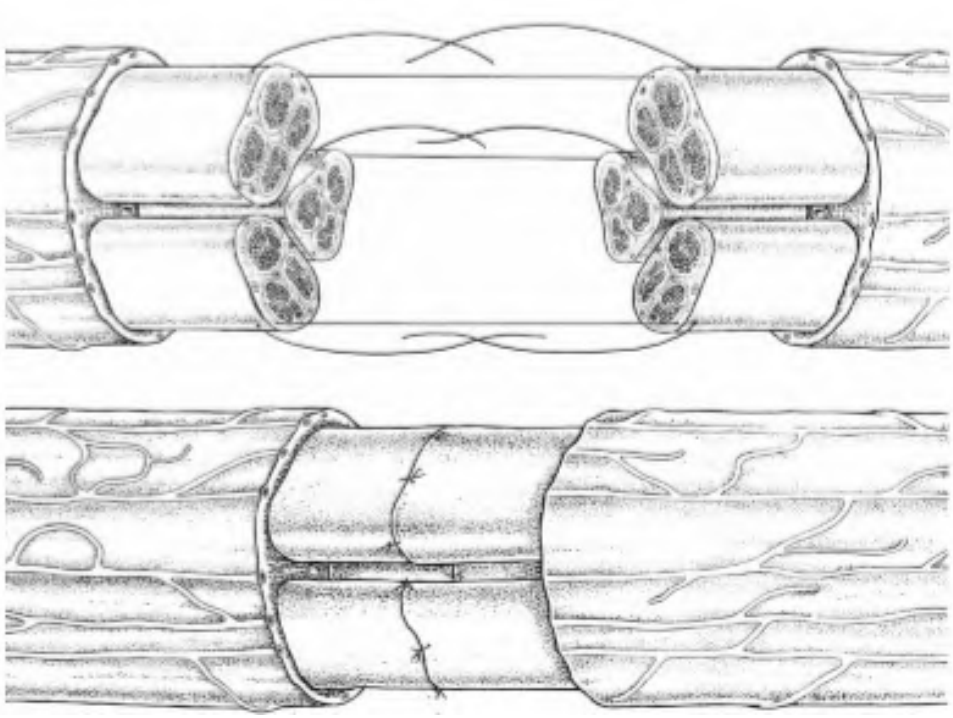

Figure 1.7: Perineural suture.
[14]

is only a limited amount of adequate nerve sites.
Availability could be solved by using **allografts**, grafts from another individual from the same species, or **xenografts**, grafts from another species. However the immune system could reject it. This leads to the need of severe immunosuppression or the use of a **decellularized nerve conduits**, where the Schwann cells of the host can migrate into. [2, 15, 16]

1.3.3 Polymer conduits

In order to obviate the drawbacks of the nerve grafts, the use of nerve tissue engineering approaches is nowadays gaining a huge interest. A synthetic ECM that acts as a suboptimal environment for nerve regeneration could show promising results. As seen with the natural nerve regeneration process, the goal is to enhance the Schwann cells to form Büngner bands and, to create a viable environment for cells to grow on while leading them to the appropriate structure that should be innervated. Apart from that, it is of great importance as well to avoid neuromas at all costs. Furthermore, other growth factors, chemicals, molecules... could also be of importance for the growth of the nerve, especially in long nerve gaps, where speeding up the process could be of great benefit. We specifically want the proximal end to reach the goal of interest, for instance a muscle, as fast as possible to avoid atrophy of that muscle. [17–19]

It is necessary that the conduits used in the process exhibit specific physical, topographical and chemical properties. First of all, we want the conduit to be biocompatible to avoid unwanted reactions of the body and promote cell adhesion, migration and proliferation. Since a second operation to remove the conduit is as well not the best option, the conduit should be biodegradable, but with an appropriate degradation rate matching the regeneration rate. If it is too fast, the support is lost before the healing process, or if it is too slow, it could lead to an unwanted reaction of the body. This goes hand in hand with the wall thickness. An appropriate porosity allowing migration of growth factors, nutrients, oxygen and waste products is required. Reports have shown that the optimal pore size should be somewhere between 10-20 μm. [18, 20] To top it all off, there is a trade-off between flexibility and stiffness: the conduit should be able to bend without kinking following the limb's movements. Moreover the guide should not collapse or dislocate in vivo. Ideally the mechanical properties of the nerve guide should resemble the mechanical

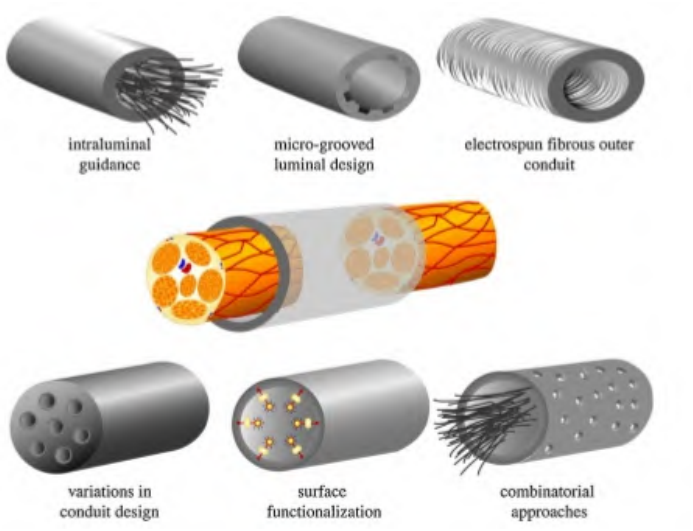

Figure 1.8: Different designs of polymer conduits.
[20]

properties of the nerves as closely as possible, see table 1.1.

Table 1.1: Mechanical properties of human nerves.

Nerve type	Elastic modulus (E)(MPa)	Ultimate tensile strength (UTS)(MPa)	Elongation at break (ϵ)($^{mm}/_{mm}$)
Intact human nerve	15.87 ± 2.21	6.78 ± 0.57	0.61 ± 0.02
Extracted human nerve	8.19 ± 7.27	8.54 ± 3.37	1.64 ± 0.34

[20]

Different designs and polymers have been proposed. The basic design is a tubular structure with a single lumen. The conduit should:

- isolate the regenerating axons from fibroblasts (cells that synthesize the ECM),
- protect the regeneration nerve against compression by the surrounding tissue,
- direct the nerve cells in the right way, which means encouraging the Schwann cells to form bands of Büngner,
- allow the revascularization to take place and
- keep the growth factors, secreted by the Schwann cells and the axon sprouts, on the inside of the tube. [20, 21]

Researchers have experimented with different nerve guide designs (figure 1.8). A first category is hollow tubes with a single lumen, that can be porous or nonporous. Inner surface microgrooves could be made to guide axonal growth in the longitudinal direction. The inside surface can also be functionalized with either bioactive molecules and peptides to enhance attachment, proliferation and migration of Schwann cells or neurotrophic factors to promote axonal regrowth.
A second design is enhancing the former with a filler in the lumen to mimic the endoneurial structure and the ECM. These fillers could be longitudinally aligned fibers, porous sponges or gels. Again it is possible to functionalize the inner surfaces.
A third approach is a multichannel graft. This mimics the internal compartmentalized structure of the nerve (fascicles). There is more surface area to be functionalized but permeability and flexibility are compromised. These conduits do not show significant improvement however. [2, 18, 20]
Despite using all these designs and adding innovative biological, topographical and chemical cues to the nerve guides, the treatment of critical sized nerve gaps is still failing. Therefore, our aim is to heal large nerve gaps by developing a scaffold presenting optimal physical and chemical properties mimicking the living nerve tissue for an effective regenerative power.

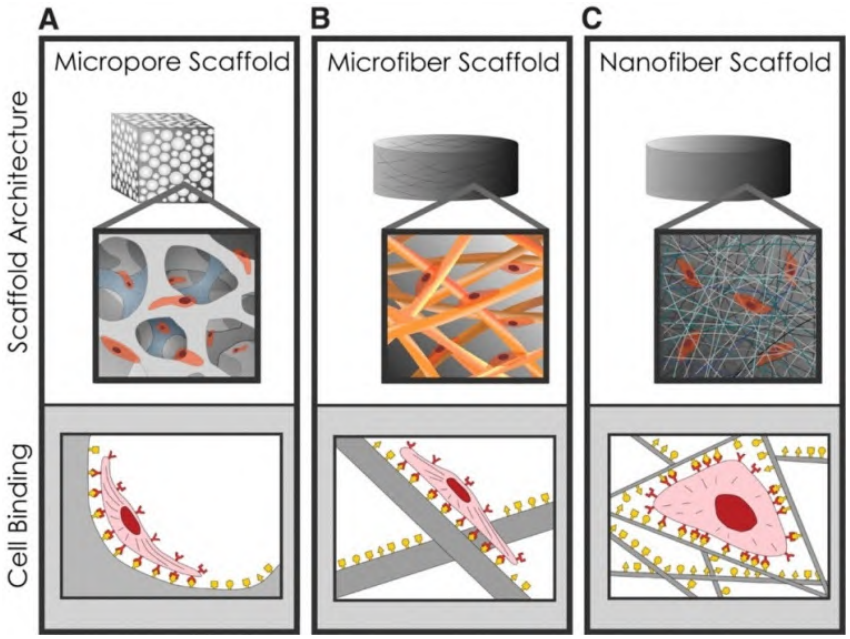

Figure 1.9: Visualization of cell attachment on nanofibrous, microfibrous and microporous scaffolds. [25]

1.3.4 Nerve conduits topographical properties

An architectural arrangement mimicking the fibrous neural ECM plays an important role for a harmonized interaction between the cells and the scaffold and will thus be adopted in this dissertation. Nanofibrous meshes have shown superior cell viability compared to other tissue engineering materials, probably because of their high surface/volume ratio, comparable to the ECM. [22] These fibers will make up the shell of a macroscopic tube, and will be created using **electrospinning**. In addition to the fibrous architecture, specific fiber conditions such as size and orientation seem to also have a great influence on cellular performances with variations between different cell types. Even if we limit our scope to nerve cells, these do not all seem to prefer the same fiber topography. This can be exemplified by oligodendrocytes and rat neural stem cells. Differentiation is optimal with a diameter of 283 $\pm$ 45 nm for the former, while the latter prefers diameters of 749 $\pm$ 153 nm and 1452 $\pm$ 312 nm. [23] The list goes on for all types of neural cells. The preferece of some cells for nanofibers instead of microfibers is justifiable as one cell is able to adhere to multiple nanofibers instead of only one. The higher surface area is beneficial for augmented cell attachment. However other cells prefer to attach to one microfiber for an enhanced proliferation, migration and differentiation. A nice visualization can be found in figure 1.9. In this dissertation different fiber diameters will be tested using neural cells. The optimal fiber diameter will be used to build a bio-mimicking fibrous nerve guide having structural similarity to the ECM. One thing all neural cells seem to have in common is their tendency to align along a grating axis. [7] This has been speculated in the work of Jha B.S. et al. showing that the end organ targeting might be improved in nerve injuries if axons can be directed to regenerate along specific tissue planes by a guide composed of 3D fiber arrays. [24] An interesting study has shown that a bi-layer conduit might be the best option for a polymer conduit to resemble an autograft as closely as possible. The inner lumen is made up out of longitudinally aligned nanofibers to promote nerve regeneration in the right direction. For the outer layer randomly organized fibers are proposed to be used, since adequate mechanical support is still in place. [25–27]

1.3.5 Nerve conduits base material

It is possible to produce nerve guides with synthetic or natural polymers as seen in figure 1.5. For the inner filler, natural polymers could be advantageous because of their biomimetic characteristics. However, synthetic polymers are preferred as the nerve guide material for several reasons including

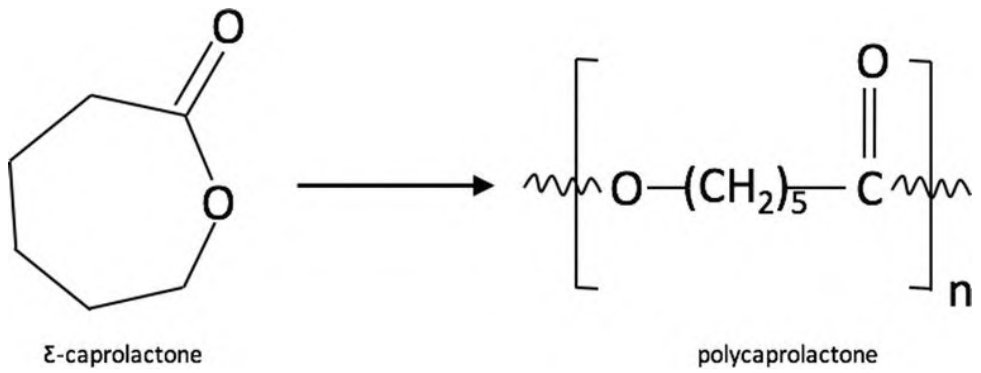

Figure 1.10: Repeating unit of polycaprolactone.
[30]

limited swelling, unaltered mechanical properties in physiological fluids and controllable degradation times. Additionally synthetic polymers are easier to reproduce in a consistent manner, are more readily available and cost less. In this dissertation the focus lies on synthetic polymers, more specifically biodegradable aliphatic polyesters. Examples include polyglycolic acid, polylactic acid, poly(L-lactic acid), poly(lactic-co-glycolic acid), polyhydroxyalkanoates, polybutylene succinate etc. This dissertation will however focus on **polycaprolactone**. [20, 25, 28]

Polycaprolactone

The first and foremost demand of an artificial conduit is biocompatibility. Polycaprolactone (PCL) is a polymer known for its biocompatible and biodegradable properties. Under physiological conditions PCL degrades by hydrolysis of its ester bonds. This makes it an interesting and widely used material in tissue engineering and biomedical applications. Furthermore the degradation products, which are succinic acid, butyric acid, valeric acid and caproic acid, are non-toxic and do not cause inflammation. Therefore a second surgery to remove the polymeric conduit is unnecessary. PCL is normally degrading in about one to two years. Defects with a lengthy repair time, such as nerve regeneration, benefit from this degradation profile. [29] PCL is an aliphatic polyester which is made by polymerization to open-ring of relatively cheap ϵ-caprolactone, see figure 1.10. It has a glass transition temperature T_g of -60 °C and a low melting point T_m of 59 - 64 °C. [28]
The research of Adam J. Reid et al. [31] or Sarah K. Pixley [18] provides us with an adequate indication that PCL can substitute the autologous graft. In their experiments rats were used with short nerve gaps and both an autologous and a PCL graft were implemented. The polymeric conduit not only showed good results, but also revealed an efficient state of degradation since it was hinted that longer nerve gaps, with longer healing time, could also benefit from using PCL conduits. The porosity, pore diameter and wall thickness of the PCL conduit also has a significant impact. Luckily it is possible to obtain different values of these parameters by optimizing the electrospinning parameters. A study done by Lauren E. Kokai [17] suggests the following parameters should be used for the external nerve guide: 80% porosity with 10-38 μm pore size and a 0.6 mm wall thickness should be used. Other sources strive for a porosity of 70%, pore size of around 10-20 μm and a wall thickness of around 100-300 μm. Another advantage of using PCL is the fact that suturing the graft at both ends of the gap is easy and the conduit maintains mechanical stability during some weeks. [17, 18, 20, 28, 30–32]

1.3.6 Bio-functionalization of nerve conduits

Acknowledging the above, PCL seems to be the ideal candidate for the polymeric conduit since it showed promising results in peripheral nerve regeneration. It is a biocompatible polymer possessing adequate mechanical properties and an appropriate degradation rate for this application etc. However PCL, just like other aliphatic polyesters, has a major drawback: the hydrophobicity and low surface energy causing inefficient cell attachment, spreading and proliferation. In fact, cells do not only respond to their environment as a purely topographical environment, but are sensitive to biochemical properties of the

surroundings as well. Cellular response on a material seems to be regulated by the composition of the material surface that dictates the adsorption of a protein layer. A property like surface wettability is as such seen to influence cellular behavior. PCL already passed several requirements such as the adjustable degradation rate and the adequate mechanical properties. Since reactions in the human body are, as opposed to a laboratory setting, occurring at the surface of the material, it would be unfortunate to neglect the properties of PCL. So instead of searching for another material, researchers have tried to modify the surface of PCL to improve the cell affinity. Incorporating specific functional groups on the surface to alter surface properties, but keep the bulk properties intact is called **surface functionalization**. Due to surface functionalization, these electrospun PCL nanofibers can be applied in biomedical applications. Bioactive molecules and cell-recognizable ligands are adsorbed to the functionalized surface facilitating the attachment of cells. Focal adhesions are formed and are important to integrate the ECM with the actin filaments of the cell cytoskeleton. A microenvironment, that is able to contact cells, is created thus enhancing their spreading, proliferation and differentiation. Examples of useful methods to introduce certain functional groups are wet-chemical routes, such as surface hydrolysis and surface aminolysis, peroxide oxidation, ozone oxidation, γ- and UV-radiation. However these techniques cannot be applied to the PCL conduits, since these start to show loss of mechanical properties, a faster degradation process or other undesirable side-effects. [26, 28, 33, 34]
In order to avoid these surface modification methods, some researchers have blended natural polymers, peptides and other bioactive molecules with the polymer solution prior to electrospinning. However a lot of drawbacks are associated with this choice such as the use of very toxic solvents because of the very limited solubility of the natural polymers, the alteration of their biological activity in toxic solvents and the weakening of the electrospun mesh that contains natural polymers. In figure 1.11 some different methods of surface modification are depicted, that could be useful for surface modification of polymers.

To obviate all the disadvantages of the above-mentioned methods and ensure an efficient nerve regeneration process, **plasma treatment** will be used in this dissertation as the surface modification technique. The advantages are numerous. First of all, uniform surface functionalization is possible even for complex shaped biomaterials like nanofibers. Next to that, since plasma treatment is a solvent-free technique, hazardous solvents are not present in the process. Plasma treatment is able to change the surface chemical composition thus leading to alterations in the wetting properties and cell-surface adhesion. More importantly, plasma treatment modifies the surface properties of PCL without altering the desired bulk properties.
A lot of different techniques of delivering plasma treatment exist. The desired outcome can be fine-tuned by changing different parameters such as the plasma source, the background gas, the treatment time and the working gas pressure to have different effects. As mentioned earlier different kinds of cells prefer different fiber conditions. It can therefore also not come as a surprise that different cellular types can have particular optimal wettabilities, which can be influenced by the parameters of the plasma treatment on specific kinds of polymers. The functionalities introduced on the surface are also able to influence specific cellular behaviors differently. Yan D. et al., for example, showed an improved cellular attachment when carboxyl and hydroxyl groups were introduced on the polymer surface. [35] A similar study has shown the difference between untreated and air plasma treated PLLA nanofibers. [36] The functionalities introduced on the nanofiber surface acted as receptor binding sites (figure 1.12). The main goal in this dissertation is to functionalize the fiber surface by a plasma activation process, which enhances cellular adhesion and proliferation. To accomplish this, a dielectric barrier discharge, sustained in argon gas (Ar) is used. [26, 28, 33, 35, 36]
A major downside of using plasma treatment is the partial hydrophobic recovery. After a plasma treatment, there is some recovery of the treated surface to the untreated state because of reactions between ambient air and the incorporated functional groups. In electrospun networks however, there is not a lot of exposure to ambient air because each nanofiber is somehow protected by its neighbors. Another important cause leading to the hydrophobic recovery of nanofibrous surfaces is the rotational and translational motion of polymeric chains or segments. The incorporated chemical groups tend to reorientate towards the bulk of the material as this might be energetically more favorable. A study done by Banik I. et al. suggests that this is the main phenomenon leading to ageing in nanofibrous polymeric meshes. [37–39]
The following section will describe plasma in general and plasma treatment of PCL in particular.

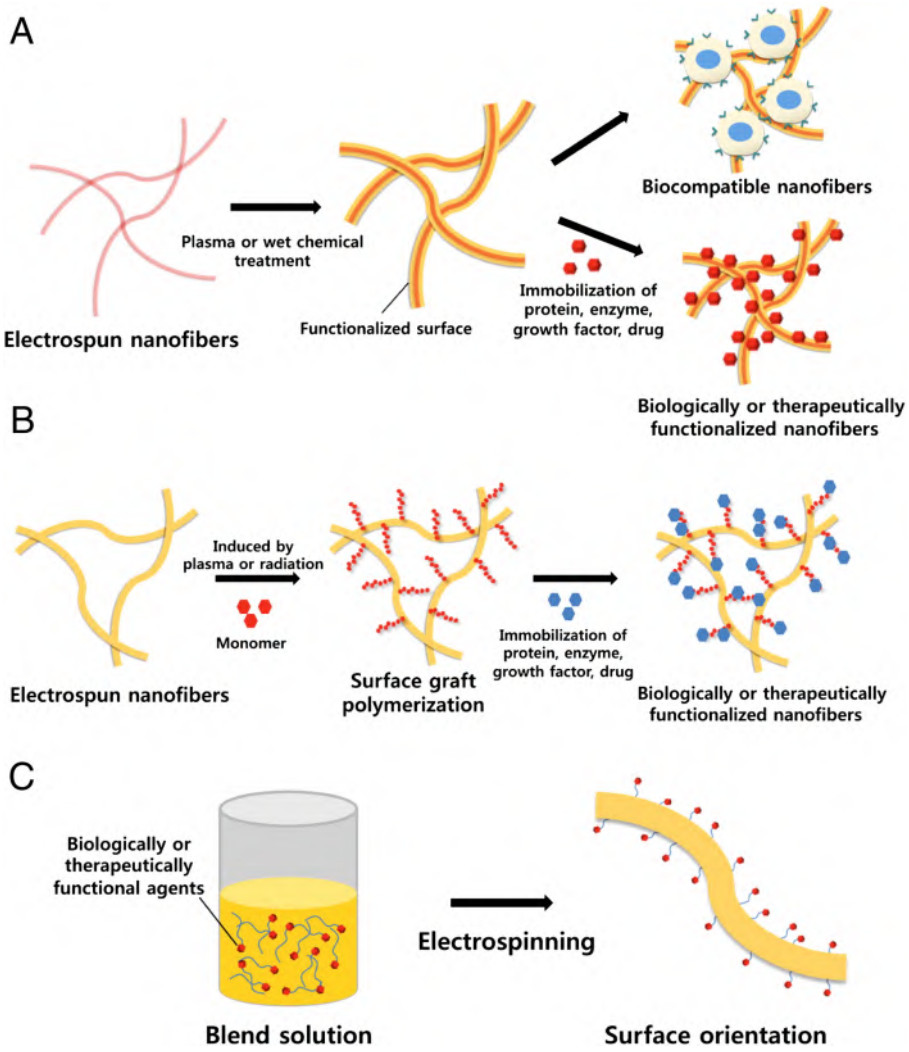

Figure 1.11: Different ways of surface modification for electrospun nanofibers. (A) Plasma treatment or wet chemical method, (B) surface graft polymerization, (C) co-electrospinning. [26]

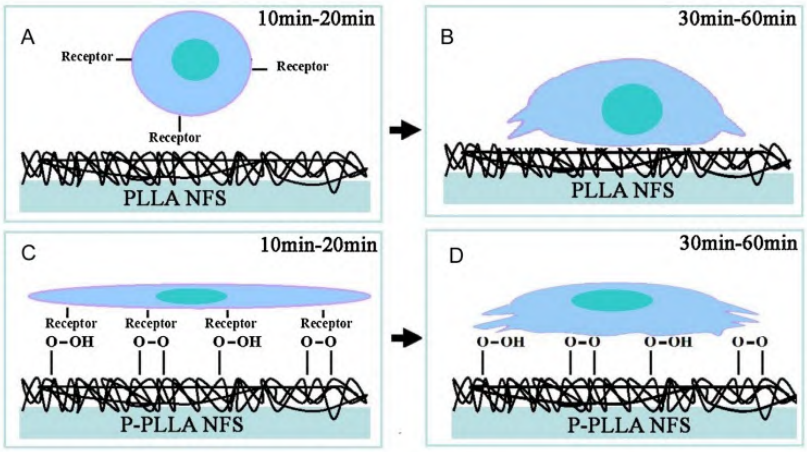

Figure 1.12: Image of cell attachment on an untreated and air plasma treated PLLA nanofiber surface. [36]

1.3.7 Surface modification by the use of plasma

Plasma

Classic physics has taught us the three states of matter: solid, liquid and gas. Solid is the lowest energy state of matter. By adding energy to a solid, it becomes liquid (melting) or immediately gaseous (sublimation). If energy is added to liquid, it becomes gaseous (vaporization). Furthermore it is possible to keep adding energy to a gas, for example by electrical discharge causing electrons to escape their atoms, this is called ionization. The gas is henceforth not only composed out of neutral particles, since it is partially or completely ionized. This implies that the mixture, that is now existing, is susceptible to electrical and magnetic fields. The phenomenon of ions, electrons, neutral particles, radicals... coexisting is called plasma and is seen as the fourth state of matter. The exited particles are able to fall back into their ground state once in a while and photons are emitted. This emission is primarily what gives plasma its glow. At first glance this seems to be quite exotic and something that only exists in laboratory set-ups, but actually 99% of all known matter is thought to be in the plasma state. Famous examples are Aurora Borealis, the sun, lightning but also fire. Not all particles making up the plasma are neutral but both negative and positive charges are almost equally present, thus plasma is known to be quasi-neutral. If this highly energetic plasma comes into contact with solids, the energy can act on the surface and modify properties for instance wettability.
Plasmas are split up into two categories: thermal and nonthermal (cold) plasmas. This division is based on the relative temperature of the existing species. If both heavy particles like ions and the lighter electrons have the same temperature, we talk about thermal plasma. The plasma is in thermodynamic equilibrium and has a temperature around 10^4 K. Thermal plasma is obviously not helpful to use close to PCL, because of its low melting temperature. The polymer conduit would be destroyed by this heat. In the nonthermal plasma, electrons and heavy particles are not in thermodynamic equilibrium. Electrons have very high temperatures ranging from 10^5 to 10^6 K, but the heavier particles remain cold because the collisions with the background gas result in an efficient energy exchange. The overall temperature of nonthermal plasmas is kept under 473 K (200 °C). Due to the low temperature it is possible to apply a non-equilibrium plasma to such a heat sensitive material as PCL.
An important source of these cold plasmas is an electrical gas discharge. A neutral gas is excited by a strong electric field. Ionization takes place and the charged particles are accelerated due to the electrical forces acting on them. The lightest particles are able to gain the most energy, these are the electrons, hence their high temperatures. As mentioned before, due to collisions with the background gas, the heavy ions are prone to more energy exchange and subsequently are kept at a lower temperature. But the very energetic electrons are still traveling in the gas volume. They collide with neutral molecules and free radicals are created. Free radicals in general can be atoms, ions or molecules, but the one thing they have in common is an unpaired valance electron, making them very chemically reactive. The chemical activity that is observed with plasma is mainly because of these radicals. The discharge is more stable and plasma reactions are easier to control at low pressures (10^{-3} - 1000 Pa). Additionally the mean free path is longer at lower pressures, so fewer collisions take place which leads to a smaller amount of chemically active species that return to the ground state.
For this reason it seems adequate to operate at very low pressures, but researchers are searching for a way to extent the region of interest to atmospheric pressure. Keeping the scaling to industrial dimensions in mind, this seems like a fitting solution. The elimination of expensive vacuum devices significantly lowers the cost. But conform to the folk wisdom and engineering rule of thumb of conservation of misery, this will come with some difficulties. A homogeneous surface treatment is harder to obtain, instabilities in the discharge are not uncommon, leading to inhomogeneous plasma. One solution is working in a pulsed regime as seen in the study of Bhoj A. N. and Kushner M. J. [40]. This restricts the discharge maintenance time and the instabilities simply have no time to unravel. A possibly better solution is used in this dissertation. The range between vacuum and atmospheric pressure is wide, this is called the medium pressure range (0.2 kPa to 50 kPa). [41] Comparison between plasma treatment at medium pressure and atmospheric pressure has been performed by De Geyter N. et al. [42], establishing that medium pressure has distinct advantages over atmospheric pressure, while still being cost effective. The pumping equipment to work at medium pressure is economically feasible.
Clearly the high energetic character of plasma is an interesting environment for reactions to occur. Depending on the outcome three processes can be distinguished: plasma polymerization, plasma treatment

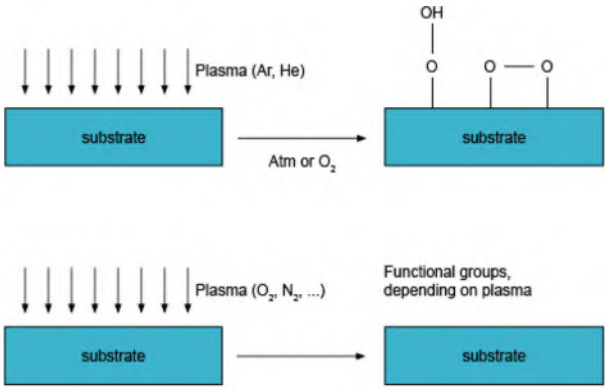

Figure 1.13: Representation of plasma treatment according to plasma gas used. [33]

and plasma etching. Only plasma treatment, so called plasma activation, at medium pressure is of interest to us in this dissertation. [28, 33, 40–43]

Plasma activation

Plasma activation is the surface functionalization technique depicted in figure 1.13. A plasma is sustained in an inert gas, typically Ar, He, O_2, N_2, NH_3 or CF_4. If Ar or He are used, free radicals are created on the surface. The free radicals can be used for cross-linking and surface grafting. While if the plasma is sustained in O_2, N_2, NH_3 or air, the interaction of highly energetic, chemically active species formed by the plasma with the polymer molecules results in the introduction of oxygen- and nitrogen containing functionalities on the surface. These are polar hydrophilic groups which render the surface obviously more hydrophilic. However, the new surface properties are not lasting. The surface tends to recover to the untreated state after the plasma treatment: the ageing effect or hydrophobic recovery. [28, 33]

Effects of plasma treatment on PCL

Different studies have been conducted to examine the effect of a plasma treatment on PCL. A first example is the work of Jacobs T. et al. [41] in 2011. A nonthermal plasma at medium pressure (5.0 kPa) was used to treat the surface of PCL using a dielectric barrier discharge (DBD). Three different background gases were used: dry air, argon and helium. The differences were studied with contact angle measurements and X-ray photoelectron spectroscopy (XPS). The results of the contact angle measurement in function of plasma energy density (in $^{mJ}/_{cm^2}$), which can be related to treatment time, can be found in figure 1.14. A decline in contact angle is clearly visible in all three background gases for increasing treatment times. An explanation for this phenomenon was found in the results of the XPS analysis. Results showed that oxygen content increases, which makes the surface more hydrophilic.
In 2013 Jacobs et al. proceeded with cell culture tests and analysis of plasma treatment on scaffolds. Their conclusions were mostly positive. The cells showed better adhesion and migration on plasma treated samples compared to untreated samples after one week of culturing. Concerning the porous scaffolds it was noted that there was not only an increased oxygen content on the outer surface but also on the interior of the 3D structure. According to the fluorescent microscopy images, improved cell-material interaction was present in the first days of the cell culturing. [44] A lot of other similar studies have been conducted, where a lot of them have been covered in an interesting review paper also by Jacobs et al. The reader is thus referred to [45].

To sum up, the main goal of this dissertation is to compare different fiber conditions and their ability to serve as a valid shell for a polymeric nerve conduit. The effects of changing the electrospinning parameters on PCL fiber diameter and orientation will be studied. Moreover, the influence of medium pressure argon plasma treatment on fiber surface chemistry will be thoroughly investigated using water contact angle (WCA) measurements, XPS and an ageing study.
Six different fiber conditions will be the subject of neural cell tests in order to find the ideal fiber condi-

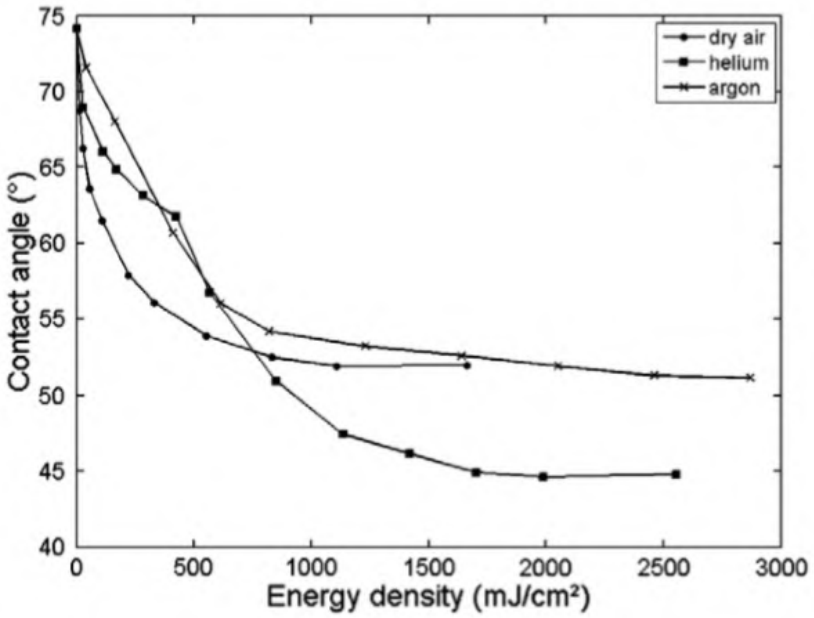

Figure 1.14: Contact angle as function of energy density during plasma treatment in dry air, argon and helium.

[41]

tion for an optimal cell attachment and proliferation. The same will be done on non-treated samples to compare both situations.

Chapter 2

Experimental set-up and analysis techniques - overview

2.1 Electrospinning

Nowadays, a promising biofabrication technique, called electrospinning has the capacity to make a similar structure as the ECM which can enhance cell adhesion, growth and can direct cell migration. This process is able to produce more or less consistent fibers, with a diameter ranging from 2 nanometer to a few micrometers, a desirable porosity and an optimal fiber alignment, out of various natural and synthetic polymers. The technique is being used in a wide variety of applications among which tissue engineering. Electrospinning can be done at room temperature in ambient conditions. A possible set-up is illustrated in figure 2.1. It consists of a syringe with a needle, connected to an injection pump, a high voltage power supply and a collector. A polymer solution or melt is introduced into the syringe and a small droplet, maintained by the surface tension, forms at the needle. A high voltage is then applied between the needle and the collector. When the electrical field reaches a critical value, the repulsive electrical forces overcome the surface tension, leading to the formation of a Taylor cone. A jet of the polymer solution is fired out of the Taylor cone towards the collector. In the space between the needle and the collector, the solvent evaporates or the melt cools down, leaving behind thin fibers of the polymer. In this dissertation a cylindrical collector, rotating at a certain speed, is used. The set-up is depicted in figure 2.2. On the cylindrical collector a sheet of aluminum foil is attached and small circular glass plates, known as coverslips, with a diameter of 12 mm, are taped to this sheet. The fibers are collected on these coverslips which are easy to examine and treat.
In this set-up it is possible to change a lot of parameters, in this way we can search for e.g. the desired fiber diameter. These parameters can be split into 3 categories. First, the **solution parameters** such as the concentration of the solution, the viscosity and the molecular weight. Secondly it is possible to change things like the applied voltage, the distance between the tip and the collector, the rotating speed in case of a rotating collector or the polymer feeding rate in the syringe. These are called **process parameters**. At last we have **ambient parameters**, such as humidity of the air, temperature etc. These parameters can influence the quality of the fibers, the diameter of the fibers and the alignment of the fibers. [46]

2.1.1 Electrospinning of PCL fibers

The tools for the polymeric conduits so far are PCL and electrospinning, but the question remains: "Do they go hand in hand?" Researchers have tried to answer this question extensively the last couple of years. The process all begins with a solution: the solute is obviously PCL, but what about the solvent(s). Chloroform was widely used as a solvent, but it creates fibers in the microscale range rather than nanofibers. Other researchers have tried relatively highly toxic solvents, such as trifluoroethanol, dichloromethane and hexafluoropropanol which were able to produce bead-free PCL nanofibers. [24, 48, 49] Unfortunately these processes lacked reproducibility and do therefore not lead to a significant breakthrough. The search for adequate and non-toxic solvents led Van Der Schueren et al. to try the binary solvent system, formic acid and acetic acid, for the first time. It showed good solubility, good

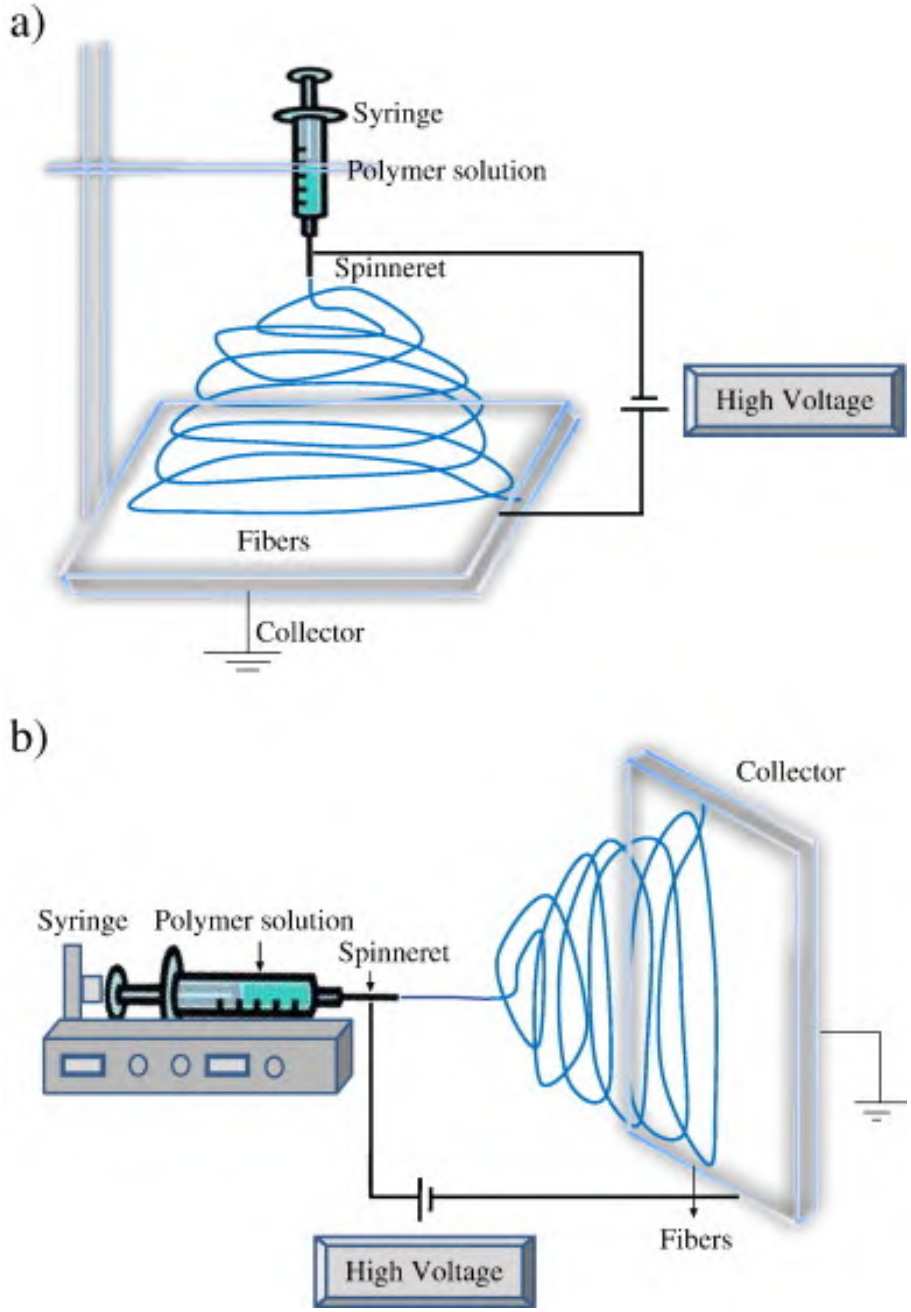

Figure 2.1: Set-up of electrospinning, (a) vertical and (b) horizontal. [46]

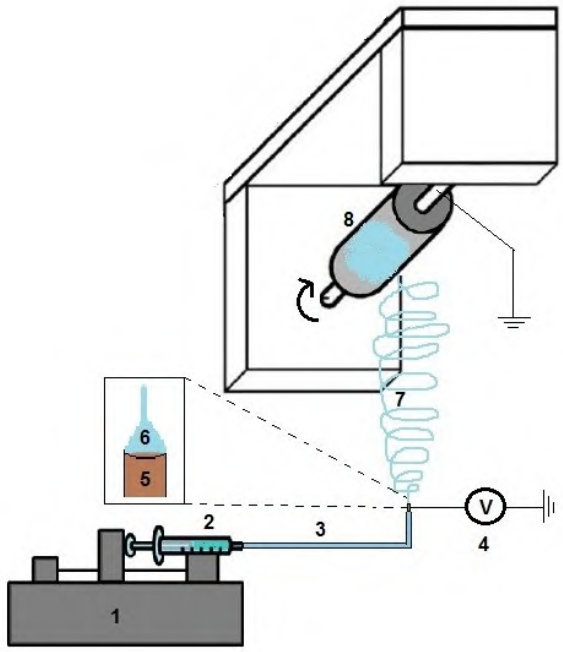

Figure 2.2: Set-up of electrospinning with cylindrical collector, (1) syringe pump, (2) syringe containing the polymer solution, (3) capillary tube, (4) high voltage power supply, (5) copper tip, (6) Taylor cone, (7) polymer jet, (8) cylindrical collector.
[47]

electrospinnablility and was able to produce nanoscale bead-free fibers. Furthermore they also showed that the average diameter decreased with decreasing polymer concentration and the diameter distribution decreased with increasing the amount of formic acid. [50]
In the former section, other parameters of the electrospinning process were given. Research has shown trends in the morphology of the nanofibers when altering separate parameters. Kanani et al. [51] reported that the diameter increases with increasing voltage, but not significantly. The work of Ghobeira R. [47] further examined the effect of altering other parameters on the fiber diameter and alignment. Since a rotating cylindrical collector is used, a first important parameter is the rotational speed that dictates the fiber alignment between randomly oriented and aligned fibers. A rotational speed of 100 rotations per minute (rpm) is used for randomly oriented fibers, while for aligned fibers 3000 rpm seems to do the trick. Another possible modification of the process is the distance from the collector to the tip. As this distance decreases, the diameter increases. A usually overlooked ambient parameter that showed an important influence on the fiber morphology, is the relative humidity. In fact, an increase in humidity exhibited an increase in fiber diameter as well.

2.2 Dielectric barrier discharge

A common way to create a nonthermal plasma at low or sub-atmospheric pressure is, as mentioned earlier, a dielectric barrier discharge (DBD). An electrical discharge is sustained between two electrodes (comparable to a capacitor) with an insulating material in between, called the dielectric barrier. This dielectric material can be glass, quartz, a ceramic, enamel, mica, plastics, silicon rubber or teflon. Typically the discharge gap is 0.1 - 10 mm. As with a capacitor, alternating or pulsed high voltage in the range V_{rms} = 1 - 100 kV is required. The most typical configuration for a volume DBD uses planar and parallel electrodes as in figure 2.3. Another common way uses circular coaxial electrodes. For specialized applications, a kaleidoscope of other set-ups has been developed which can be found in advanced literature concerning DBD. [52] The set-up used in this dissertation can be found in figure 2.4.

Table 2.1: Characteristic microdischarge properties.

Quantity	Value	Quantity	Value
Duration	1-10 ns	Total Charge	0.1 - 1 nC
Filament Radius	about 0.1 mm	Electron Density	$10^{14} - 10^{15}\ cm^{-3}$
Peak Current	0.1 A	Electron Energy	1-10 eV
Current Density	100 - 1000 $^{A}/_{cm^2}$	Gas Temperature	Close to average gap temperature

[53]

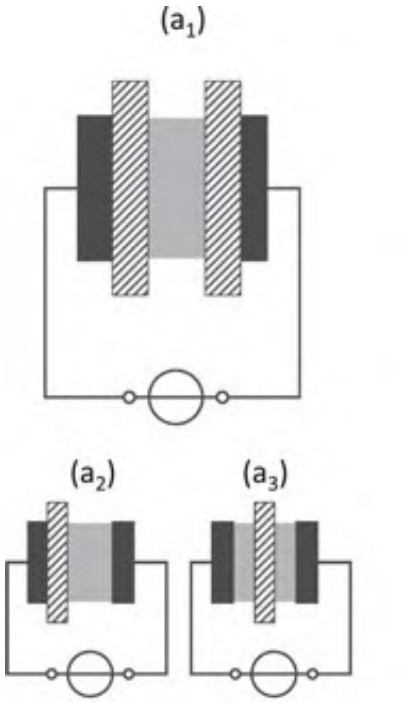

Figure 2.3: Basic planar configuration of volume DBDs: (a_1) symmetric, (a_2) asymmetric, (a_3) floated dielectric. The dark regions indicate the electrodes, the light region is the plasma region and the shaded area is the dielectric barrier.

[52]

The high electrical field is present between the electrodes, but when it exceeds the breakdown voltage, dielectric breakdown occurs. This can be in the form of streamer discharge or filamentary discharge and only happens in small channels. Due to the high applied voltage, accelerated electrons collide with the gas molecules. The energy exchange can be large enough for another electron to escape the molecule, ionizing the molecule left behind. These new free electrons can again do the same and a chain reaction occurs. The space charge and additional electric field, created by the electron avalanche, leads to local secondary electron avalanches. Distinct plasma channels, working independently, start to exist. These channels are very short and are called microdischarge filaments that are in a way comparable to transient high pressure glow discharges in a small channel of weakly ionized plasma. Some properties are listed in table 2.1. [53]
But eventually the dielectric breakdown leads to charging of the surfaces of the insulator. The total electric field is decreased because of the opposing newly induced electric field and the discharge extincts. The dielectric acts as a resistor and the amount of charge and current density is limited. Because of this phenomenon, the plasma is kept in a nonthermal state. Despite the distinct microdischarge filaments, studies have shown that a surface is treated uniformly at micron scale. [42,52–55]

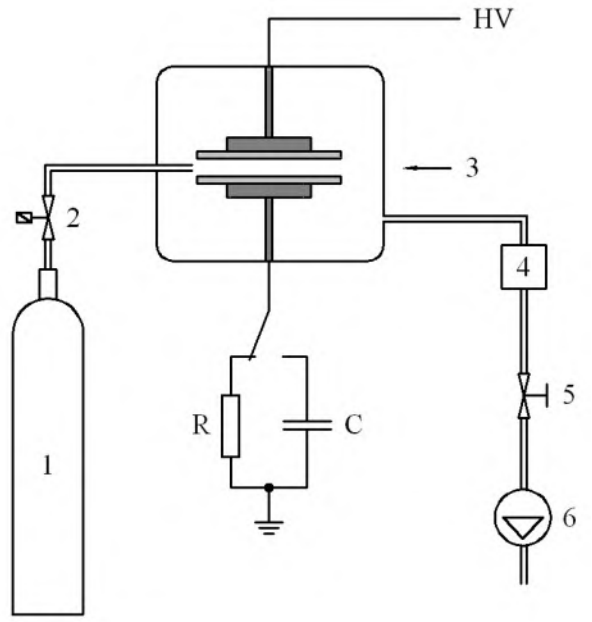

Figure 2.4: Experimental set-up of the DBD discharge, (1) gas cylinder, (2) mass-flow controller, (3) plasma chamber, (4) pressure gauge, (5) needle valve, (6) pump.
[42]

2.3 UV sterilization

After the entire treatment a last important need has to be fulfilled. Inside the body, living organisms such as bacteria, yeasts and viruses, present on the biodegradable scaffold, can cause unwanted infections. The process of killing these unwanted contaminations is called sterilization. It is of utmost importance that the used sterilization method ensures that the properties of the plasma-treated PCL nanofibrous conduit are kept the way they were. This is to make sure that the scaffolds will fulfill their intended purposes post-sterilization. [56] Ethylene oxide (EtO) and γ irradiation are common techniques, but other techniques, such as autoclave and heat treatment, exist as well. However, because of the PCL low melting temperature, methods involving higher temperatures melt PCL fibers leading to a complete deterioration of the topographical strucutre. Moreover irradiation methods lead to ionizing reactions in PCL chains causing alteration in crystallinity and molecular weight thus severly damaging surface and bulk properties. Therefore UV sterilization can serve as an alternative. It is fast, cheap, does not need too high temperatures and leaves no toxic residues. Only under long exposure duration, alterations of the structural properties are noticed. [56].
UV irradiation results in excitation of electrons and accumulation of photoproducts. This causes damage to DNA molecules and prevents DNA replication, leading to inactivation of microorganisms. [57] The UV range is rather broad with a wavelength range of 10 - 400 nm. Research has found that at 254 nm the UV absorbance is highest, leading to the most efficient way of inactivating and killing microorganisms. Ghobeira et al. conducted two studies where plasma-treated PCL fibers and films were sterilized using the following 3 different methods: UV (254 nm), ethylene oxide and H_2O_2 plasma sterilization. The results showed that an exposure of 3 hours to UV did not cause any morphological damage to the samples, in contrast to what was observed with the H_2O_2 plasma sterilization. Moreover UV sterilization did not alter the plasma chemistry induced at the sample surface that was altered when using ethylene oxide. The cytocompatibility was not affected by UV sterilization as well. [58,59] Therefore, in this dissertation, the samples will be exposed to 3 hours of UV (254 nm) for sterilization prior to the in-vitro cell tests. [60]

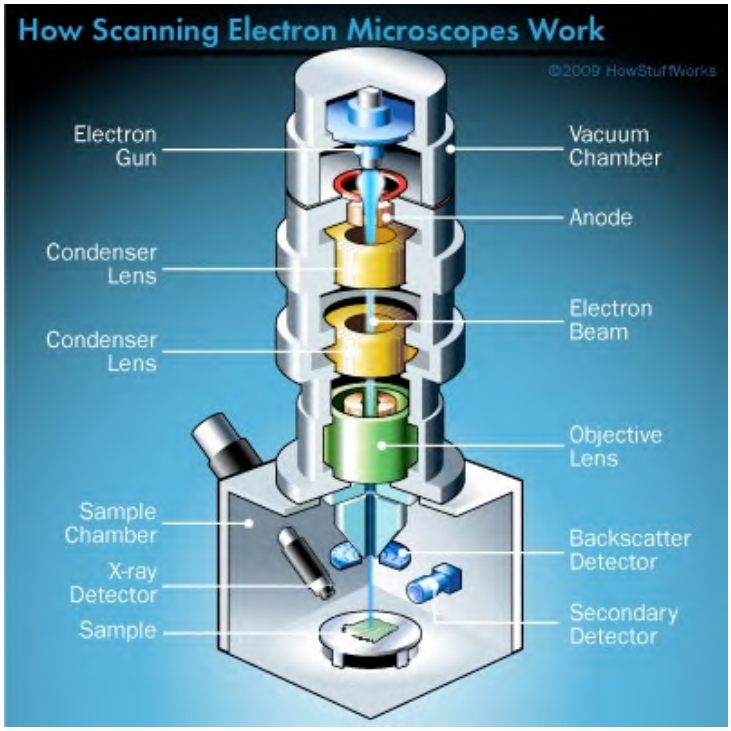

Figure 2.5: Components of a scanning electron microscope. [61]

2.4 Analysis techniques

2.4.1 SEM

Scanning electron microscopy (SEM) is used, among other analysis techniques, to visualize the surface morphology of a sample. The inside of a SEM can be found in figure 2.5. An electron gun producing electrons is the first component present in the SEM chamber. A positively charged anode, found underneath the electron gun, attracts the negatively charged particles. A hole is present in the middle of the circular anode to force the electrons into a beam right through the center of the anode. Similarly to light microscopy, lenses are needed to focus the beam on a specimen. Instead of glass lenses, magnetic lenses are used in this case, since the charged electrons are influenced by a magnetic field. The lenses work together to focus the electron beam on the correct spot of the sample. The sample is mounted into the sample chamber that ensures that it stays very still. Changing the angle of the sample or moving it inside the chamber is possible.
When the electron beam hits the specimen, a number of interesting phenomena occur e.g. the backscattering of electrons (high energy electrons due to elastic scattering), production of characteristic X-rays and Auger electrons etc. For the surface topography we are only interested in the production of secondary electrons. Once the primary electrons hit the atoms in the sample, they are scattered inelastically and cause secondary electrons to escape from the inner shells. These electrons have low energy, so only the electrons from the top layers manage to escape the sample and are thus detected by an Everhart-Thornley detector. The detector uses the information to form an image onto a computer screen. The beam scans the sample to get information about its complete surface. A resolution of less than 0.5 nm is possible. Another important feature is the use of a vacuum pump to eliminate the influence of the particles in the air on the beam and the sample. For nonconducting samples a charge build-up might occur. In order to solve this issue, the sample is sputter coated with a very thin layer of conducting material e.g. gold on its top surface. [62–64]

2.4.2 Contact angle measurements

Water contact angle (WCA) measurement is an analysis technique used to measure the wettability of a solid surface. It is an easy and straightforward technique. A droplet of distilled water or another liquid is brought into contact with a solid surface. The interaction of the solid, liquid and vapor molecules will result in the formation of a small spherical droplet. The angle between the solid-liquid interface and the tangent of the liquid-vapor interface in the point where all three phases meet is measured. In figure 2.6 the contact angle is denoted by θ. The interactions between the distinct phases are denoted as γ_{SL}, γ_{LV} and γ_{SV}.

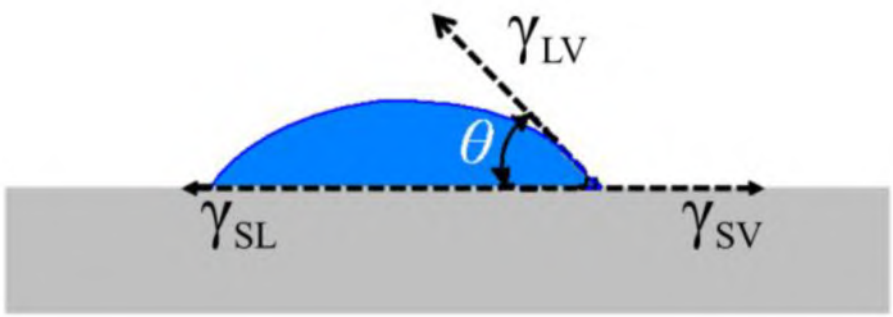

Figure 2.6: Contact angle.
[65]

The shape of the droplet can be explained on a molecular level. Take a look at figure 2.7. Imagine a water molecule in the bulk of the droplet. In every direction the molecule experiences the same pull, giving zero net force. This is not the case anymore on the surface of the droplet where the molecules are pulled inward. The liquid contracts to a state with lowest energy and the tension that arises is called surface tension. The contact angle is the result of the interaction of the tensions at the three different interfaces, where thermodynamic equilibrium is the goal.

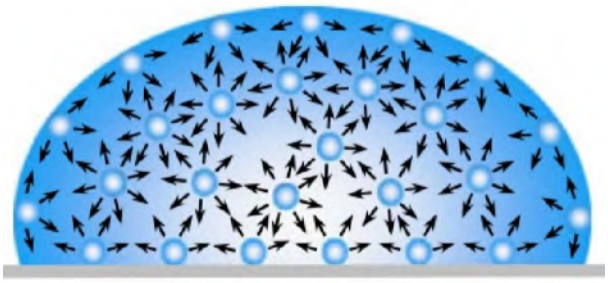

Figure 2.7: Molecular forces at work in a droplet of water.
[66]

We make a distinction at a 90° angle. If the contact angle is smaller than 90° then we call the solid surface hydrophilic, so it is characterized by high wettability. If the angle bigger than 90°, we talk about a hydrophobic surface, so low wettability. Visually it is clear that a low wettability results in the formation of a nice, firm droplet while high wettability will spread out this droplet. [65, 66]

2.4.3 XPS

X-ray photoelectron spectroscopy is used to detect the chemical composition of the surface layers. The main physical phenomenon here is the photoelectric effect. Electromagnetic radiation is absorbed by an atom and an electron of the inner shell will be ejected. The energy $h\nu$ of the electromagnetic ray is known, since it is to be equal to the kinetic energy of the emitted electron E_{kin} plus the atom binding

energy E_b and the work function W_f, which is the energy needed for the electron to escape the sample into the vacuum immediately outside of the solid. The equation is visualized in figure 2.8.

$$h\nu = E_{kin} + E_b + W_f \tag{2.1}$$

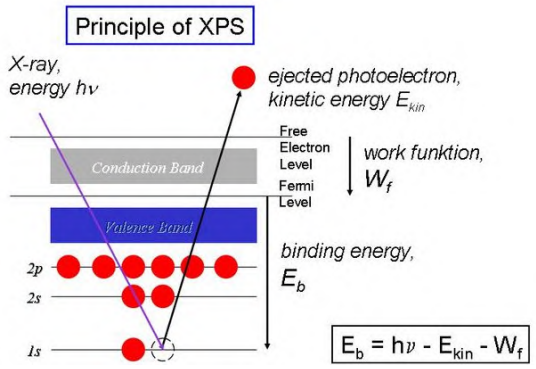

Figure 2.8: Energy diagram of photoelectric effect in XPS.
[67]

A typical XPS set-up is shown in figure 2.9. The electromagnetic radiation used is a monoenergetic X-ray beam. Ultra-high vacuum (UHV) is needed to have a long mean free path of the photoelectrons leaving the sample, not to collide with other molecules on their way to the hemispherical electron analyzer. This device spreads the electrons according to their kinetic energy. It is comparable to a prism in which light is dispersed according to its wavelength. At the other side of the analyser, the electrons are collected by an electron multiplier. One electron can trigger an avalanche of electrons by means of secondary emission on successive dynodes. The energy spectrum can tell us which elements and in what concentration they are present on the surface layer of the sample. [67–69]

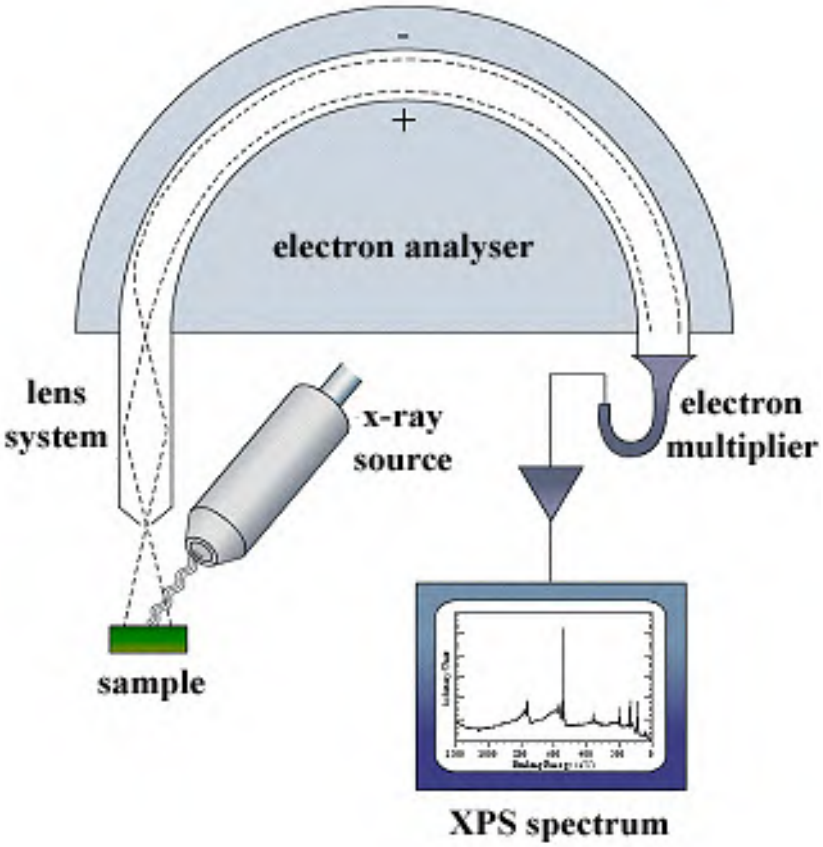

Figure 2.9: Typical set-up of an X-ray photoelectron spectrometer.
[70]

Chapter 3

Results and discussion

3.1 Electrospinning of the PCL fibers

In order for PCL fibers to be electrospun, the polymer granules needed to be dissolved into appropriate solvents to get a polymer solution with a specific concentration. The solvent system used was a mixture of formic acid and acetic acid with a ratio of 9:1. In these experiments 25 ml of solution was made, with 22.5 ml formic acid and 2.5 ml of acetic acid. A certain mass of PCL was added to get a desired concentration using the following equation:

$$c = \frac{m_{PCL}}{V_{sol}} \tag{3.1}$$

With c the weight concentration of PCL in $^{g}/_{ml}$, m_{PCL}, the mass of PCL in g and V_{sol} the volume of the solution, in this case 25 ml. The resulting mass of PCL used to obtain different concentrations can be found in table 3.1.
As in subsection 2.1.1 different conditions of the fibers are the result of altering the electrospinning parameters. These are subdivided into fixed parameters (see table 3.2) and parameters that can be changed. Temperature is one of the fixed parameters since it cannot be changed in the electrospinning chamber. However, as it couldn't be controlled as well, it was not stable at all times, but it depended on the weather conditions. Therefore, in order to minimize the variations in fiber quality caused by fluctuations in temperature, electrospinning was only done at temperatures between 20 and 24 °C. Several other process-related, solution-related and environmental parameters affecting the fiber quality, diameter and alignment can be varied. The most influential parameters were the polymer concentration, the collector-to-tip distance (CTD), relative humidity (RH) and the rotating speed of the collector. Therefore, their effect will be studied thoroughly, since they affect the morphology of the fibers to a greater extent.

To obtain different fiber alignment, the only thing that needed to be adjusted was the rotating speed of the mandrel. For random fibers, the collector rotated at 100 rpm and for aligned fibers the collector rotated at 3000 rpm. This is clear in figures 3.1a and 3.1b. The polymer concentration, CTD and RH were the same, but the rotating speed was different, resulting in a different alignment. This is due to the mechanical force implemented by the high rotational speed that leads to the stretching of the fibers and thus to their aligned deposition.
Intuitively, the mechanical stretching caused by the high rotational speed exhibits a thinning of the fibers,

Table 3.1: Different concentrations and corresponding mass of PCL dissolved in solution.

c $[^{g}/_{ml}]$	$m_{PCL}[g]$
0.2	5
0.24	6
0.28	7
0.32	8

Table 3.2: Fixed parameters of the electrospinning process.

V	Feeding rate	Temperature
32 kV	0.5 - 0.7 $^{ml}/_{hour}$	20 - 24 °C

Table 3.3: Effect of the rotating speed on the fiber diameter.

Concentration (wt%)	CTD (cm)	rotational speed (rpm)	RH (%)	diameter (nm)
20	15	**100**	± 50	202 ± 29
20	15	**3000**	± 50	238 ± 81
32	20	**100**	± 50	1280 ± 395
32	20	**3000**	± 50	1091 ± 463

this was however not the case since aligned fibers had bigger diameters than the random fibers. A possible explanation for this is the fact that the high rotational speed led to augmented solvent evaporation and the fibers dried in an earlier stage of jet stretching and travelling. This compensated for the mechanical forces exerted by the rapidly rotating mandrel. The effect was not visible at the highest concentration, being 32 wt%, because the solidification happens so fast, only the mechanical stretching was of importance. These predictions are evidenced in table 3.3 and figure 3.1. [47]
This leaves us with the concentration, the CTD and the RH. These parameters were the main influences of the fiber diameter. For the concentration 20 wt%, 24 wt%, 28 wt% and 32 wt% were used and for the CTD 20 cm, 17.5 cm, 15 cm and 10 cm were used. These conditions were carefully investigated together to find fibers with a more or less fixed diameter. The RH also had a minor effect on the fiber morphology. As with temperature, this was also depending on the weather conditions. Two situations were investigated: low RH (± 20%) and high RH (± 50%). The higher humidity was accomplished by putting hot water in the electrospinning machine as a humidifier. After spinning the software ImageJ was used to measure 50 fiber diameters per sample and determine the mean diameter and standard deviation. Some conditions led to an appropriate fiber diameter to continue the study. SEM images (at 1000x magnification) of the fiber conditions can be found in figure 3.1. Since electrospinning is not such a reproducible process and depends on a lot of ambient conditions, in every batch (± 20 samples that were electrospun at the same time) one samples had to be tested to see if the mean fiber diameter was acceptable to continue with.

The parameters of the electrospinning for all fiber conditions can be found in tables 3.2, 3.7 and 3.8. It should be noted that other combinations of parameters could also lead to an appropriate fiber diameter, but the ones listed in the tables were most likely to turn out good.

By taking a quick look at the electrospinning parameters and the SEM images in figure 3.1 some trends are visible. Starting with the concentration of the solution, it is clear that if the concentration was higher, the fiber diameter was bigger. This can be attributed the amount of entanglements between the molecular chains at a higher concentration. In the applied electric field, there is more resistance against the jet stretching, which obviously leads to larger diameters. A higher concentration leads to a higher viscosity influencing the coulumbic repulsion and electrostatic forces that have a smaller influence on the jet stretching compared to less viscous solutions, because of bigger viscoelastic forces. A third consequence of a higher concentration is the rapid jet solidification. The time for stretching, due to the voltage difference, is thus smaller, again leading to bigger diameters. These predictions are evidenced in table 3.4. [47]

The CTD influenced the fiber morphology as well. First of all, decreasing the CTD caused an increase in fiber diameter, which can be explained by phenomena occurring in the larger traversing distance. After a straight jet is fired from the nozzle towards the mandrel. it becomes prone, during its path, to bending instabilities and whipping motion (the spiralling as can be seen in figures 2.1 and 2.2), that elongates the fibers. A bigger CTD was however desirable over a small CTD because of the risk of incomplete evaporation of the solvent. If the drying is not complete, a decrease in fiber diameter uniformity is seen. These predictions are evidenced in table 3.5. [47]

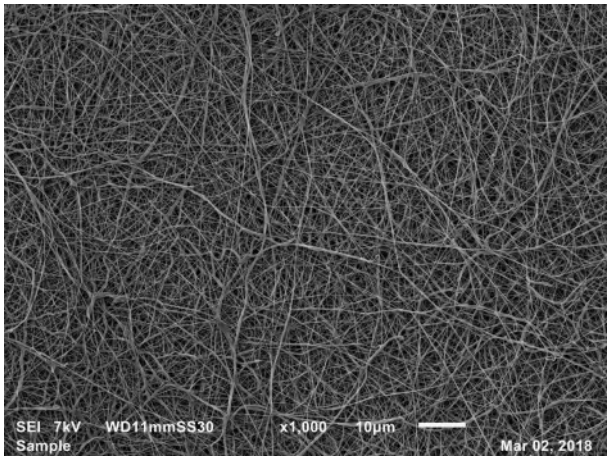

(a) R1: 202 ± 29 nm

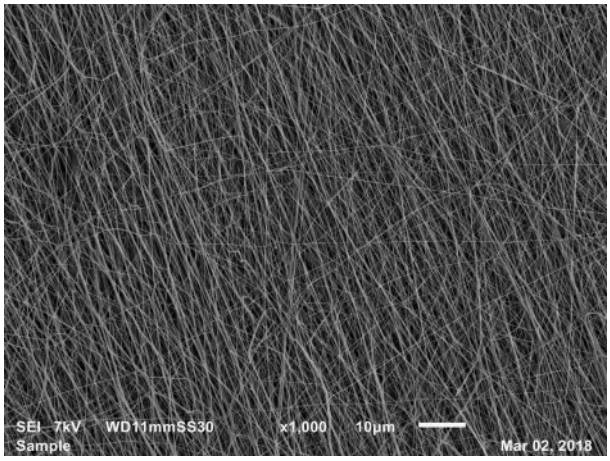

(b) A1: 238 ± 81 nm

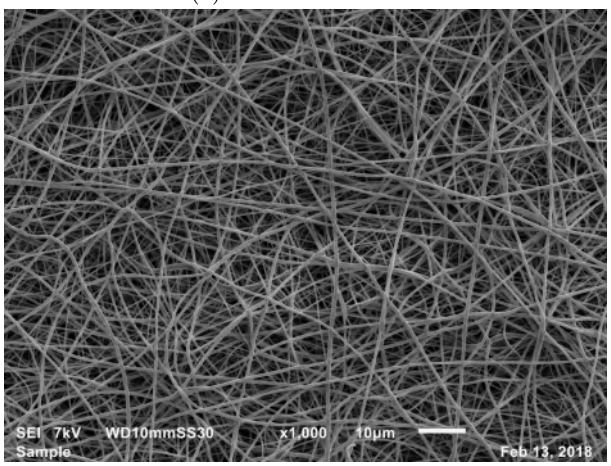

(c) R2: 420 ± 114 nm

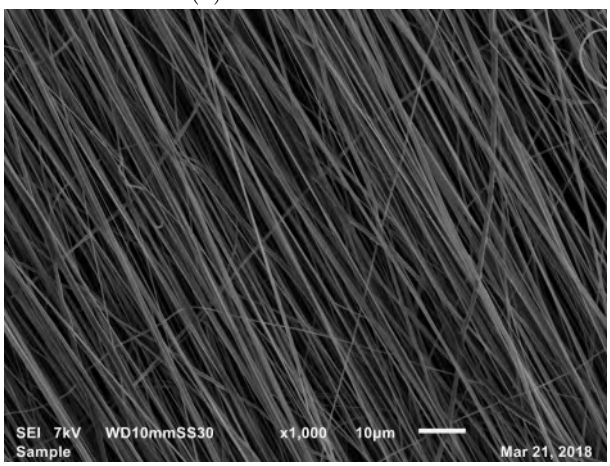

(d) A2: 573 ± 240 nm

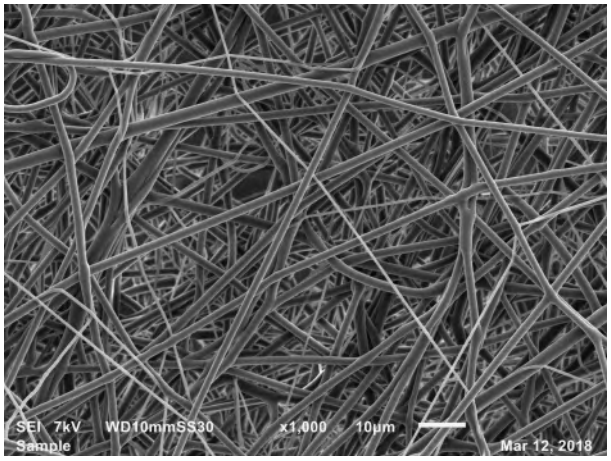

(e) R3: 1280 ± 395 nm

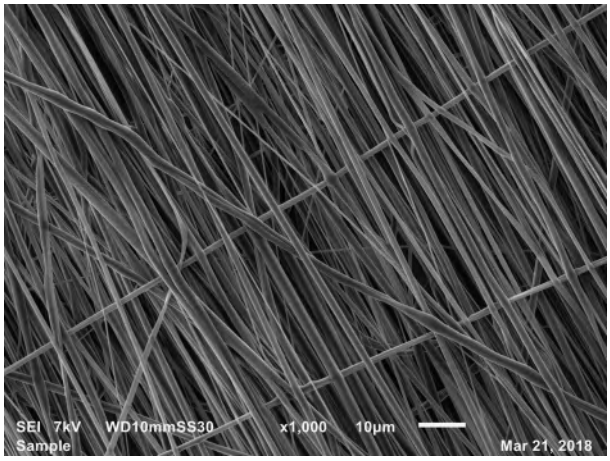

(f) A3: 1091 ± 463 nm

Figure 3.1: SEM images (magnification 1000) of the different fiber conditions. (a) randomly oriented fibers with small diameter, (b) aligned fibers with small diameter, (c) randomly oriented fibers with intermediate diameter, (d) aligned fibers with intermediate diameter, (e) randomly oriented fibers with large diameter, (f) aligned fibers with large diameter. The mean diameter and standard deviation of the samples can be found underneath every SEM image.

Table 3.4: Effect of the polymer concentration on the fiber diameter.

Concentration (wt%)	CTD (cm)	rotational speed (rpm)	RH (%)	diameter (nm)
20	15	100	± 50	202 ± 29
24	15	100	± 50	359 ± 60
32	15	100	± 50	1564 ± 585
20	15	3000	± 50	238 ± 81
24	15	3000	± 50	346 ± 159
32	15	3000	± 50	1638 ± 589

Table 3.5: Effect of the CTD on the fiber diameter and diameter uniformity.

Concentration (wt%)	CTD (cm)	rotational speed (rpm)	RH (%)	diameter (nm)
24	**10**	100	± 50	696 ± 278
24	**15**	100	± 50	420 ± 114
32	**10**	3000	± 50	2504 ± 1093
32	**15**	3000	± 50	1638 ± 589
32	**20**	3000	± 50	1091 ± 463

A minor influence of the RH on the fiber diameter was also seen. In literature this ambient parameter is overlooked, but its effect is not to be underestimated. A higher RH led to a larger fiber diameter. This can be explained by looking at two effects of the increased presence of water vapor in the electrospinning chamber. Firstly, more water molecules will be absorbed by the jet. The solution turns into a solid, which is called precipitation, faster, since PCL is less soluble in water than in the original solvent. After solidification, elongation is stopped and the fibers have a larger diameter. Secondly, the larger amount of water molecules in the chamber leads to induced molecular polarization, resulting in a drop of the excess charge on the polymer jet, reducing the intensity of the electrical field. The drawdown force on the jet is weaker, resulting in limited elongation and thus larger fiber diameter. These predictions are evidenced in table 3.6. [47, 71, 72]

In the following experiments, aligned and random fibers with small, intermediate and large fiber diameters will be used. The different used parameters are summarized in table 3.7 and 3.8.
For simplicity the fiber conditions will be abbreviated from now on: R1, R2 and R3 stand for randomly oriented fibers with small, intermediate and large diameter respectively. A1, A2 and A3 stand for aligned fibers with small, intermediate and large diameter respectively.

3.2 Analysis of plasma treatment

3.2.1 Electrical characterization of the DBD discharge

The voltage applied to the electrodes and the resultant current of the discharge were measured to observe the electrical characterization of the DBD. The voltage and current waveforms in argon are given in figure 3.2. A sinusoidal voltage was applied, the current waveform was periodic as well and had one distinct discharge pulse peak linked with each positive and negative voltage half cycle. The DBD was therefore operating in glow mode. The plasma is diffuse and not existing in distinct microdischarges. This led to treatment uniformity. A homogeneous treatment is beneficial for the application in mind. The applied discharge power at medium pressure was 1.4 W. [73, 74]

Table 3.6: Effect of the relative humidity on the fiber diameter.

Concentration (wt%)	CTD (cm)	rotational speed (rpm)	RH (%)	diameter (nm)
24	15	100	± **20**	359 ± 60
24	15	100	± **50**	420 ± 114

Table 3.7: Electrospinning parameters for the randomly oriented fibers R1, R2 and R3 (rotational speed: 100rpm).

Diameter (nm)	Concentration (wt%)	CTD (cm)	RH (%)
202 ± 29	20	15	± 50
420 ± 114	24	15	± 50
1280 ± 395	32	20	± 50

Table 3.8: Electrospinning parameters for the aligned fibers A1, A2 and A3. (rotational speed: 3000rpm).

Diameter (nm)	Concentration (wt%)	CTD (cm)	RH
238 ± 81	20	15	± 50
573 ± 240	24	10	± 50
1091 ± 463	32	20	± 50

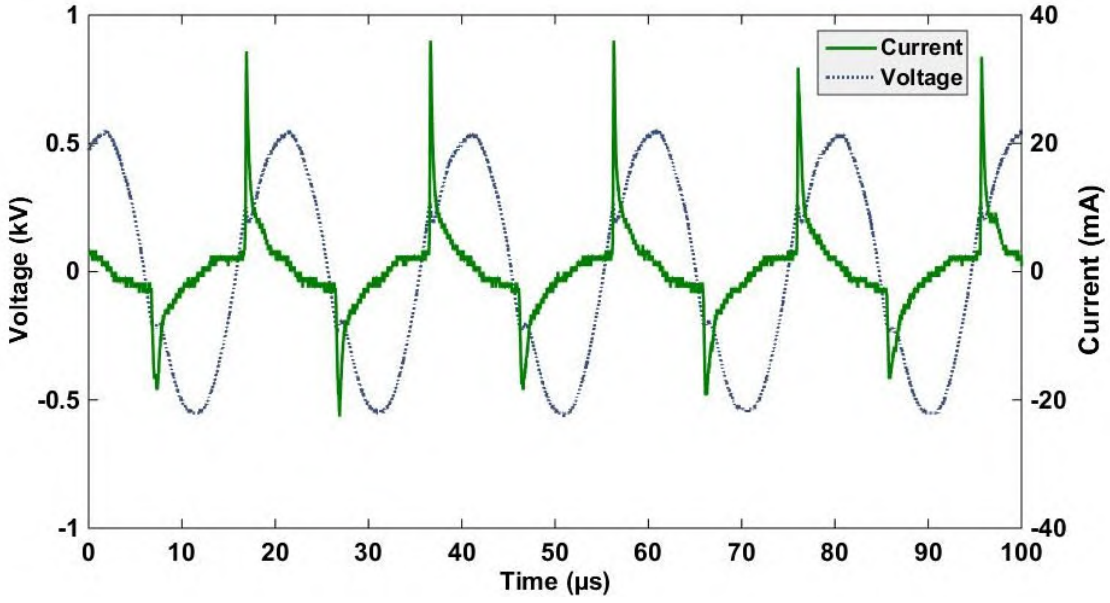

Figure 3.2: Voltage and current waveforms of the DBD sustained in argon.

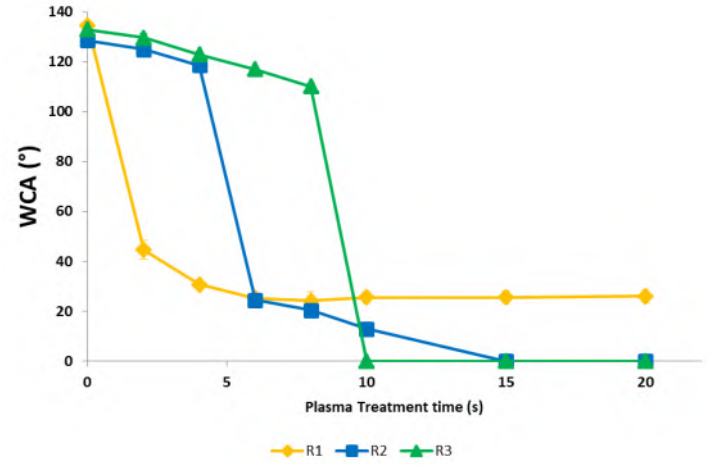

(a) Random fibers

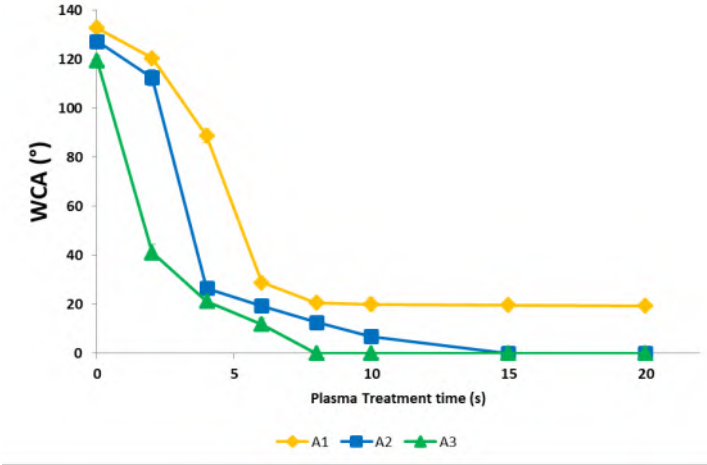

(b) Aligned fibers

Figure 3.3: WCA (°) vs plasma treatment time (s) for (a) random fibers and (b) aligned fibers.

3.2.2 Water contact angle

Figure 3.3 and table 3.9 shows the evolution of the WCA for argon plasma treatment on all fiber conditions. In the untreated state all samples have a WCA around 130°, thus very hydrophobic. The WCA on untreated PCL films is 74° however. [59] This indicates that the nanofibrous structure leads to a decrease in wettability. The porous structure is full of inter-fiber spaces able to entrap air, which in turn hinders the water drops to penetrate into the structure. [75] The different WCAs on the untreated samples for the different fiber conditions, further illustrates the dependency of the wettability on the surface morphology. The thin fibers have a higher WCA compared to the thick fibers. The diameter of the fibers is a major influence on the porosity and the roughness of the electrospun mesh, which in turn influence the spreading of a water drop. A larger fiber diameter is related to higher roughness. Two phenomena lead to thermodynamic equilibrium of the shape of the water drop. Homogeneous wetting is the penetration of water into the roughness grooves, leading to a decrease in WCA. This is described by the Wenzel equation. Heterogeneous wetting is the entrapment of air bubbles into the roughness

Table 3.9: WCA of the untreated and argon plasma-treated samples with a treatment time of 15s.

	R1	R2	R3	A1	A2	A3
WCA (°) Untreated	134.6 ± 2.1	128.6 ± 2.9	132.9 ± 2.4	132.7 ± 2.1	127.2 ± 1.1	119.3 ± 1.9
WCA (°) after 15s treatment time	25.6 ± 2.5	0	0	19.6 ± 0.4	0	0

Table 3.10: Surface oxygen content on untreated samples and plasma-treated after saturation for the different fiber conditions.

	R1	R2	R3	A1	A2	A3
Initial % oxygen	24.17	24.45	24.36	24.40	24.20	24.61
% oxygen after saturation	30.35	30.16	30.92	30.21	30.04	30.49

grooves, so water cannot penetrate it anymore, leading to an increase in WCA. This is described by the Cassie-Baxter equation. Competition between homogeneous and heterogeneous wetting, leading to a minimization of Gibbs energy of the system, determines the resulting contact angle on a rough surface. [76] Additionally as the fiber diameter increases, the porosity also increases, leading to more entrapment of air bubbles and increasing the WCA. [77] All these effects influence the WCA, either decreasing or increasing it. This explains the small differences in WCA. Since the WCA is decreasing with increasing fiber diameter, the homogeneous wetting should be the main actor of the system. The WCA on the aligned fibers is smaller than on the randomly oriented fibers, because of the decrease in porosity. [47]
The effect of the plasma treatment is very pronounced. After a few seconds of treatment a very steep drop in WCA is measured. The higher wettability suggests that hydrophilic groups are introduced on the surface of the fibers. The oxygen content will thoroughly be examined with XPS analysis (figure 3.4). The evolution of the WCA has close links with the differences in oxygen incorporation of the distinct fiber diameter and alignment. A closer look at figure 3.3a shows a faster decrease for smaller fiber diameters (R1: sudden decrease from 134.6° to 44.7° at 2s; R2: sudden decrease from 118.6° to 24.5° at 6s; R3: sudden decrease from 110.1° to 0° at 10s). A possible explanation is found in the surface-to-volume ratio and porosity, since the former is higher for the small fibers, a higher surface area is treated, in a shorter treatment time. The water is able to penetrate the mesh 'earlier' (shorter treatment time). The latter increases for increasing diameter, and, as in the untreated case, there is more air entrapment. The air entrapment (WCA↗) and the oxygen containing functionalities (WCA↘) counteract. Larger fibers have more air entrapment and less treated surface area, so it is harder for the water to penetrate the mesh. But after 10s of treatment time, enough oxygen containing functionalities are introduced to overcome the effect of air entrapment. Now the bigger pore size enables the water drop to fully penetrate inside the mesh, the drop of low tension cannot be held on the surface anymore. This explains why the WCA drops to 0° for R2 and R3, but saturates at a value of 25.6°. It also explains why the sudden decreases are bigger.
In contrast, for the aligned fibers, the opposite is observed. A closer look at figure 3.3b shows a faster decrease for larger fiber diameters (A1: sudden decrease from 88.7° to 28.9° at 6s; A2: sudden decrease from 112.3° to 26.5° at 4s; A3 sudden decrease from 119.3° to 41° at 2s). The sudden decreases are smaller and less steep compared to those for the random fibers, the higher packing density for the aligned fibers reduces the exposed surface area to the treatment and thus makes plasma incorporation harder. The porosity is smaller for aligned fibers, so the influence of the porosity is less pronounced in these cases, subsequently the WCA follows the trend seen in the XPS analysis. The homogeneous wetting, described by the Wenzel equation, remains a main actor of the system, as with the untreated case. The surface roughness is larger for larger fiber diameters, so more penetration of water into the grooves, thus a smaller WCA and the evolution of A2 and A3 to 0, while A1 reaches a saturation value of 19.6°.

3.2.3 XPS

To further explain the decrease in the WCA following plasma treatment, the elemental composition of the surface of the PCL fibers was analyzed using XPS measurements. All fiber conditions were studied at different argon plasma treatment times: 2s, 4s, 6s, 8s, 10s, 15s and 20s. In the untreated case, the different fiber conditions do not show a significant difference in oxygen content, that was around 24.5 %. Plasma treatment was shown to incorporate functional groups according to the literature study. The longer the plasma treatment time, the higher the oxygen content until a saturation point, corresponding to around 30 % of oxygen is reached at approximately 15s. Therefore, the improved surface wettability is caused by the incorporation of oxygen-containing functionalities on the nanofibers, as was suggested in the WCA measurements (figure 3.4).

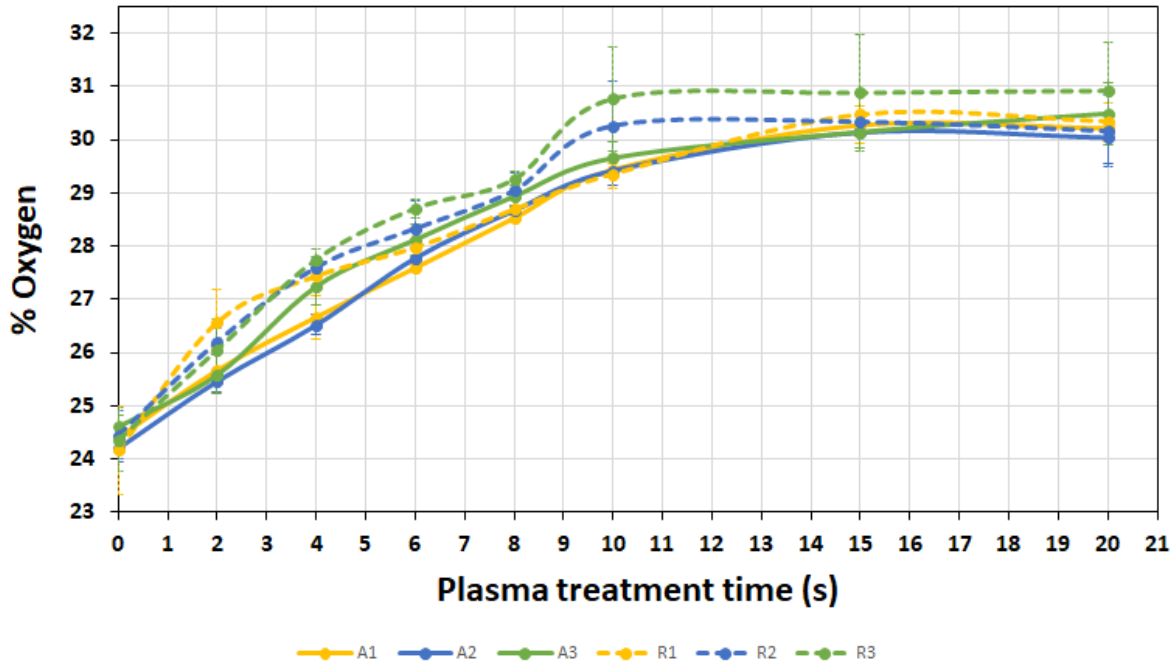

Figure 3.4: % Oxygen vs plasma treatment time (s) for the different fiber conditions.

Nonthermal plasma sustained in pure argon gas contains several species such as nonreactive excited atoms, nonreactive ions, photons, electrons and molecules which are able to break chemical bonds. These species can break C-C and C-H bonds or excite the polymer. Polymer radicals are formed, which can react with other radicals in the neighbouring polymer chains, forming a cross-linked network. In theory argon plasma treatment would only lead to cross-linking and double bond formation since argon plasma should only contain nonreactive argon species, but the working environment is not entirely pure. Oxygen trace is present in the plasma chamber because of impurities in the working gas, gaseous products desorbed from the reactor wall during the treatment and some residual air left in the plasma chamber. The radicals will react with atomic oxygen, molecular oxygen, ozone and OH radicals, hence the surface will be oxidized by the incorporation of oxygen containing functionalities such as C-O (hydroxyl), O-C=O (carboxyl) and C=O (carbonyl). Post-treatment oxidation also plays an important role in the appearance of oxygen at the surface of the fibers. [32, 41, 44, 78]
A closer look at figure 3.4 shows that, although all fiber conditions show a negligible difference in oxygen content in the untreated state, the oxygen content develops in a slightly different way during plasma treatment. For the randomly oriented fibers, the saturation is reached earlier. Morevover, in both orientations the biggest diameter has slightly higher surface oxidation compared to the smallest diameters. For the aligned fibers, the macromolecules are really packed and straight, making plasma incorporation harder. The molecular chains need thus more treatment time to be broken and functionalized. Furthermore, a bigger diameter is caused by a polymer jet experiencing less stretching and thinning, leading to less ordering in the molecular chain arrangement. This implicates that more molecular chains are exposed to plasma resulting in more bonds to be broken, thus more functionalities that can be incorporated into the sample.

3.2.4 SEM images of the damage after plasma treatment

To determine eventual fiber damage after plasma treatment, SEM images were taken after 15s and 1 min of plasma treatment and compared with the untreated case. Figure 3.5 shows the random fibers before and after plasma treatment, while figure 3.6 shows the same for the aligned fibers. After 15s of plasma treatment, minor to no damage is observed, but after 1 min the samples start to show significant damage. Two phenomena take place: some fibers are melting together and some fibers get thinner, this leads to a very big standard deviation when calculating the mean fiber diameter. The melting is caused

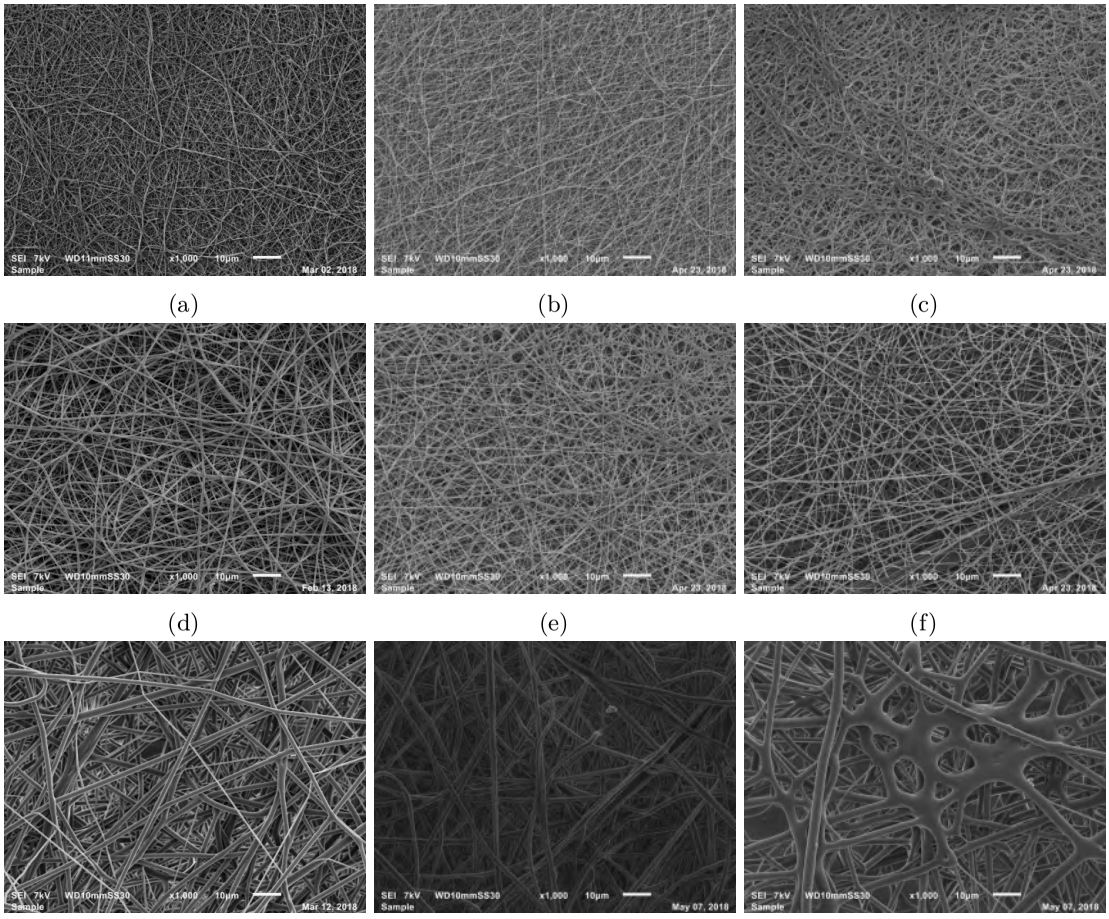

(a) (b) (c)

(d) (e) (f)

(g) (h) (i)

Figure 3.5: SEM images (magnification 1000x) of the randomly oriented fibers after plasma treatment. First column is untreated, second column is treated for 15 seconds, third column is treated for 1 minute. The plasma is sustained in argon gas. The first row is the smallest diameter, the second row is the intermediate diameter and the third row is the largest diameter.

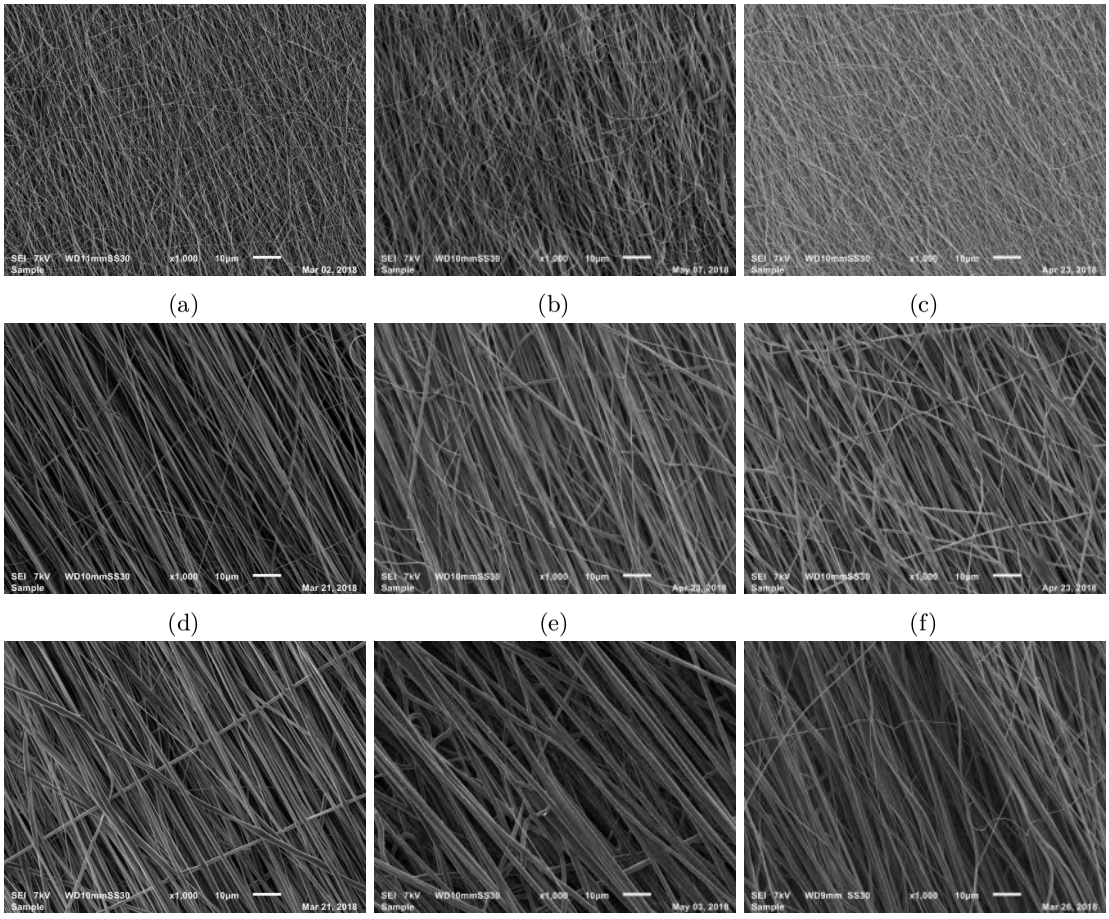

(a) (b) (c)

(d) (e) (f)

(g) (h) (i)

Figure 3.6: SEM images (magnification 1000x) of the aligned fibers after plasma treatment. First column is untreated, second column is treated for 15 seconds, third column is treated for 1 minute. The plasma is sustained in argon gas. The first row is the smallest diameter, the second row is the intermediate diameter and the third row is the largest diameter.

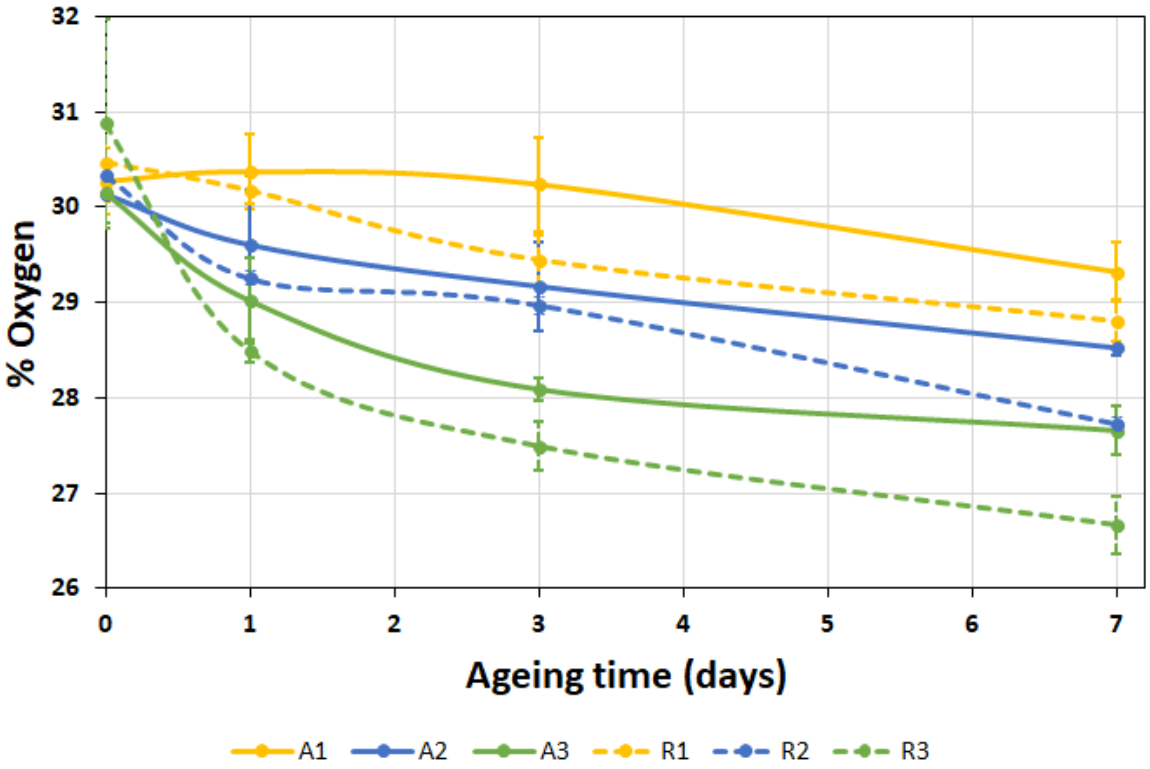

Figure 3.7: Evolution of the surface content of oxygen as a function of ageing time (days) for the different fiber conditions.

by the electrodes that get heated during the treatment because of the high energy supplied by the plasma source. The thinning could be explained by the ion etching effect of the plasma: ions interact with the polymeric fibers on the surface. The unwanted reactions cause degradation of the polymer chain called chain scissions, leading to formation of oligomers and desorption of volatile products from the PCL fibers of the surface. [78] PCL contains O_2 functionalities (ester groups), so its surface presents high susceptibility to plasma etching. [79] Etching leads to a rougher surface, but in general there is not such an aggressive etching present in argon plasma. [78–80]
By comparing the different fiber conditions with each other, it is clear that the bigger the diameter, the more the fibers are damaged. Again poor molecular arrangement and crystallinity are seen in the biggest fibers. This increases the degree of freedom for the polymer chains to move, making them more susceptible to deformations. Very pronounced deformation is seen after 1 min for the randomly oriented fibers with the largest diameter. The alignment is responsible for better mechanical properties. The porous structure, seen in random fibers, can weaken the resilience against deformations as well.

3.2.5 Ageing

The nanofibrous mesh topographically mimics the ECM. Argon plasma treatment adds polar groups to the surface to increase surface wettability thus chemically mimicking the natural ECM. An adequate treatment time, that still preserves the morphology good enough, while sufficiently altering the surface chemistry for its intended use, is of crucial importance. After 15s of plasma treatment, saturation is seen by XPS measurements and the SEM images show no damage to the fibers. Therefore, this treatment time is used for the rest of the dissertation. In the introduction, hydrophobic recovery has briefly been discussed. The surface modification due to the argon plasma treatment is not permanent. Therefore, the effect of storing the plasma-treated samples in air has been tested for all fiber conditions by performing XPS measurements after 1 day, 3 days and 7 days. The results can be found in figure 3.7 and in table 3.11. For all fiber conditions a small decrease in oxygen content is seen. Two phenomena are contributing to this ageing effect. Firstly, post-plasma treatment reactions of the surface with atmospheric minorities

such as CO_2 and H_2O, neutralize the implemented polar groups. Because of the fibrous structure however, the fibers are protecting one another from contact with ambient air, so this is not the major influence of the hydrophobic recovery. Instead the reorientation of the polar groups towards the bulk of the material has an impact that should not be underestimated. This explains the minor differences between the fiber conditions. Samples with aligned fibers experience less hydrophobic recovery: the alignment of the molecular chains hinders the incorporated functional groups to move and reorientate. The less packed density of the molecular chains forming the random fibers enables the incorporated groups to rotate and translate more. In the same way, the smaller diameter fibers undergo less ageing because of the increased packing density of the molecular chains. This can be explained in a similar way as with the damage from the plasma treatment. High crystallinity leads to a lower degree of freedom to move and less possibility to reorientate the functional polar groups towards the bulk. [37–39]

Table 3.11: XPS measurement of oxygen content (in %) after ageing times of 0 days, 1 day, 3 days and 7 days for all the fiber conditions.

Ageing time	0 days	1 day	3 days	7 days
% oxygen A1	30.27 ± 0.34	30.37 ± 0.39	30.24 ± 0.19	29.32 ± 0.31
% oxygen A2	30.13 ± 0.064	29.61 ± 0.58	29.17 ± 0.46	28.53 ± 0.07
% oxygen A3	30.14 ± 0.31	29.02 ± 0.45	28.09 ± 0.12	27.66 ± 0.26
% oxygen R1	30.53 ± 0.42	30.18 ± 0.14	29.45 ± 0.26	28.81 ± 0.22
% oxygen R2	30.34 ± 0.11	29.25 ± 0.07	28.97 ± 0.09	27.72 ± 0.07
% oxygen R3	30.88 ± 1.09	28.49 ± 0.12	27.50 ± 0.25	26.67 ± 0.31

3.3 Cell tests

As mentioned in the introduction, different nerve cells prefer different fiber conditions. These six different conditions will be compared with distinct cell tests. For each different condition, the untreated and treated samples will hopefully show some interesting differences concerning the viability, adhesion and proliferation of the nerve cells. From the results we should be able to pick an optimal nanofibrous polymer mesh to continue the work on peripheral nerve repair. For the cell tests, olfactory ensheathing cells (OECs) are utilized. These can be compared to Schwann cells. Schwan cells ensheath the non-myelinated neurons in the PNS, where OECs ensheath the non-myelinated neurons of the olfactory system, that is responsible for our sense of smell. [81] In the introduction it has been mentioned that Schwann cells are able to form Büngner bands and research has shown that additional transplantation of OECs can enhance axonal regeneration and could thus facilitate the peripheral nerve repair process. [82] Furthermore, studies have shown that OECs also play a role in CNS repair, adding even more importance to this research. [83] Important characteristics of the nanofibrous mesh have been named a few times already in the introduction. These cell test are helpful in checking the necessary requirements. Cellular adhesion to a material's surface (cell capture efficiency) is a major characteristic in the occurrence of cell growth, spreading, proliferation and differentiation. [36] The fluorescent microscopic images after live/dead staining of OECs cultured for 3 days (figure 3.8 and 3.9) show the cells that survived and died, indicated by green and red respectively. In most of the different condition (random vs aligned, small vs intermediate vs large diameter and untreated vs plasma treated) more living cells than dead cells are seen after 3 days. The live/dead staining shows a lot of cells on R1 in the treated and untreated case (figure 3.8a and 3.8b). The effect of the plasma treatment is primarily the more elongated morphology of the cells, which is an indication of better cell attachment. The spread out morphology is seen in all plasma treated samples (figures 3.8b, 3.8d, 3.8f, 3.9b, 3.9d and 3.9f). On the aligned fibers the cells spread out and elongate in the same direction, thus following the fiber alignment of the nanofibrous mesh. This can be used to guide nerve cells in the right direction during nerve repair.
The actin staining, (figures 3.10 and 3.11) after 3 days of cell culturing, confirms this as well. In the introduction (section 1.1) it was mentioned that neurons have a cytoskeleton with intermediate filaments containing actin. By staining the actin within the cells, the cytoskeleton can be visualized. The same

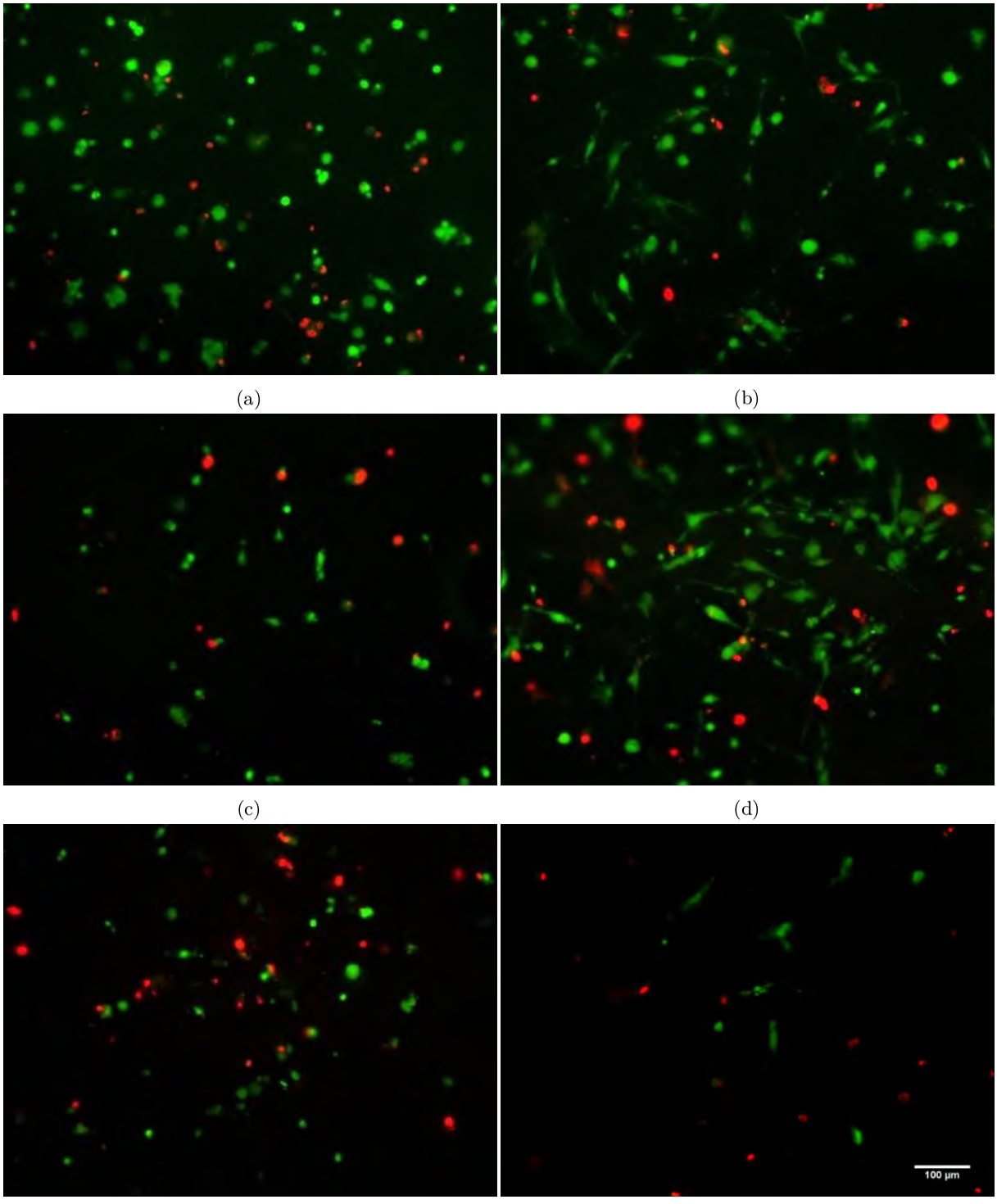

Figure 3.8: Fluorescent micrographs after live/dead staining of OECs cultured for 3 days on randomly oriented PCL nanofibrous samples. The left column ((a), (c) and (e)) are the untreated conditions, the right column ((b), (d) and (f)) are the samples treated by plasma sustained in argon for 15s. The fibers in (a) and (b) have the smallest diameter, the fibers in (c) and (d) have the intermediate diameter and the fibers in (e) and (f) have the biggest diameter. (scale bar: 100 μm)

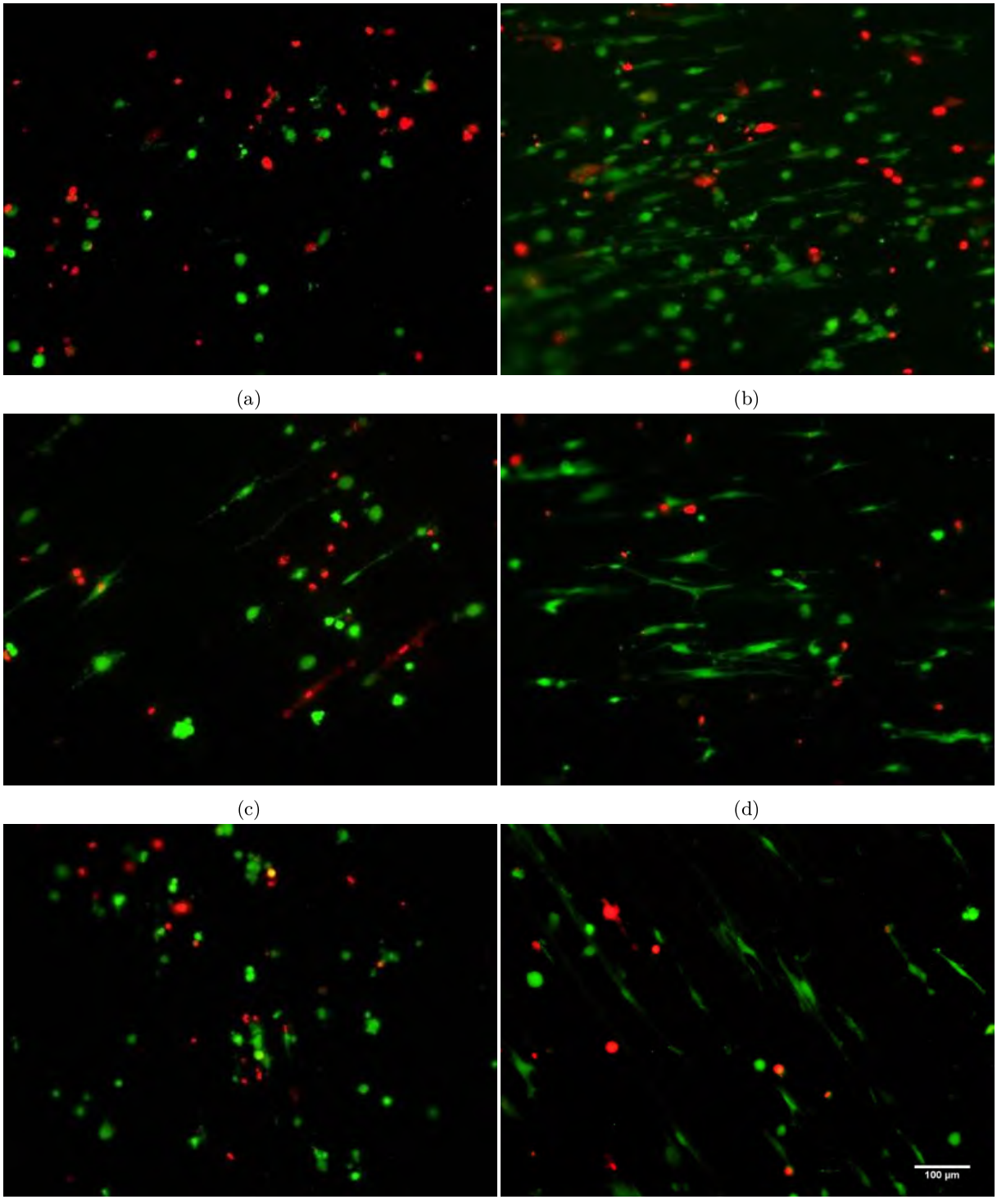

Figure 3.9: Fluorescent micrographs after live/dead staining of OECs cultured for 3 days on aligned PCL nanofibrous samples. The left column ((a), (c) and (e)) are the untreated conditions, the right column ((b), (d) and(f)) are the samples treated by plasma sustained in argon for 15s. The fibers in (a) and (b) have the smallest diameter, the fibers in (c) and (d) have the intermediate diameter and the fibers in (e) and (f) have the biggest diameter. (scale bar: 100 μm)

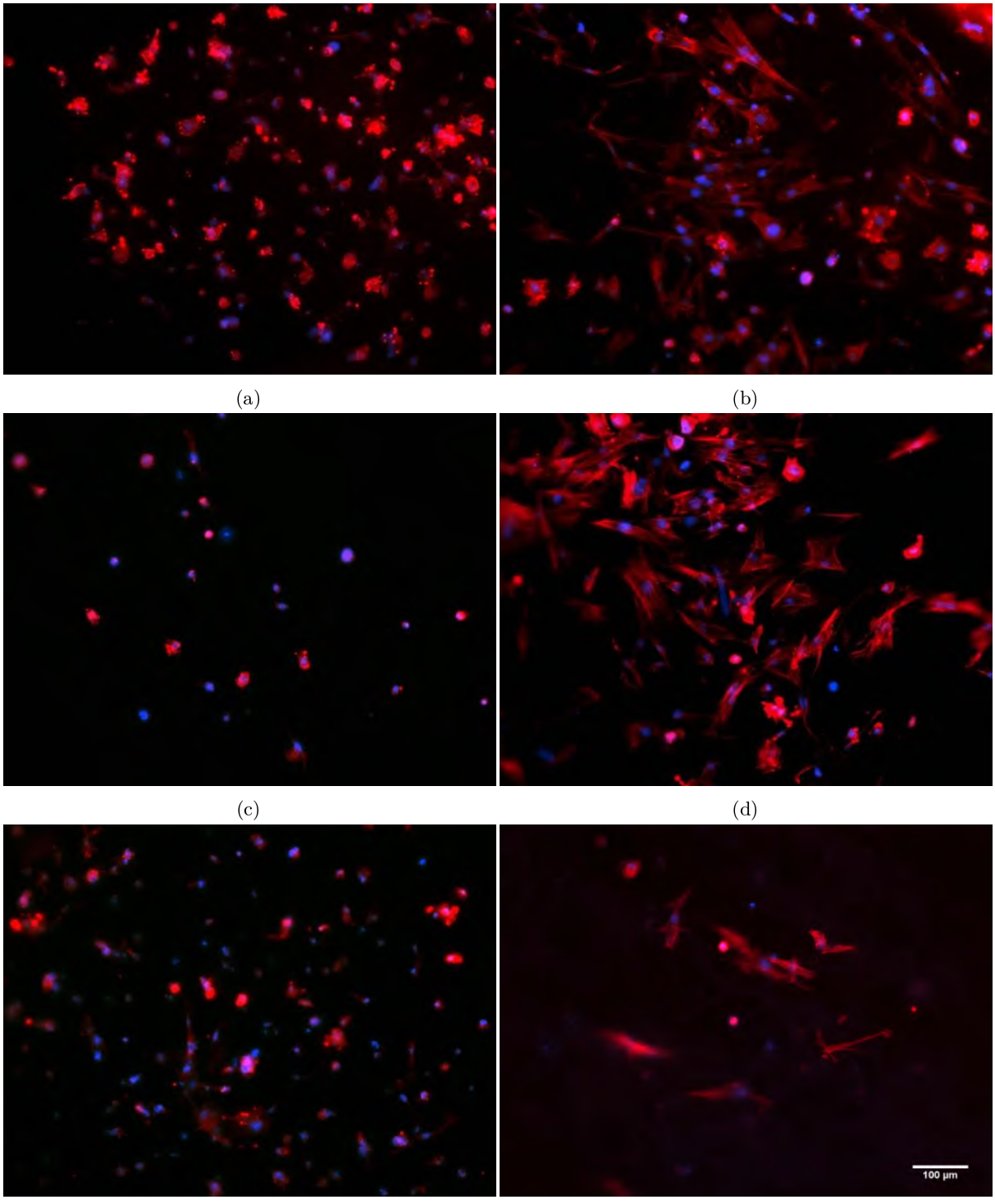

(a) (b)

(c) (d)

(e) (f)

Figure 3.10: Actin stainning of OECs cultured for 3 days on randomly oriented PCL nanofibrous samples. The left column ((a), (c) and (e)) are the untreated conditions, the right column ((b), (d) and (f)) are the samples treated by plasma sustained in argon for 15s. The fibers in (a) and (b) have the smallest diameter, the fibers in (c) and (d) have the intermediate diameter and the fibers in (e) and (f) have the biggest diameter. (scale bar: 100 μm)

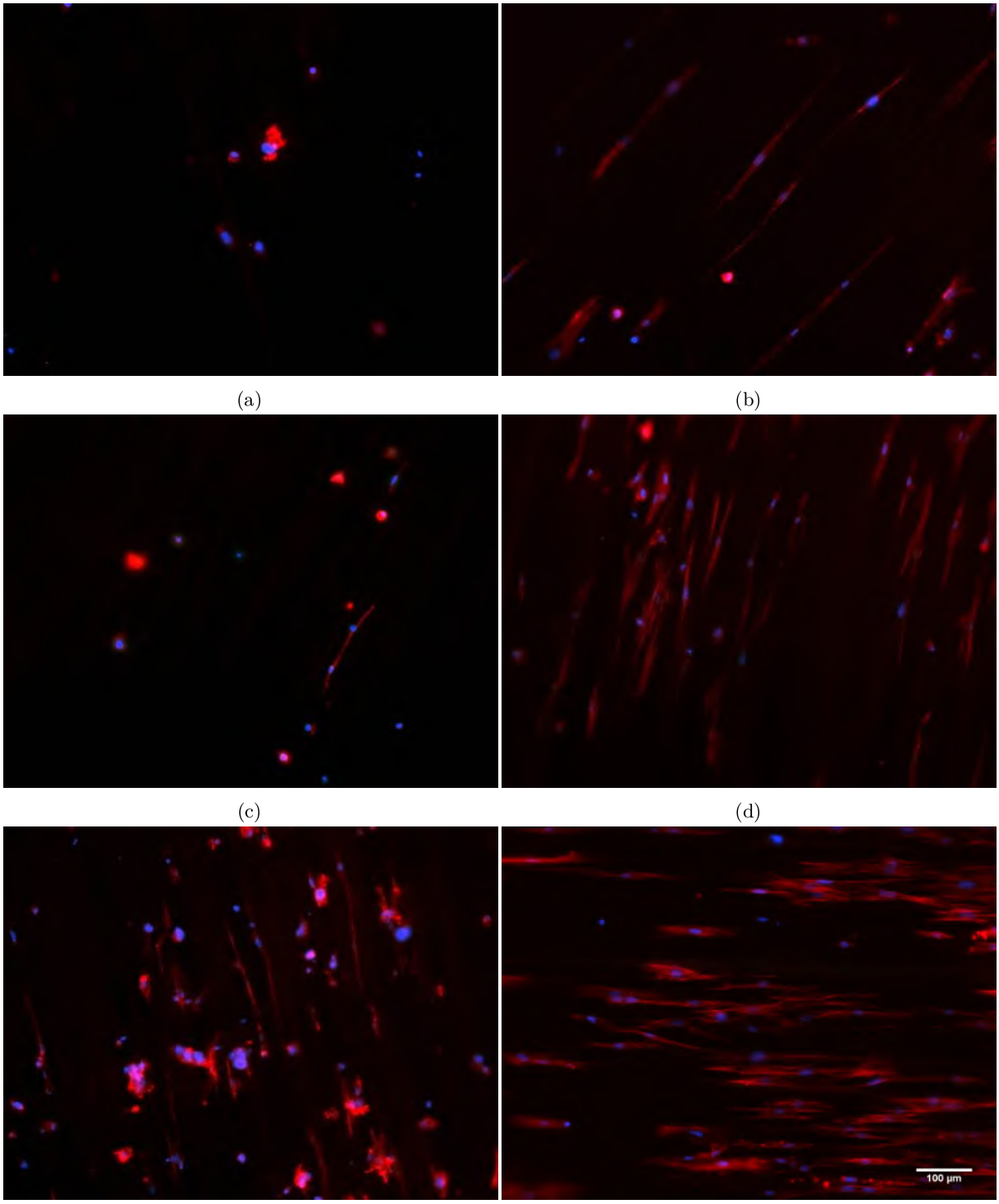

Figure 3.11: Actin stainning of OECs cultured for 3 days on aligned PCL nanofibrous samples. The left column ((a), (c) and (e)) are the untreated conditions, the right column ((b), (d) and (f)) are the samples treated by plasma sustained in argon for 15s. The fibers in (a) and (b) have the smallest diameter, the fibers in (c) and (d) have the intermediate diameter and the fibers in (e) and (f) have the biggest diameter. (scale bar: 100 μm)

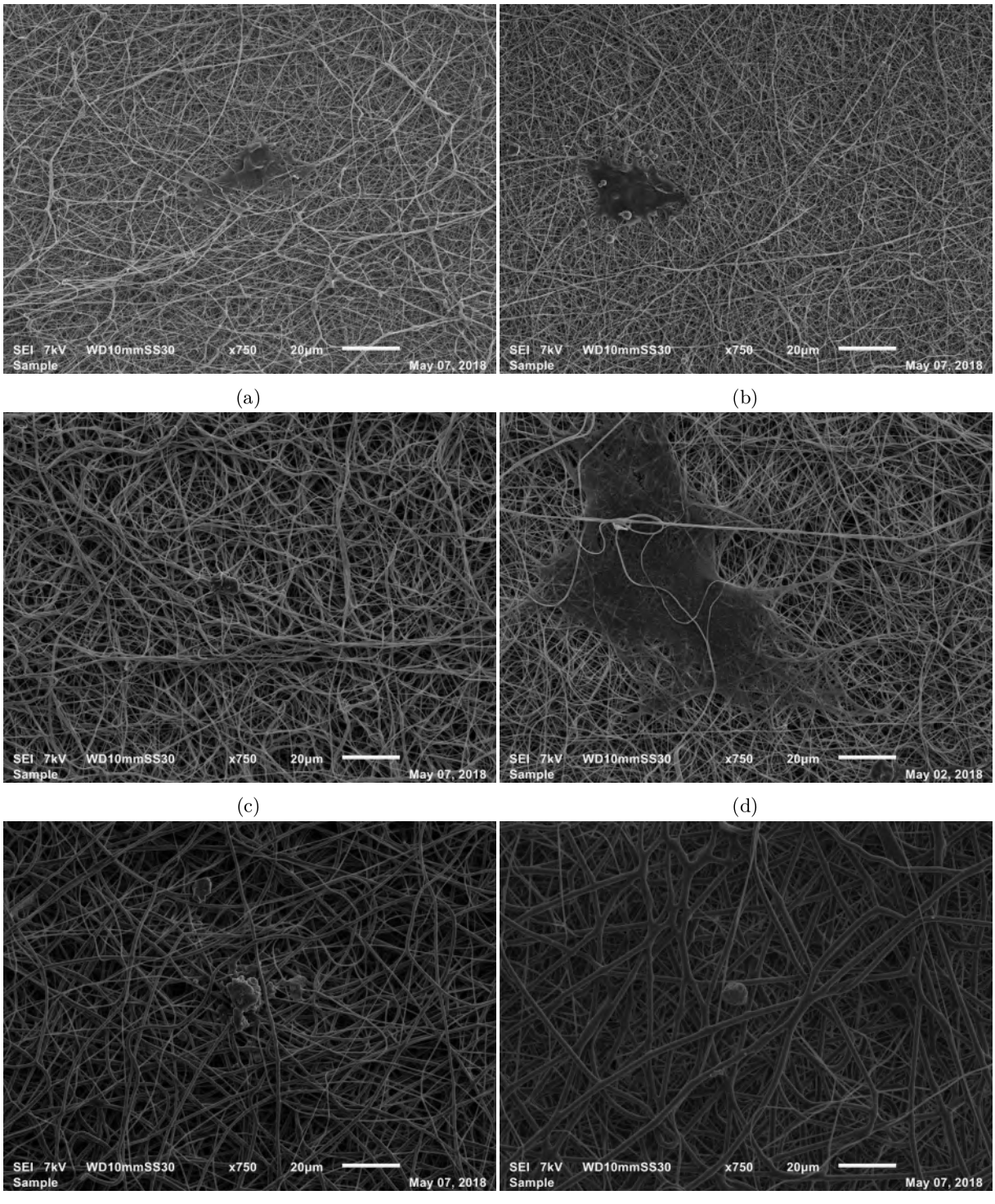

Figure 3.12: SEM images (magnification 750x) of OEC on the different randomly orientated nanofibrous meshes after three days of culturing. Left column ((a), (c) and (e)) are untreated, right column ((b),(d) and (f)) are argon plasma treated for 15s. The fibers in (a) and (b) have the smallest diameter, the fibers in (c) and (d) have the intermediate diameter and the fibers in (e) and (f) have the biggest diameter.

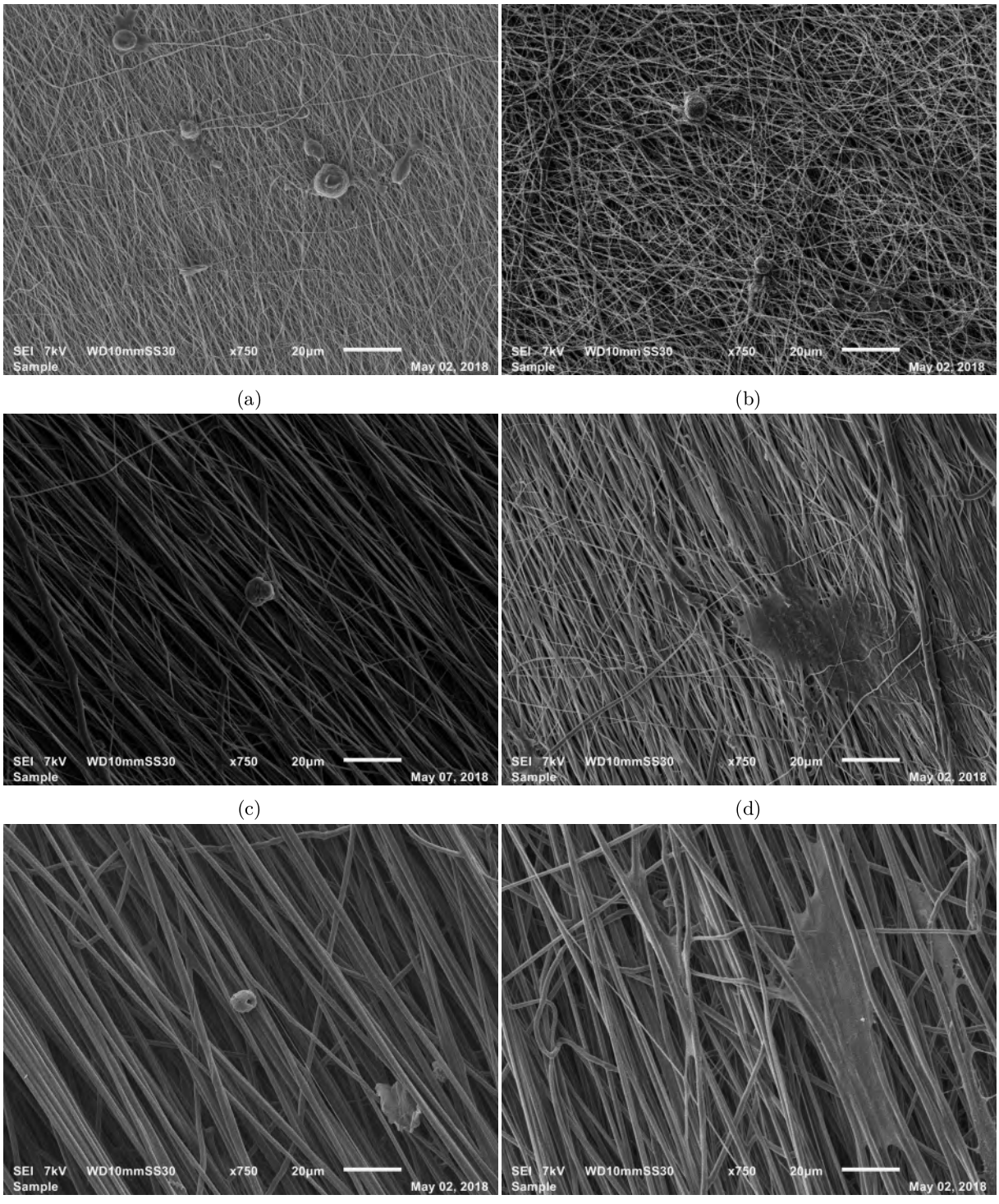

Figure 3.13: SEM images (magnification 750x) of OEC on the different aligned nanofibrous meshes after three days of culturing. Left column ((a), (c) and (e)) are untreated, right column ((b),(d) and (f)) are argon plasma treated for 15s. The fibers in (a) and (b) have the smallest diameter, the fibers in (c) and (d) have the intermediate diameter and the fibers in (e) and (f) have the biggest diameter.

conclusions can be drawn from this. The plasma treatment increases the cell spreading, while untreated cells have a rounded morphology, indicating poor cellular attachment. Again the aligned fibers show highly directional spreading.
Even on the SEM images the difference between treated and untreated is clear. The cells are small and round on the untreated samples, indicating poor cellular attachment. For the plasma treated conditions the cells are elongated and spread out. For the treated A3 sample (figure 3.13f) the cell is even migrating into the bulk of the sample. A promising image because the cell is integrating into the scaffold as if it were a genuine ECM.
The oxygen containing functionalities, incorporated by the argon plasma treatment, might be the cause of the improved cellular attachment. Higher wettability leads to better adsorption of proteins, because the oxygen containing functionalities act as receptor binding sites. The receptors on the cell surface are able to bind to the plasma treated nanofibers (figure 1.12). Important mediators in cell-material interactions are the transmembrane proteins: integrins. At focal adhesion sites, the cell binds to the sample with these integrins. They cluster together and evoke signalling pathways, that alters the structure of the filaments of the cytoskeleton among others. The untreated samples do not have a lot of these focal adhesion sites, because they lack oxygen functionalities. The cells that do attach show a three-dimensional rounded morphology. The plasma treated samples are occupied with focal adhesive sites, the cells show a two-dimensional spreading and elongation. [36, 84] After 3 days however there are quite a lot of dead cells in some conditions of the live/dead staining images (figures 3.8d, 3.8e, 3.8f, 3.9a and 3.9b). This could indicate some cytotoxicity of the PCL fibers. The plasma treatment cannot be responsible for this since the dead cells occur in both treated and untreated cases. There is however another possibility. Because of the porous structure, cells are able to infiltrate the mesh and consequently the PBS (section A.6.2) is unable to rinse away the infiltrated cells, that might not have attached properly to the mesh.

After 7 days of cell culturing, there is not a lot of difference. Cells in the untreated state stay rounded and small, while in the treated state the cells spread out. The few cells that stayed rounded and small on the treated samples (figure 3.14d), after 3 days of culturing become however well spread out (figure 3.12d). The main difference between the treated samples is seen in the migration of the cells inside the bulk. The pores in the R1 sample are too small for the elongated cells to migrate into and the cells form a covering sheet on top of the mesh (figure 3.14b). The cells on the samples with large fiber diameter (figures 3.14f and 3.15d) are able to move inside the bulk as was seen after three days of culturing. The treated, aligned fibers show that the cells are following the fiber direction in spreading.

The samples were again studied after 10 days of culturing to check the proliferation (cell growth and cell division) of the cells. The live/dead staining in figures 3.16 and 3.17 indicates most cells are still alive. For random fibers, there is a clear difference between the untreated and the argon plasma treated samples. A lot of living cells are present on the treated random fibers, much more than on the untreated random fibers. Plasma treatment does not only enhance adhesion of the cells, but also their proliferation. The difference is smaller between the untreated and treated aligned fibers, still the treated fibers show better proliferation and spreading. The morphology is checked again on SEM images (figures 3.18 and 3.19). The conclusions are the same. Cells prefer plasma treated samples, clearly indicated by the large spreading. The cells are migrating through the porous structure of the fibers with the large diameter (figures 3.18f and 3.19f). The cells on the untreated samples are rounded and very small.

A quantifiable distinction can be made with PrestoBlue®, showing the metabolic activity of the cells, comparable to an MTT assay. The metabolic activity is compared to cells seeded on coverslips coated with poly-L-lysine, this is a positive control, meaning that cells are having a good attachment and proliferation on these. The metabolic activity was checked after 3 days, 7 days and 10 days.
The resulting graphs are given in figure 3.20. The first thing that needs to be cleared out is the negative values obtained on day 3, this is an indication that the assay was not sensitive enough to measure proliferation. These results are consequently not very useful. In most cases the metabolic activity peaks on day 7 and decreases on day 10. This could indicate 100% confluence. The coverslips are entirely covered in cells and there is no room left. Studies have shown that proliferation stops due to confluence, but cellular migration might be activated, which should be beneficial once a polymeric conduit is placed in vivo. [85]
Another observation is that all values are below 1, so in all cases there is poorer cellular proliferation on

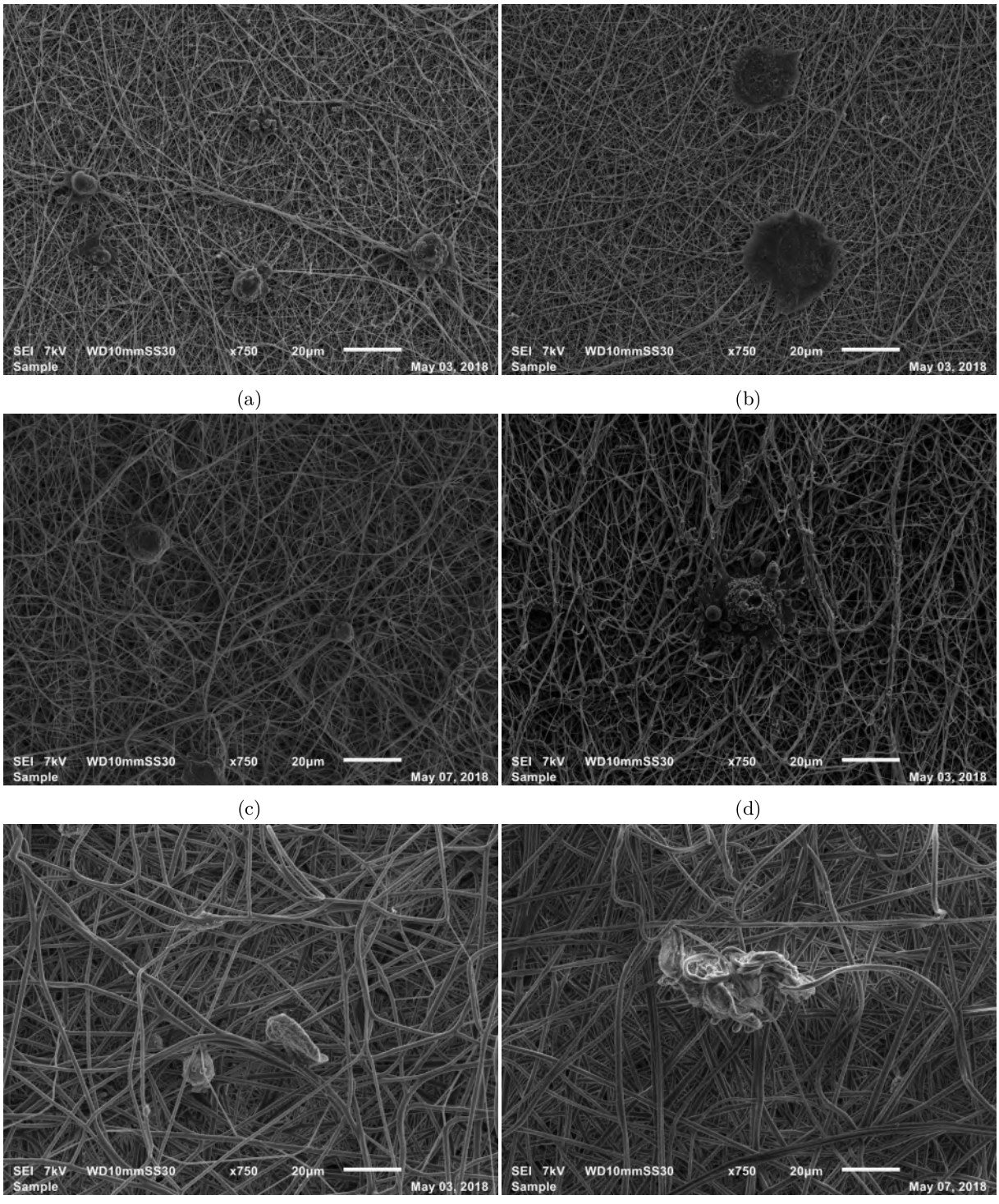

Figure 3.14: SEM images (magnification 750x) of OEC on the different randomly oriented nanofibrous meshes after 7 days of culturing. Left column ((a), (c) and (e)) are untreated, right column ((b),(d) and (f)) are argon plasma treated for 15s. The fibers in (a) and (b) have the smallest diameter, the fibers in (c) and (d) have the intermediate diameter and the fibers in (e) and (f) have the biggest diameter.

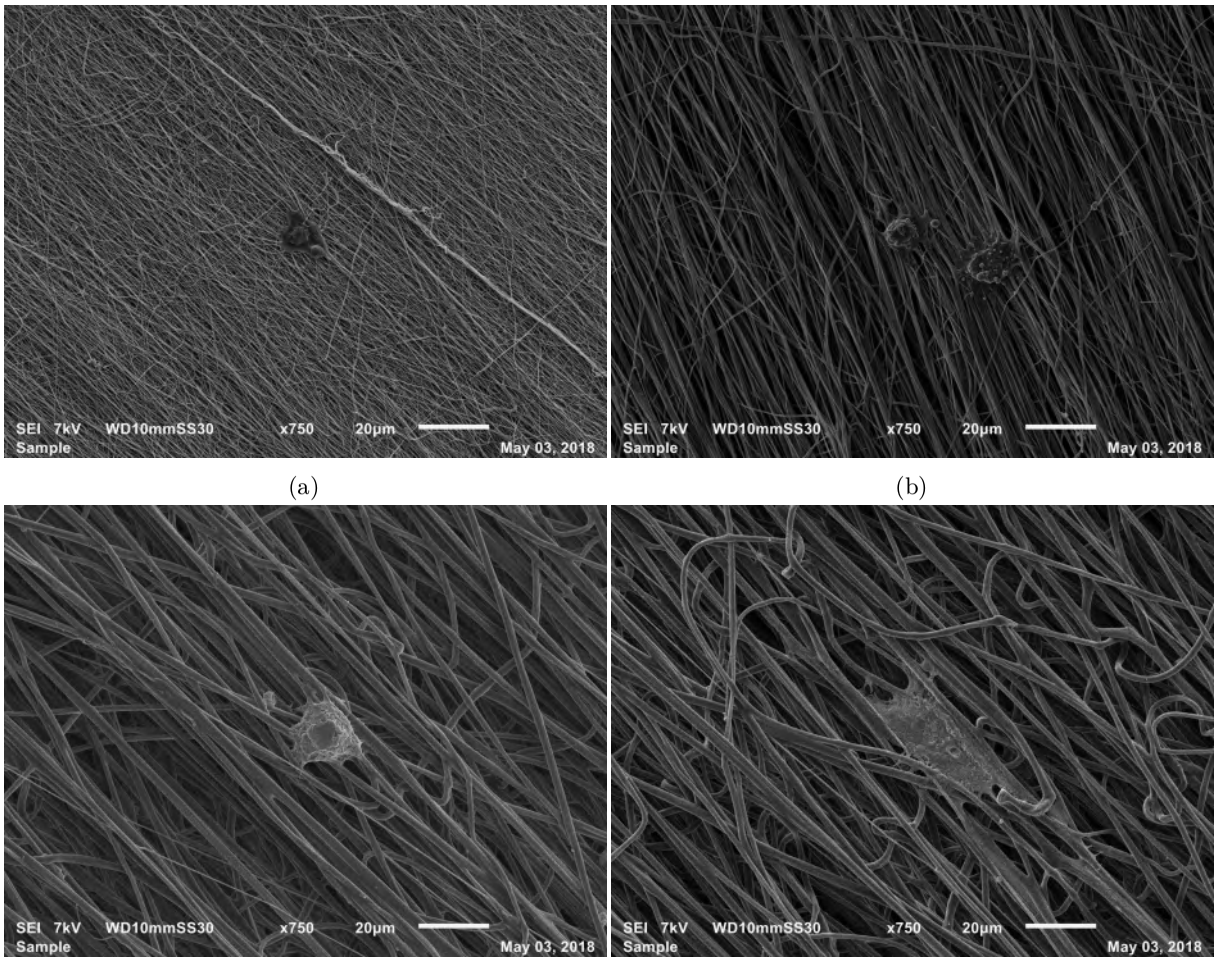

(a) (b)

(c) (d)

Figure 3.15: SEM images (magnification 750x) of OEC on the different aligned nanofibrous meshes after 7 days of culturing. (a) Untreated A1, (b) Untreated A2, (c) Untreated A3 and (d) Treated A3.

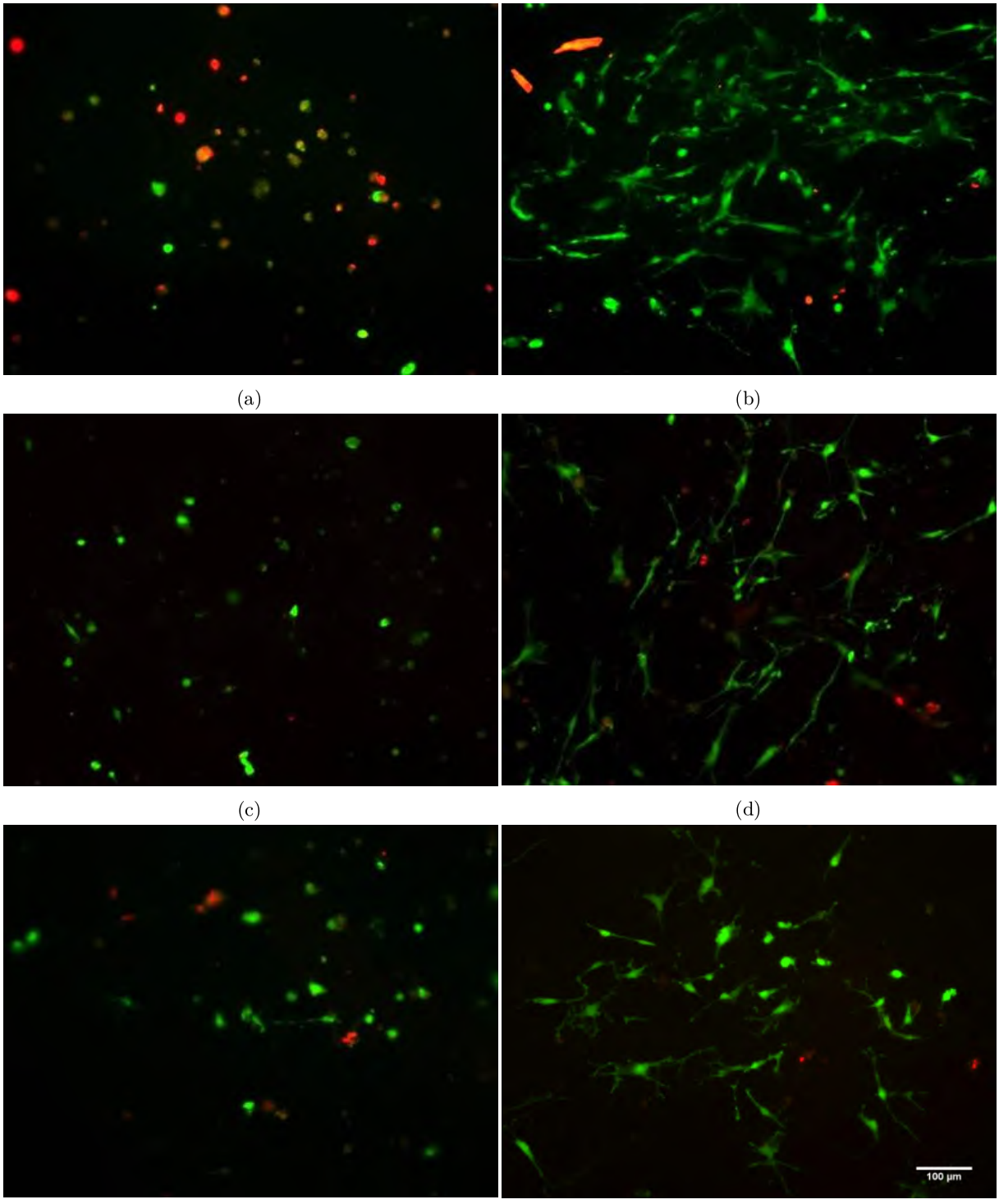

(a) (b)

(c) (d)

(e) (f)

Figure 3.16: Fluorescent micrographs after live/dead staining of olfactory ensheathing cells cultured for 10 days on randomly oriented PCL nanofibrous samples. The left column ((a), (c) and (e)) are the untreated conditions, the right column ((b), (d) and (f)) are the samples treated by plasma sustained in argon. The fibers in (a) and (b) have the smallest diameter, the fibers in (c) and (d) have the intermediate diameter and the fibers in (e) and (f) have the biggest diameter. (scale bar: 100 μm)

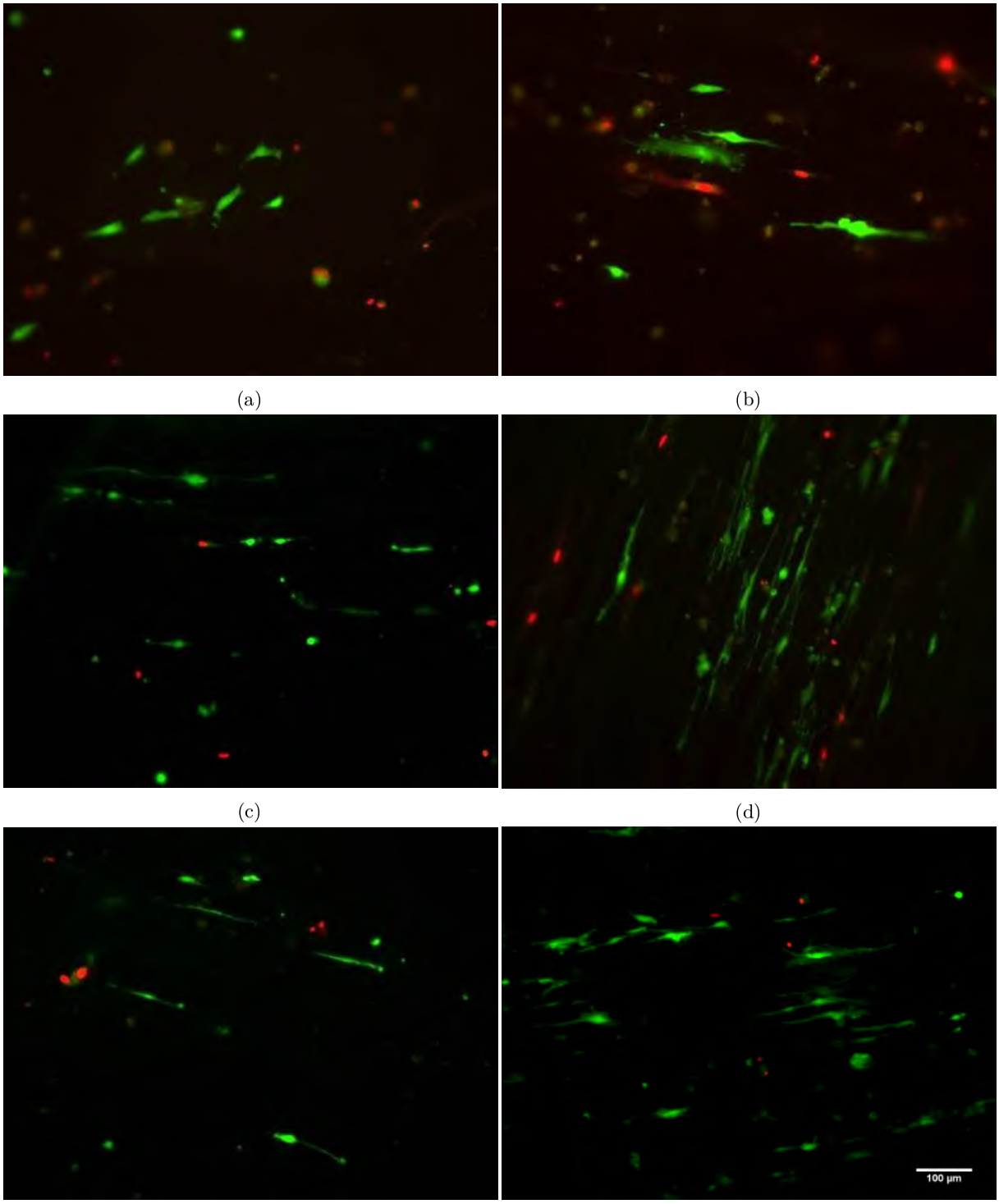

(a) (b)

(c) (d)

(e) (f)

Figure 3.17: Fluorescent micrographs after live/dead staining of olfactory ensheating cells cultured for 10 days on aligned PCL nanofibrous samples. The left column ((a), (c) and (e)) are the untreated conditions, the right column ((b), (d) and (f)) are the samples treated by plasma sustained in argon. The fibers in (a) and (b) have the smallest diameter, the fibers in (c) and (d) have the intermediate diameter and the fibers in (e) and (f) have the biggest diameter. (scale bar: 100 μm)

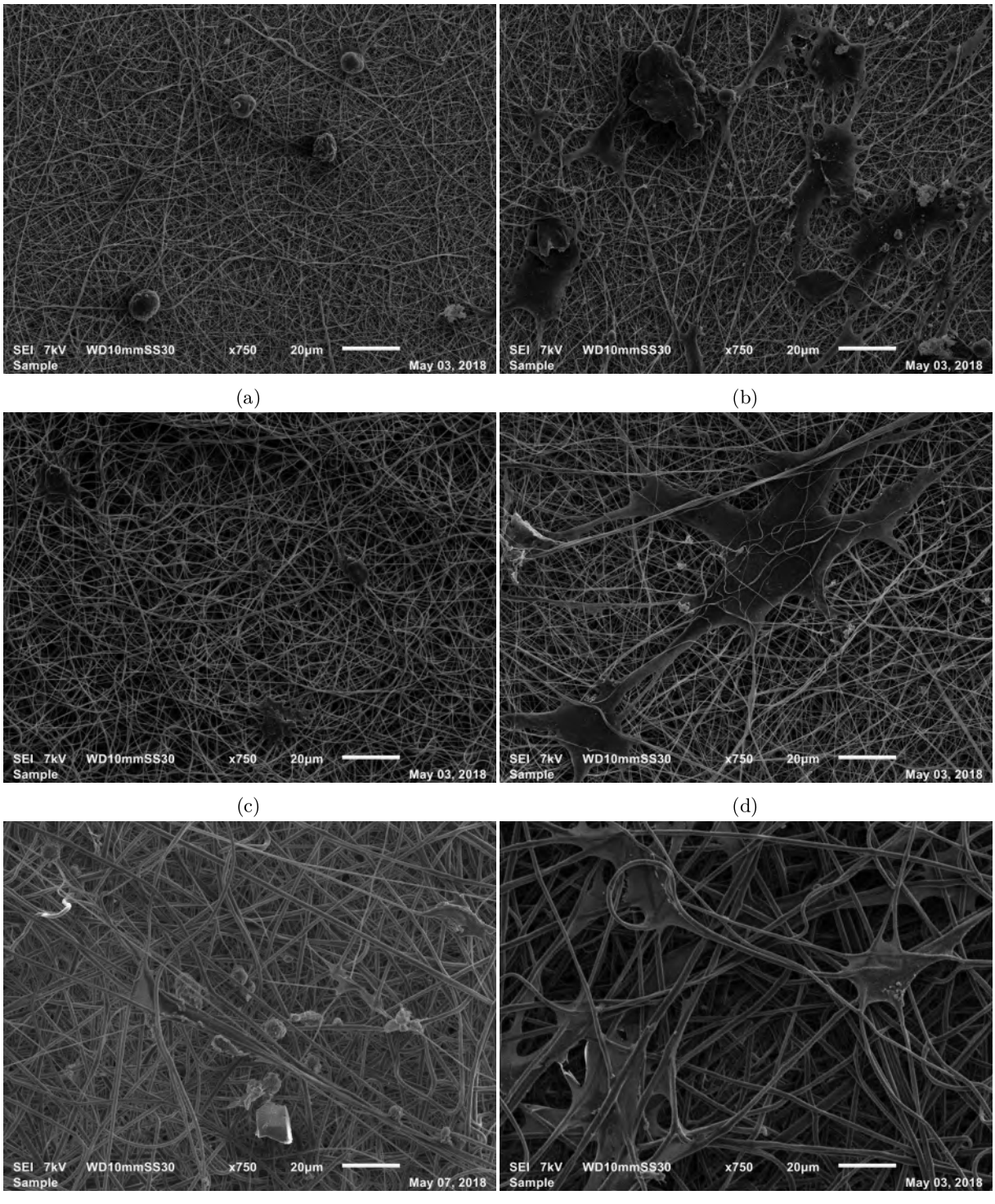

Figure 3.18: SEM images (magnification 750x) of OEC on the different randomly oriented nanofibrous meshes after 10 days of culturing. Left column ((a), (c) and (e)) are untreated, right column ((b),(d) and (f)) are argon plasma treated for 15s. The fibers in (a) and (b) have the smallest diameter, the fibers in (c) and (d) have the intermediate diameter and the fibers in (e) and (f) have the biggest diameter.

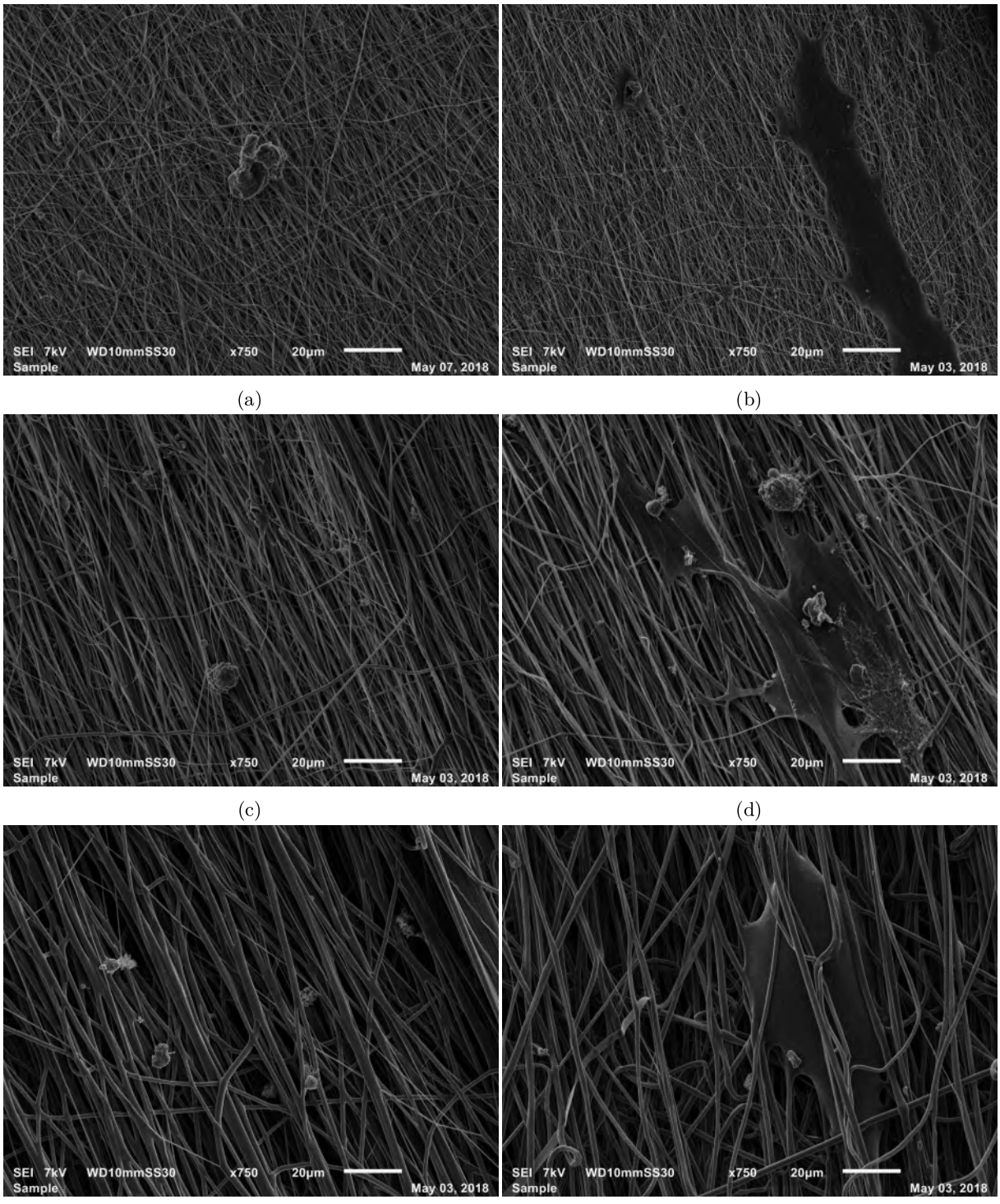

Figure 3.19: SEM images (magnification 750x) of OEC on the different aligned nanofibrous meshes after 10 days of culturing. Left column ((a), (c) and (e)) are untreated, right column ((b),(d) and (f)) are argon plasma treated for 15s. The fibers in (a) and (b) have the smallest diameter, the fibers in (c) and (d) have the intermediate diameter and the fibers in (e) and (f) have the biggest diameter.

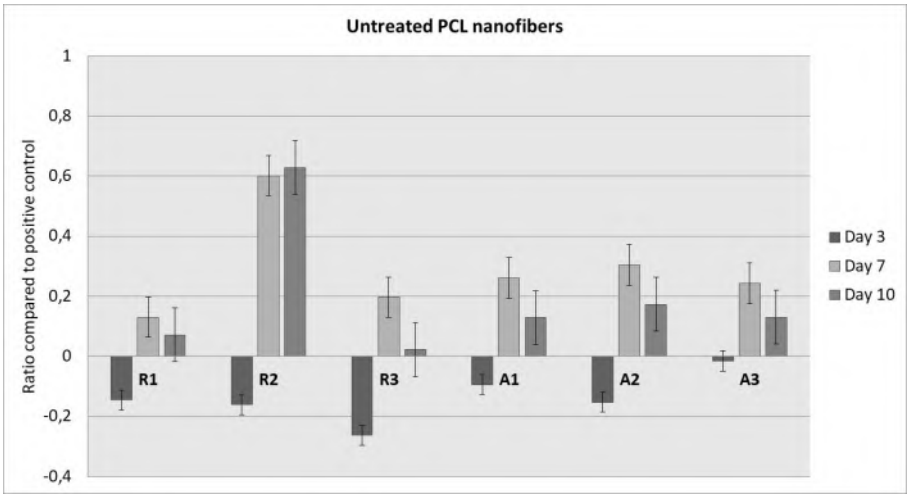

(a)

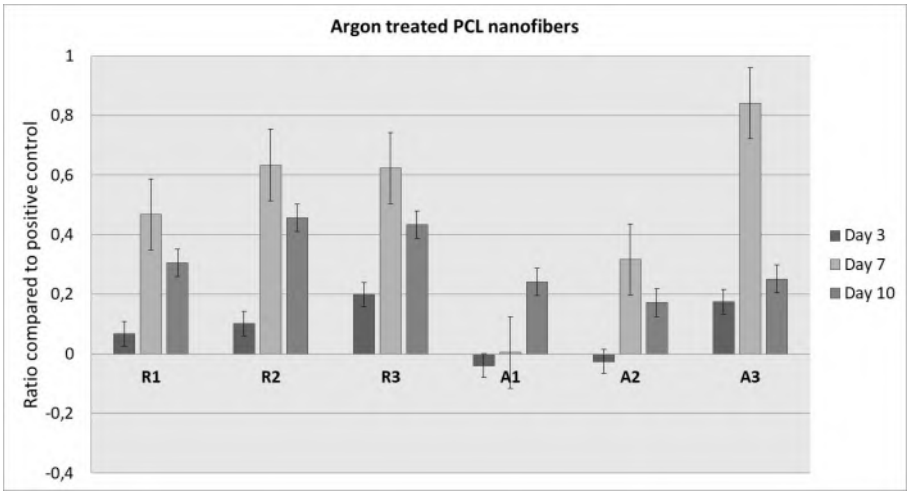

(b)

Figure 3.20: PrestoBlue® assay on day 3, day 7 and day 10. (a) Untreated fiber conditions, (b) argon plasma treated fiber conditions.

the PCL nanofibers than on the positive control. In the majority of the cases the treated fibers show better cellular proliferation, however this is not generally the case. On the basis of the PrestoBlue® it is dangerous to draw conclusions about a preferential surface state, luckily it was already made clear with the other cell tests that attachment and spreading is better on the treated samples. Finally OEC proliferation seems to be the highest on day 7 for the argon treated A3 fibers. But cellular proliferation is also high on all random, argon treated fibers.

The preference for argon plasma treated fibers is very clear, but concerning the topography the distinction is less pronounced. Since the OECs are infiltrating the porous structure in the R3 and A3 samples, these seem to be the conditions of interest to proceed the research with. The metabolic activity of these samples are also the highest (on day 7). No clear preference was made for random or aligned fibers, but the cell morphology was different however. The elongated and highly directional spreading on the aligned fibers can lead the OECs to grow in the appropriate direction. This would be preferable for the inner lumen of a polymeric conduit.

Chapter 4

Conclusion

This master's dissertation describes a host of advancements concerning the fabrication of nanofibrous meshes suitable for peripheral nerve regeneration purposes, which is a common clinical problem. These results can be interesting for people working in the field of tissue engineering. For starters, the electrospinning of PCL fibers was performed in the binary solvent system formic acid and acetic acid. The possibility to shape the fibers into adequate topographies has been researched. The focus was the effects of the rotational speed of a cylindrical mandrel as collector, the polymer concentration of the solution, the CTD and the frequently overlooked ambient parameter RH. Altering the rotational speed led to different alignment. Aligned fibers were electrospun by rotating the collector at a high speed, because of the additional mechanical forces. The diameter of the fibers was altered by adjusting the polymer concentration, CTD and RH. The resulting mean fiber diameter increased with increasing polymer concentration, increasing RH and decreasing CTD. The goal of this part was to create six different fiber conditions: randomly oriented or aligned fibers with small, intermediate or large diameter.

The effects of a DBD argon plasma treatment on the different fibers conditions have also been studied extensively. A drop in the WCA and an increase in surface oxygen content were present on all fiber conditions, but the different topographies led to differences as well, concluding that the surface morphology and the surface energy are two properties influencing the wettability. The surface oxygen content also developed in a slightly different way for each fiber condition. For the random fibers, the saturation is reached earlier since the molecular chains of the aligned fibers are really packed and straight. This makes the incorporation of functional groups harder, the molecular chains thus need more treatment time to be broken and functionalized. The larger diameters have a slightly higher surface oxygen content, regardless of the alignment, because of the ordering in the molecular chains. A larger fiber has lesser ordering, so more chains are exposed to the plasma, thus more functionalities. The poor molecular arrangement in larger fibers led to a decrease in mechanical strength. The larger fibers were prone to more damage after a plasma treatment. The alignment also augmented the mechanical strength of the mesh. The hydrophobic recovery was studied as well. The major phenomenon for the ageing effect was the reorientation of functional groups towards the bulk. The different mechanical properties of the different fibers were again the main reason of the variation in ageing behavior. At 15s the fibers were still intact. The main reason for the plasma treatment was the bad biochemical properties of the surface of the fibers. These were altered without changing the bulk of the material. This led to 12 different conditions: untreated or argon plasma treated, randomly oriented or aligned fibers with small, intermediate or large diameter.

These conditions were tested and compared to each other concerning their potential to be used as a nanofibrous mesh for polymer conduits used in peripheral nerve regeneration. In the introduction it has been established that cells are sensitive to both their topographical as their biochemical environment. The electrospun nanofibers were responsible for the topographical cues, while the argon plasma treatment was responsible for the biochemical cues. The cellular attachment, morphology and proliferation of OECs were tested on the 12 different conditions. Live/dead staining showed the cell viability. None of the samples showed a high dead rate for the cells. The actin staining enabled the visualization of the morphology of the OECs. The untreated samples show rounded cells, indicating poor cellular attachment, while the treated samples show a elongated morphology. The attachment is made very clear on the SEM

images as well. Some interesting cell behavior related to the topography were seen on the actin stained fluorescent micrographs and the SEM images. The cells show a directional spreading on the aligned fibers, which is a promising result to direct the cells to the right structure to be innervated. The cells were also migrating to the inside of the bulk on the larger fibers, because of the adequately porous structure. The nanofibrous meshes mimic the ECM quite good in these cases.

The next step in this research is the fabrication of actual polymeric conduits instead of meshes on coverslips. My suggestion is a bi-layer conduit where the inner lumen is built up out of plasma treated aligned fibers with a mean diameter of around 1200 nm. The outer lumen should consist of randomly oriented fibers , so nutrients can reach the inner volume, but cellular ingrowth deep into this volume should be hindered, especially for cells like fibroblasts. These synthesize the ECM, so the available place for the nerve regeneration could be diminished. A little inwards migration could be beneficial, since, during the degradation of the polymer, the ECM should replace the conduit continuously.

Bibliography

[1] J. G. Betts, P. Desaix, E. Johnson, J.E. Johnson, O. Korol, D. Kruse, B. Poe, and J.A. Wise. *Anatomy and Physiology.* OpenStax, 2013.

[2] D. Arslantunali, T. Dursun, D. Yucel, N. Hasirci, and V. Hasirci. Peripheral nerve conduits: Technology update. *Med Devices (Auckl)*, 7:405–424, 2014.

[3] C. Reeve. What is a neurofilament? *WiseGEEK*. Consulted on 22 january 2018 via http://www.wisegeek.com/what-is-a-neurofilament.htm.

[4] G. Evans. Peripheral nerve injury: A review and approach to tissue engineered constructs. *The Anatomical Record*, 263(4):396–404, 2001.

[5] J. T. Kevenaar and C. C. Hoogenraad. The axonal cytoskeleton: from organization to function. *Frontiers in Molecular Neuroscience*, 8(44), 2015.

[6] E.A. Huebner and S.M. Strittmatter. Axon regeneration in the peripheral and central nervous systems. *Material Science and Engineering: C Materials and Biological Applications*, 48:339–351, 2009.

[7] A. T. Nguyen, S.R. Sathe, and E.K. Yim. From nano to micro: topographical scale and its impact on cell adhesion, morphology and contact guidance. *Journal of Physics: Condensed Matter*, 28, 2016.

[8] R. W. Williams, M.J. Bastiani, B. Lia, and L.M. Chalupa. Growth cones, dying axons, and developmental fluctuations in the fiber population of the cat's optic nerve. *Journal of Comparative Neurology*, 246(1):32–69, 1986.

[9] K. W. Tosney and L.T. Landmesser. Growth cone morphology and trajectory in the lumbosacral region of the chick embryo. *Journal of Neuroscience*, 5(9):2345–2358, 1985.

[10] J. W. Fawcett and R. J. Keynes. Peripheral nerve regeneration. *Annual Review of Neuroscience*, 13:43–60, 1990.

[11] S. Lee and S. W. Wolfe. Peripheral nerve injury and repair. *Journal of the American Academy of Orthopaedic Surgeons*, 8(4):243–252, 2000.

[12] I. Chizuka. Peripheral nerve regeneration. *Neuroscience Research*, 25(2):43–60, 1996.

[13] S. Sunderland. The anatomy and physiology of nerve injury. *Muscle and Nerve*, 13(9):771–784, 1990.

[14] Lundborg G. A 25-year perspective of peripheral nerve surgery: Evolving neuroscientific concepts and clinical significance. *Journal of Hand Surgery*, 25(3):391–414, 2000.

[15] X. Gu, F. Ding, and D.F. Williams. Neural tissue engineering options for peripheral nerve regeneration. *Biomaterials*, 35(24):6143–6156, 2014.

[16] P. Konofaos and J.P. Ver Halen. Nerve repair by means of tubulization: past, present, future. *Journal of Reconstructive microsurgery*, 29(3):149–164, 2013.

[17] L. E. Kokai, Y.C. Lin, N.M. Oyster, and K.G. Marra. Diffusion of soluble factors through degradable polymer nerve guides: Controlling manufacturing parameters. *Acta Biomaterialia*, 5(7):2540–2550, 2009.

[18] S. K. Pixley, T.M. Hopkins, K.J. Little, and D.B. Hom. Evaluation of peripheral nerve regeneration through biomaterial conduits via micro-ct imaging. *Material Science and Engineering: C Materials and Biological Applications*, 1(6):185–190, 2016.

[19] A. Subramanian, U.M. Krishnan, and S. Sethuraman. Development of biomaterial scaffold for nerve tissue engineering: Biomaterial mediated neural regeneration. *Journal of Biomedical Science*, 16(108), 2009.

[20] V. Chiono and C. Tonda-Turo. Trends in the design of nerve guidance channels in peripheral nerve tissue engineering. *Progress in Neurobiology*, 131:87–104, 2015.

[21] Sarazin P., X. Roy, and B.D. Favis. Controlled preparation and properties of porous poly(l-lactide) obtained from a co-continuous blend of two biodegradable polymers. *Biomaterials*, 25(28):5965–5978, 2004.

[22] S. Agarwal, J.H. Wendorff, and A. Greiner. Use of electrospinning technique for biomedical applications. *Polymer*, 49:5603–5621, 2008.

[23] G. T. Christopherson, H. Song, and H.Q. Mao. The influence of fiber diameter of electrospun substrates on neural stem cell differentiation and proliferation. *Biomaterials*, 30:556–564, 2009.

[24] D. S. Jha, R.J. Colello, J.R. Bowman, S.A. Sell, K.D. Lee, J.W. Bigbee, G.L. Bowlin, W.N. Chow, B.E. Mathern, and D.G. Simpson. Two pole air gap electrospinning: Fabrication of highly aligned, three-dimensional scaffolds for nerve reconstruction. *Acta Biomaterialia*, 7:203–215, 2011.

[25] Ghobeira R. Cools, Pieter and S. Van Vrekhem. *Non-thermal plasma technology for the improvement of scaffolds for tissue engineering and regenerative medicine: a review.* IntechOPen, 2016.

[26] H. S. Yoo, T. G. Kim, and T. G. Park. Surface-functionalized electrospun nanofibers for tissue engineering and drug delivery. *Advanced Drug Delivery Reviews*, 61:1033–1042, 2009.

[27] Zhu Y., A. Wang, S. Patel, K. Kurpinski, E. Diao, X. Bao, G. Kwong, W.L. Young, and S. Li. Engineering bi-layer nanofibrous conduits for peripheral nerve regeneration. *Tissue Engineering part C: Methods*, 17(7):705–715, 2011.

[28] Morent R., Nathalie De Geyter, T. Desmet, P. Dubruel, and C. Leys. Plasma surface modification of biodegradable polymers: A review. *Plasma Processes and Polymers*, 8(3):171–190, 2011.

[29] A. Vishwakarma, P. Sharpe, S. Shi, and M. Ramalingam. Elsevier Science Publishing Co Inc, 2014.

[30] T. Osathanon, P. Chanjavanakul, P. Kongdecha, P. Clayhan, and N.C.N. Huynh. *Polycaprolactone-Based Biomaterials for Guided Tissue Regeneration Membrane.* 2017.

[31] A.C. Reid, A. J. adn de Luca, A. Faroni, S. Downes, M. Sun, G. Terenghi, and P.J. Kingham. Long term peripheral nerve regeneration using a novel pcl nerve conduit. *Neuroscience Letters*, 554:125–130, 2013.

[32] A. Martins, E.D. Pinho, S. Faria, I. Pashkuleva, A.P. Marques, P.L. Reis, and N.M. Neves. Surface modification of electrospun polycaprolactone nanofiber meshes by plasma treatment to enhance biological performance. *Small*, 5:1195–1206, 2009.

[33] T. Desmet, R. Morent, N. De Geyter, C. Leys, E. Schacht, and P. Dubruel. Non-thermal plasma technology as a versatile strategy for polymeric biomaterials surface modification: A review. *Biomacromolecules*, 10(9):2351–2378, 2009.

[34] K. Webb, V. Hlady, and P.A. Tresco. Relative importance of surface wettability and charged functional groups on nih 3t3 fibroblast attachment, spreading, and cytoskeletal organization. *Journal of Biomedical Materials Research*, 41:422–430, 2009.

[35] D. Yan, J. Jones, X.Y. Yuan, X.H. Xu, J. Sheng, J.C. Lee, G.Q. Ma, and Yu Q.S. Plasma treatment of electrospun pcl random nanofiber meshes (nfms) for biological property improvement. *Journal of Biomedical Materials Research*, page 963–972, 2013.

[36] W. Liu, J. Zhan, Y. Su, T. Wu, C. Wu, S. Ramakrishna, S.S. Mo, X. an Al-Deyab, and M. El-Newehy. Effects of plasma treatment to nanofibers on initial cell adhesion and cell morphology. *Colloids and Surfaces B: Biointerfaces*, 113:101–106, 2013.

[37] Banik I., K.S. Kim, Yun Y.I., Kim D.H., Ryu C.M., and Park C.E. Inhibition of aging in plasma-treated high-density polyethylene. *Journal of Adhesion Science and Technology*, 16:1155–1169, 2002.

[38] Banik I., K.S. Kim, Y.I. Yun, D.H. Kim, Ryu C.M., C.S. Park, G.S. Sur, and C.E. Park. A closer look into the behavior of oxygen plasma-treated high-density polyethylene. *Polymer*, 44:1163–1170, 2003.

[39] R. Morent, N. De Geyter, C. Leys, L. Gengemvre, and E. Payen. Study of the ageing behaviour of polymer films treated with a dielectric barrier discharge in air, helium and argon at medium pressure. *Surface and Coatings Technology*, 201:7847–7854, 2007.

[40] A. N. Bhoj and M. J. Kushner. Repetitively pulsed atmospheric pressure discharge treatment of rough polymer surfaces: Ii. treatment of micro-beads in he/nh3/h2o and he/o2/h2o mixtures. *Plasma Sources Science and Technology*, 17(3), 2008.

[41] T. Jacobs, N. De Geyter, R. Morent, T. Desmet, P. Dubruel, and C. Leys. Plasma treatment of polycaprolactone at medium pressure. *Surface and Coatings Technology*, 205:543–547, 2011.

[42] N. De Geyter, R. Morent, C. Leys, L. Gengembre, E. Payen, S. Van Vlierberghe, and E. Schacht. Dbd treatment of polyethylene terephthalate: Atmospheric versus medium pressure treatment. *Surface and Coatings Technology*, 202:3000–3010, 2008.

[43] S. K. Pankaj, Z. Wan, and K.M. Keener. Effects of cold plasma on food quality: A review. *Foods*, 7(1), 2018.

[44] T. Jacobs, H. Declercq, N. De Geyter, M. Cornelissen, P. Dubruel, C. Leys, and R. Morent. Improved cell adhesion to flat and porous plasma-treated polycaprolactone samples. *Surface and Coatings Technology*, 232:447–455, 2013.

[45] Jacobs T., R. Morent, N. De Geyter, P. Dubruel, and C. Leys. Plasma surface modification of biomedical polymers: Influence on cell-material interaction. *Plasma Chemistry and Plasma Processing*, 32:1039–1073, 2012.

[46] N. Bhardwaj and S.C. Kundu. Electrospinning: A fascinating fiber fabrication technique. *Biotechnology Advances*, 68(3):325–347, 2010.

[47] R. Ghobeira, Vercruysse C., Asadian M., N. Declercq, H.and De Geyter, R. Cornelissen, and R. Morent. Wide-ranging fiber diameter scale of random and highly aligned pcl fibers electrospun using an unusual non-toxic solvent system. *European Polymer Journal (submitted).*

[48] S.H. Lee, E. J. adn Teng, T. S. Jang, P. Wang, S.W. Yook, H.E. Kim, and Y.H. Koh. Nanostructured poly(epsilon-caprolactone)-silica xerogel fibrous membrane for guided bone regeneration. *Acta Biomaterialia*, 6:3557–3565, 2010.

[49] C. Luo, E. Stride, and M. Edirisinghe. Mapping the influence of solubility and dielectric constant on electrospinning polycaprolactone solutions. *Macromolecules*, 45:4669–4680, 2012.

[50] L. Van der Schueren, B. De Schoenmaker, Ö.I. Kalaoglu, and K. De Clerck. An alternative solvent system for the steady state electrospinning of polycaprolactone. *European Polymer Journal*, 47:1256–1263, 2011.

[51] A. G. Kanani and S.H. Behrami. Effect of changing solvents on poly(-caprolactone) nanofibrous webs morphology. *Journal of Nanomaterials*, 2011, 2011.

[52] R. Brandenburg. Dielectric barrier discharges: progress on plasma sources and on the understanding of regimes and single filaments. *Plasma Sources Science and Technology.*, 26(5), 2017.

[53] U. Kogelschatz, B. Eliasson, and W. Egli. Dielectric-barrier discharges: Principle and application. *Journal de Physique IV Colloque*, 7:47–66, 1997.

[54] H. E. Wagner, R. Brandenburg, K.V; Kozlov, A. Sonnenfeld, P. Michel, and J.F. Behnke. The barrier discharge: Basic properties and applications to surface treatment. *Vacuum*, 71:417–436, 1997.

[55] U. Kogelschatz. Dielectric-barrier discharges: Their history, discharge physics, and industrial applications. *Plasma Chemistry and Plasma Processing*, 23, 2003.

[56] Z. Dai, J. Ronholm, Y. Tian, B. Sethi, and X. Cao. Sterilization techniques for biodegradable scaffolds in tissue engineering applications. *Journal of Tissue Engineering*, 7, 2016.

[57] A.P. Fraise, J.Y. Maillard, and S.A. Sattar. MA: Blackwell Publishing, 4th ed malden edition, 2004.

[58] R. Ghobeira, C. Philips, V. De Naeyer, H. Declercq, P. Cools, N. De Geyter, R. Cornelissen, and R. Morent. Comparative study of the surface properties and cytocompatibility of plasma-treated polycaprolactone nanofibers subjected to different sterilization methods. *Journal of Biomedical Nanotechnology*, 13:699–716, 2017.

[59] R. Ghobeira, C. Philips, H. Declercq, P. Cools, N. De Geyter, R. Cornelissen, and R. Morent. Effects of different sterilization methods on the physico-chemical and bioresponsive properties of plasma-treated polycaprolactone films. *Biomedical Materials*, 12, 2017.

[60] S. T. Summerfelt. Ozonation and uv irradiation—an introduction and examples of current applications. *Aquacultural Engineering*, 28:21–36, 2003.

[61] J. Atteberry. How scanning electron microscopes work. Consulted on 24 december 2017 via https://science.howstuffworks.com/scanning-electron-microscope.htm.

[62] Oatley C.W., W.C. Nixon, and R.F.W. Pease. Scanning electron microscopy. *Advances in Electronics and Electron Physics.*, 21:181–247, 1966.

[63] M. Gans. How a scanning electron microscope works.wmv. *Youtube*. Consulted on 24 december 2017 via https://www.youtube.com/watch?v=vwxyszpttsi, 2013.

[64] R. Reichelt. *Science of Microscopy.* Springer, New York, 2007.

[65] Y. Yang and T. Cho. Effect of annealing temperature on the water contact angle of pvd hard coatings. *Materials*, 6(8), 2013.

[66] Y. Yuan and T. R. Lee. Contact angle and wetting properties. *Surface Science Techniques*, 51, 2013.

[67] X-ray photoelectron spectroscopy (xps). *Leibniz Institute for Solid State and Materials Research Dresden.* Consulted on 27 december 2017 via https://www.ifw-dresden.de/institutes/ikm/research-teams-and-topics/micro-and-nanostructures/available-methods/xps/.

[68] Channel electron multiplier/detector. *Indian Institute of Technology, Kanpur.* consulted on 27 december 2017 via https://www.iitk.ac.in/ibc/cem.pdf.

[69] A. Juarez. Introduction to hemispherical deflection analysers. *Atomic and Molecular Physics Group, University of Manchester*. Consulted on 27 december 2017 via http://es1.ph.man.ac.uk/research/facilities/introhda.pdf.

[70] K. Lahtonen. Electron spectroscopy (xps,aes,ups). *Tampere University of Technology.* Consulted on 27 december 2017 via http://www.tut.fi/en/research/research-fields/photonics/surface-science/electron-spectroscopy/index.htm, 2012.

[71] L. Huang, N.N. Bui, S.S. Manickam, and J.R. McCutcheon. Controlling electrospun nanofiber morphology and mechanical properties using humidity. *Journal of polymer science part B: Polymer physics*, 49:1734–1744, 2011.

[72] S. De Vrieze, T. Van Camp, A. Nelvig, B. Hagström, P. Westbroek, and K. De Cletch. The effect of temperature and humidity on electrospinning. *Journal of materials science*, 44:1357, 2009.

[73] F. Massines and G. Gouda. A comparison of polypropylene-surface treatment by filamentary, homogeneous and glow discharges in helium at atmospheric pressure. *Journal of Physics D: Applied Physics.*, 31(24):3411–3420, 1998.

[74] R. Brandenburg and Y. Golubovskii. Diffuse barrier discharges in nitrogen with small admixtures of oxygen: Discharge mechanism and transition to the filamentary regime. *Journal of Physics D: Applied Physics.*, 38(13):2187–2197, 2005.

[75] L.S. Dolce, S.D. Quiroga, M. Gherardi, R. Laurita, A. Liguori, P. Sanibondi, A. Fiorani, M. Calza, V. Colombo, and M.L. Focarete. Carboxyl surface functionalization of poly(l-lactic acid) electrospun nanofibers through atmospheric non-thermal plasma affects fibroblast morphology. *Plasma Processes and Polymers*, 11:203–213, 2014.

[76] A. Marmur. Wetting on hydrophobic rough surfaces: to be heterogeneous or not to be? *Langmuir*, 19:8343–8348, 2003.

[77] D. Cho, S. Chen, Y.J. Jeong, and Y.L. Joo. Surface hydro-properties of electrospun fiber mats. *Fibers and Polymers*, 16:1578–1586, 2015.

[78] N. De Geyter, R. Morent, T. Desmet, M. Trentesaux, L. Gengembre, P. Dubruel, C. Leys, and E. Payen. Plasma modification of polylactic acid in a medium pressure dbd. *Surface and Coatings Technology*, 204:3272–3279, 2010.

[79] D. M. Correia, C. Ribeiro, G. Botelho, J. Borges, C. Lopes, F. Vaz, S.A.C. Carabineiro, A.V. Machado, and S. Lanceros-Méndez. Superhydrophilic poly(l-lactic acid) electrospun membranes for biomedical applications obtained by argon and oxygen plasma treatment. *Applied Surface Science*, 371:74–82, 2016.

[80] C. Zandén, N. Hellström Erkenstam, T. Padel, J. Wittgenstein, J. Liu, and H.G. Kuhn. Stem cell responses to plasma surface modified electrospun polyurethane scaffolds. *Nanomedicine: Nanotechnology, Biology and Medicine*, 10:949–958, 2014.

[81] S.C. Barnett and J. S. Riddell. Olfactory ensheathing cells (oecs) and the treatment of cns injury: advantages and possible caveats. *Journal of Anatomy*, 204:57–67, 2004.

[82] M.T. Moreno-Flores, J. Diaz-Nido, F. Wandosell, and J. Avila. Olfactory ensheathing glia: Drivers of axonal regeneration in the central nervous system? *Journal of Biomedical Biotechnology*, 2:37–43, 2002.

[83] C. Radtke and J.D. Kocsis. Peripheral nerve injuries and transplantation of olfactory ensheathing cells for axonal regeneration and remyelination: fact or fiction? *International Journal of Molecular Sciences*, 13:12911–12924, 2012.

[84] Bates O. Lepzelter, D. and M. Zaman. Integrin clustering in two and three dimensions. *Langmuir*, 28:5379–5386, 2012.

[85] A. Szöör, L. Ujlaky-Nagy, G. Toth, J. Szöllosi, and G. Vereb. Cell confluence induces switching from proliferation to migratory signaling by site-selective phosphorylation of pdgf receptors on lipid raft platforms. *Cellular Signalling*, 28:81–93, 2016.

[86] F. Roloff, S. Ziege, W. Baumgärtner, K. Wewetzer, and G. Bicker. Schwann cell-free adult canine olfactory ensheathing cell preparations from olfactory bulb and mucosa display differential migratory and neurite growth-promoting properties in vitro. *BMC Neuroscience*, 14, 2013.

Appendix A

Materials and methods

A.1 Fiber material

The fibers were made from PCL pellets with a molecular weight of 80 000 $^{g}/_{mol}$. PCL was dissolved in a mixture of commercially available formic acid and acetic acid with a ratio of 9 to 1 to obtain the following concentrations: 20%, 24%, 28% and 32%. The solution was continuously stirred with a magnetic stirrer, 3 hours was sufficient for the concentrations 20% and 24%, but 4 hours for 28% and 32%. This was all performed at room temperature. All chemicals were purchased from Sigma-Aldrich in Belgium and used without additional purifications.

A.2 Electrospinning

Electrospinning was used to fabricate the fibers from the prepared PCL solution using the instrument Nanospinner 24, inovenso, Turkey. It consists of the following parts: a syringe pump, a high voltage power supply and an electrically conductive collector which is grounded and a rotating cylindrical metallic mandrel with a height of 1 cm and a radius of 5 cm. A plastic syringe was filled with the solution and pumped to the copper nozzle through a capillary tube. The CTD was adjusted to 20 cm, 17.5 cm, 15 cm and 10 cm. The rotating speed of the collector was 100 rpm for random fibers and 3000 rpm for the aligned fibers. The humidity was either low (± 20%) or high (± 50%). Under normal conditions, the low humidity was obtained and by putting hot water in the electrospinning chamber as a humidifier, the high humidity could be obtained. A voltage regulated DC power supply applied a voltage of 32 kV, this generated the polymer jet. The collector was covered with an aluminum sheet and round coverslips with a diameter of 12 mm, attached with double sided tape, utilized to collect the fibers. After each batch of samples, one sample was taken to the SEM to check the mean fiber diameter and its standard deviation.

A.3 Plasma treatment set-up

The plasma treatment was done by a dielectric barrier discharge (DBD) reactor consisting of two main parts: a plasma chamber and a power supply. Figure A.1 show the set-up used in this dissertation. The plasma was generated between two circular copper electrodes (diameter = 4 cm). Separate square (25.0 cm^2) ceramic plates (Al_2O_3) (thickness = 0.7 mm) were used as dielectrics and covered both electrodes. The lower electrode was connected to earth, by either a capacitor (10.4 nF) or a resistor (50 Ω) and the upper electrode was connected to an AC power source (frequency = 50 kHz). The plasma chamber was connected to a pump and filled with argon gas with a controllable flow. The inter-electrode discharge gap was 4 mm. The treatment started by placing the coverslip on the lower glass plate. The pump evacuated the plasma chamber below a pressure of 0.6 kPa. Next, the reactor was filled with argon gas at a rate of 3 standard liters per minute (slm) until a subatmospheric pressure between 80 and 90 kPa was reached. The chamber was flushed for three minutes, maintaining the pressure between 80 and 90 kPa to make sure a reproducible gas composition was attained. The gas flow was lowered to 1 slm until a stable medium pressure of 5.0 kPa was reached. The plasma treatment was performed for different

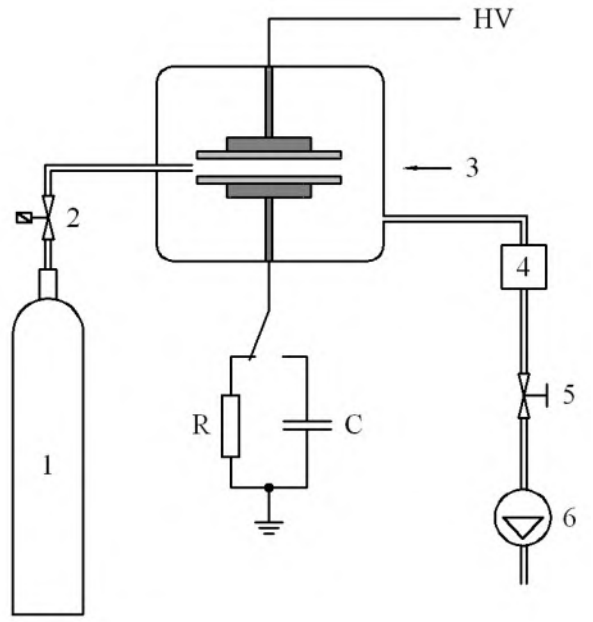

Figure A.1: Set-up of the dielectric barrier discharge.
[42]

treatment times.
The capacitor and resistor connected to the lower electrode were used to electrically characterize the discharge. The high voltage applied to the reactor was measured with a 1000:1 high voltage probe (Tektronix P6915A), connected to the upper electrode. By measuring the voltage over the resistor connected to the lower electrode, the discharge current could be obtained. A digital oscilloscope (Picoscope 3204A) and Picoscope 6 software were utilized to record and visualize the voltage and current waveforms respectively.
The capacitor, connected to the lower electrode, was used to obtain the discharge power. The charge stored on the copper electrodes is directly proportional to the voltage across this capacitor. Lissajous figures were constructed by plotting both quantities with respect to each other. The area enclosed by the Lissajous figure is equal to the electrical energy consumed per voltage cycle and, multiplied by the frequency of the feeding voltage (50 kHz), represents the discharge power. All plasma treatments were performed with an applied discharge power of 1.4 W.

A.4 Surface characterization of the fibers

A.4.1 Scanning electron microscopy

To visualize the morphology of the PCL nanofibers an SEM was used (JSM6010PLUS, JEOL, Japan). The instrument operated at an accelerating voltage of 7 kV to acquire the images. For an optimal result, the samples required a golden coating. This was feasible with the sputter coater (JFC1300 autofine coater, JEOL, Japan).
Afterwards the average nanofiber diameter was calculated using the ImageJ analysis software (National Institutes of Health, USA). The size of 50 different fibers was measured perpendicular to the long axis and the mean and standard deviation were calculated.

A.4.2 Water contact angle measurement

To evaluate the surface wettability of the PCL nanofibrous meshes, the static contact angles were measured. This was performed with the commercially available Krüss Easy Drop optical system (Krüss Gmbh in Germany). A 2 μl distilled water drop was deposited onto the samples. Rapidly after the

drop hit the mesh, the contact angle was measured. A water drop profile was obtained and by using Laplace-Young curve fitting, the contact angle was found. The measurements were executed in normal ambient conditions in a laboratory setting.

A.4.3 X-ray photoelectron spectroscopy

A PHI 5000 Versaprobe II spectrometer was used to carry out the XPS measurement. A monochromatic Al K_α X-ray source ($h\nu = 1486.6\ eV$), operating at 50 W power (beam size = 200 μm) was focused onto the sample. A pressure of at least 10^{-6} Pa was maintained inside the apparatus. Placed under an angle of 45° with respect to the sample surface normal, a hemispherical electron analyzer detected the photoelectrons. The chemical composition of the PCL samples before and after plasma treatment could be determined with the XPS measurement. This was done by extracting the binding energies of the atoms of the ejected photoelectrons in reference to carbon (C1s) at 285.0 eV. Survey scans measured two different samples with four points per sample and were documented with a pass energy of 187.85 eV. These scans were as such important to establish the elemental composition of the surface of the nanofibrous mesh. Furthermore the Multipack Software (V9.6) was needed to create a Shirley background. Together with the relative sensitivity factors, supplied by the manufacturer of the apparatus, a quantification of the elements detected on the sample could be performed.

A.5 UV sterilization

The samples were irradiated for 3 h by an UV lamp of 15W (Sylvania; 254 nm wavelength). A distance of 45 cm between the lamp and the samples was maintained and the effective UV intensity was 300 $^{\mu W}/_{cm^2}$.

A.6 Cell culture tests

A.6.1 Cell culture and cell seeding

The olfactory ensheathing cells (OECs) were derived from rats by incubating the dissected and grinded bulbus olfactorius or olfactory bulb (neural structure responsible for transmission of olfactory information to the brain) in DMEM/F12 (Gibco) solution with 0.1% trypsin (Sigma; T9201) at 37°C for 1 hour on a shaker. Studies have shown that OECs harvested from the olfactory bulb enhance neurite outgrowth better and migrate faster than OECs harvested from the olfactory mucosa. [86] Afterwards DMEM/F12 with a 10% foetal calf serum (FSC) was added to neutralize the olfactory bulb. A cell strainer (70 μm) was used to filter the cell suspension, which was centrifuged for 5 minutes at 100 rpm. The supernatant was removed. Cells were resuspended in DMEM/F12 with 10% FCS and 1% P/S before being seeded in a culture flask. Three hours later, unattached cells were put in a new culture flask. The second culture flask was incubated with a poly-L-lysine (0.1 $^{mg}/_{ml}$) (Sigma; P5899) solution for 2 hours, washed with sterile water and let to dry out. A poly-L-lysine coating was achieved on the inside of the culture flask in this way. Three days later, the medium was refreshed. When the cells reached 80-90% confluence, they were split.

A.6.2 Live/dead staining (CaPi) and fluorescence microscopy

Live/dead staining with calcein AM/propidium iodide was carried out to evaluate cell viability, attachment, morphology and proliferation of OECs. First of all the PCL fibers were rinsed, then the supernatant was replaced with 1 ml phosphate buffered saline (PBS) supplemented with 2 μl (1 $^{mg}/_{ml}$) prodium iodide (Sigma-Aldrich; P4170) and 2 μl (1 $^{mg}/_{ml}$) calcein AM (ANaspec; 89201). Afterwards the cells were incubated in the dark for a duration of 10 min at room temperature. The samples were washed with PBS and checked under a fluorescence microscope (Olympus IX 81).

A.6.3 Actin staining

The intermediate actin filaments of the OEDs could be visualized by first fixing the samples with 4 % paraformalfehyde for a duration of 20 min. The samples were washed three times with PBS and

permeabilized with 0.5 % Triton X-100 (Sigma-Aldrich; T8787) for five minutes in distilled water. Next the cells were washed again with PBS and subsequently incubated with rhodamine phalloidin (Thermo Fisher Scientific; R415; 1/100). A last PBS wash was carried out and finally the samples were mounted with Vectashield Antifade Mounting Medium with DAPI (Vectorlabs; H-1200).

A.6.4 PrestoBlue® assay

Within the cytosol a reducing environment is maintained in viable cells. First 100 μl PrestoBlue® was added to each well. The samples were placed, for two hours, in an incubator (37°C, 5% CO_2. The PrestoBlue® (Invotrogen, A13262) reagent enters a living cell, then resazurin (non-fluorescent blue compound) is reduced in this environment to resorufin (highly fluorescent red compound). Finally, 200 μl of the supernatant was transferred to a 96-well plate. The amount of metabolically active cells was represented by this fluorescence, which could be measured using a Victor 3 1420 multilabel counter (PerkinEnlmer) at an excitation wavelength of 535 nm and an emission wavelength of 605 nm. The measurements were done in fivefold. The metabolic activity was compared to OECs seeded on coverslips coated with poly-L-lysine, this is a positive control. The values presented in this master's dissertation are expressed as a ratio to this control.

A.6.5 Protocol of cell fixation for SEM analysis

The SEM was used again to analyze the morphology of the cells adhering and proliferating on the PCL nanofibrous membranes. The cells were washed with PBS and fixed with 2.5 % glutaraldehyde in 0.1 M cacodylate buffer for a duration of one hour. Next, the cells were dehydrated through immersion in an increasing series of alcohol: 50 %, 70 %, 85 %, 85 %, 95 % and 100 % ethanol with a 10 min immersion in each solution. The immersion in 100 % ethanol was carried out twice, utilizing a fresh solution the second time. Dehydration occured and the nanofibers containing the cells were transferred to a 100 % hexamethyldisilazane (HMDS) solution, where they are stored for 10 min. HMDS is subsequently replaced by a fresh HMDS solution and left under the fume hood to evaporate. The same procedure as the samples without cells was used to visualize them under the SEM. They were coated with gold and viewed with the SEM operating at a accelerating voltage of 7 kV.